By Architects. For Architects.
By Engineers. For Engineers.

Architecture
Civil and Structural Engineering
Mechanics of Materials
Building and Construction
Urban Planning and Development
Transportation Issues in Construction
Geotechnical Engineering and Engineering Geology
Designing, Operation and Service
of Construction Site Engines

Architecture and Engineering

Volume 8 Issue 2 (2023)

ISSN: 2500–0055

CONTENTS

Architecture

EVOLUTION OF TEMPLE ELEVATIONAL FORM WITH SQUARE CIRCLE METHOD: LAKSHMAN TEMPLE IN SIRPUR

Mamta Dewangan[1]*, Vandana Agrawal[2]

[1]Department of Architecture, Government Girls Polytechnic, Raipur, Chhattisgarh, India

[2]Department of Architecture, National Institute of Technology, Raipur, Chhattisgarh, India

*Corresponding author's e-mail: mamta.dew01@gmail.com

Abstract

One of the fundamental methods for shaping the constructional geometry of any building is the use of basic shapes: circles and squares. The circle represents vitality or energy, while the square represents strength. In world history, the concept of geometry traces its origins to construction in Egypt and Babylonia, where proportional systems were described through mathematical equations. They later became known as the Pythagorean Theorem, named after Pythagoras. In Ancient India, the concept of geometry starts with the construction of *altars* for *Vedic* sacrifices, as per the instructions of the *Śulbasūtras*. This involved creating circles and squares, converting squares to circles and vice versa, resulting in altars of various shapes and proportionate systems. The intersection of these basic shapes, the square and the circle, is the key to constructional building geometry. For instance, *Vesica* Piscis is a geometrical element derived from the circle-circle intersection. It has been applied by researchers to examine the geometry of both ancient and modern buildings. Similarly, the Square-Circle Sequence (SCS) is a method derived from the square-circle intersection. Gandotra (2011) used it to study the constructional geometry of the Hindu temples in North India (*Nāgara temples*). Meister (1985) also applied the square-circle intersection geometric constructional method to define the proportionate system of the Hindu temples in India. Finally, this study attempts to correlate these types of constructional geometry in the evolution of elevational form of *Nāgara temples* through *Lakshman temple in Sirpur*. It determines that the building's elevational form may be derived from the basic shapes of the circle and the square.

Keywords: Elevational form, Śulbasūtras, Vesica Piscis, square-circle sequence, circle-circle intersection, square-circle intersection, Lakshman Temple in Sirpur.

Introduction

Early in history, humans built their huts and erected their tents with an intuitive notion of geometry. Basic ideas of shape and form could have emerged from observing the sky and nature, and could then have been developed further for practical needs, such as measuring and calculating area sizes (Srinivasan, 2010). Thus, geometry (where "geo" means "earth" and "metron" means "measurement", as per ancient Greek etymology) is a branch of mathematics that deals with shape, form and measurement, with the visual component being dominant. To create geometric shapes, figures or areas need to be enclosed by a boundary that consists of a specific amount of curves, points and lines. The most common, basic geometric shapes are the circle and various polygons.

The origins of geometry go back to the insights obtained with certain mathematical equations and formulas in Ancient Greece, India, Egypt, Babylonia, and China. The difference in approach between these civilizations can be illustrated by how they would solve for x in this equation: $x^2 = N$ (the concept of the square root) (Joseph, 1997).

The geometric principles expounded in the *Śulbasūtras* (800–500 BCE) have often been considered the beginning of mathematics on the Indian subcontinent (Sinha et al., 2011). The term *"śulba"* or *"śulva"* comes from the root *"śulv"*, which can be a verb, "to measure" (Harding, 2004), or a noun, "string, cord or rope" (Price, 2000). Vedic literature has forty parts: the four Vedas plus six additional sections, consisting of six parts each. These sections are the Vedas, the Vedāṅgas, the Upāṅgas, the Upa-Vedas, the Brāhmaṇas, and the Prātishākhyas. The *Śulbasūtras* form part of the Kalpa Sūtras, which, in turn, are part of the Vedāṅgas. There are four main *Śulbasūtras*: the Baudhāyana, the Āpastamba, the Mānava, and the Kātyāyana (Price, 2000). The *Śulbasūtras* describe the construction of altars of various shapes, depending on the particular ritual (Seidenberg, 1961): specifically, square and circular altars for domestic sacrifices, and other shapes like śyena citi (falcon-shaped), rathachakra citi, and kūrma citi for special sacrifices.

Using squares and circles in construction as per the *Śulbasūtras*

The construction of citis (altars or ceremonial platforms) starts with geometrical and arithmetical calculations and ends up with detailing. Geometrical measurements are performed by drawing arcs with different radii and centers using a cord, or *śulba* (Price, 2000).

The procedure starts with drawing the *prācī*, which is a line in the east-west direction (Price, 2000). According to ancient Indian texts (Mayamata and Mānasāra), directions were determined with the gnomon method. In this method, an umbrella-shaped gnomon — measuring 24, 18 or 12 aṅgulas (fingers) in length; 6, 5 or 4 aṅgulas (respectively) at the base; and 2, 1 or ¾ aṅgulas (respectively) at the top — is installed on the selected area and leveled with water. A circle (defined as a shape that is created by a set of points in a plane that are equally distant from a fixed point, i.e., the center) is drawn starting from the gnomon's bottom, with a radius twice the length of the gnomon. Two points are marked on the circumference of the circle when the shadow of the gnomon passes through them, before and after noon. The straight line joining these two points is roughly taken to be the east-west line (*prācī*). The line that bisects the east-west line is, therefore, the north-south line. The bisecting is done in the usual manner. Two circles are drawn, with the respective ends of the east-west line functioning as their centers and the length equaling their radius. They intersect

at two points, creating a Vesica Piscis shape; the straight line joining the points of intersection bisects the east-west line at right angles and indicates the north-south line. The intermediate quarters are outlined in the same manner: by constructing the Vesica Piscis between the points of the previous sections (Acharya,1994; Dagens, 1985) (Fig. 1).

After the *prācī* is laid down EOW, the circles are used to create a square; the steps are shown in Fig. 2.

Step 1 — The *prācī* is drawn EOW, and the intersection of two circles, with radii equaling the length of the *prācī*, gives us the north and south directions.

Step 2 — New circles are drawn in a similar manner in all directions, all with the same radius (OE) and with the E as the center.

Step 3 — The intersection point of two circles at the east and north direction gives us the north-east direction (A). The respective intersection points in the other directions are B, C, and D, producing the required square.

Verse I, 48 of Baudhāyana *Śulbasūtras* states, "The diagonal of a rectangle produces both areas that its length and breadth produce separately. This is seen in rectangles with sides three and four, twelve and five, fifteen and eight, seven and twenty-four, twelve and thirty-five, fifteen and thirty-six". The statement is directly related to the Theorem of Pythagoras, and the numbers it mentions are the "Pythagorean Triples", which the ancient Indians used for constructing various right angles.

Verse I, 50 of Baudhāyana *Śulbasūtras* says that a square is equal to the sum of the two unequal squares. The geometrical construction is described in Fig. 3. And verse I, 51 of Baudhāyana *Śulbasūtras* mentions that a square is also equal to the difference between two unequal squares. This geometrical construction is described in Fig. 4 (Price, 2000).

In verse I, 52 of Baudhāyana *Śulbasūtras,* the diagonal of a square is described as the side of another square with two times the area (Fig. 5)*.* Let us suppose that the side of a square is one unit; then the diagonal is its square root ($\sqrt{2}$), or *dvi-karaṇī* (meaning "that which produces 2", or "double-
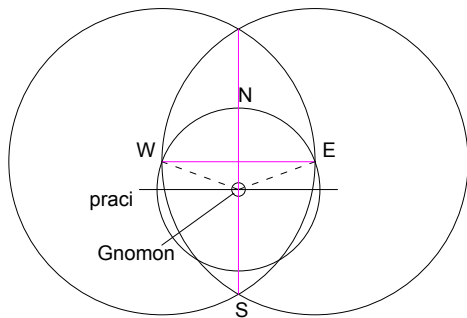
Fig. 1. The gnomon method as per Mayamata and Mānasāra, used for identifying the site's orientation (drawn by the author)
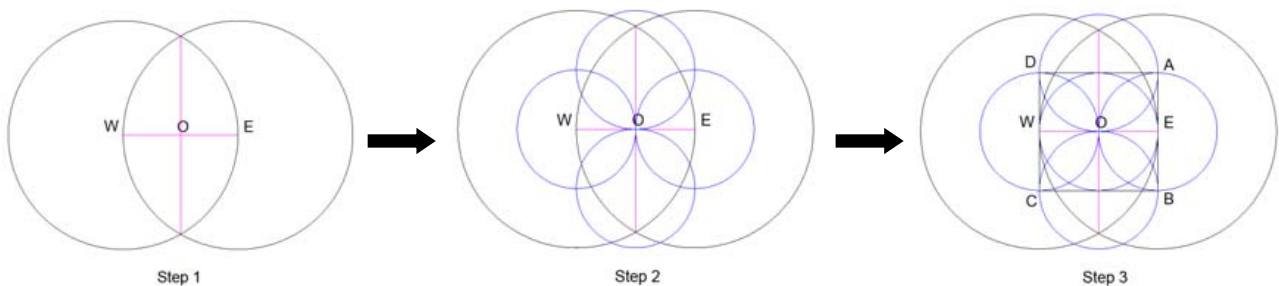
Fig. 2. Step-by-step process of constructing a square from the given *prācī* (drawn by the author)
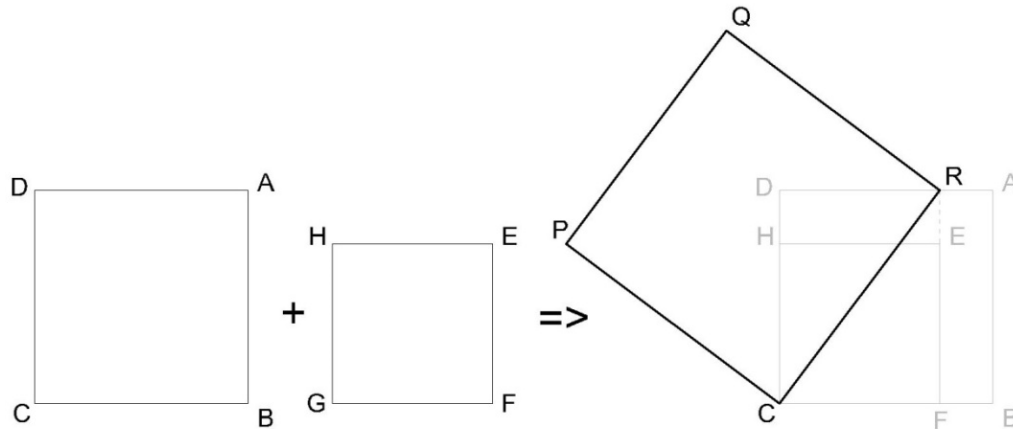
Fig. 3. Sum of two unequal squares. ABCD > EFGH. Adding the two squares leads to DR = CF = GF; then CR is the side of the square whose area is equal to the areas of ABCD and EFGH (drawn by the author)
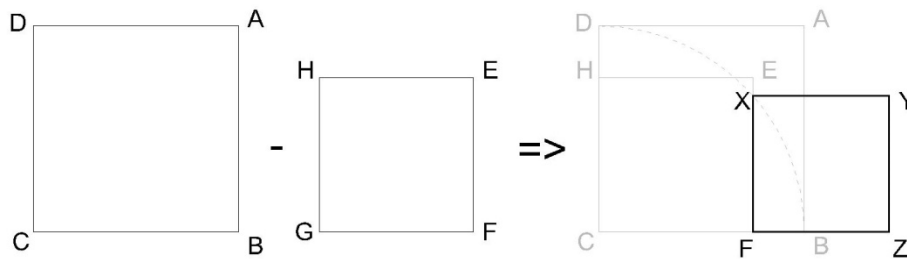
Fig. 4. Difference between two unequal squares. ABCD> EFGH, $CX^2 = CF^2 + XF^2$. If CB = CX, then $FX^2 = CB^2 – CF^2$, where FX is the side of the square whose area is equal to the difference between the areas of ABCD and EFGH (drawn by the author)

maker") (Henderson, 2000). If a rectangle is then formed with the proportion of one to the square root of two, its diagonal would be *tri-karaṇī* ("that which produces 3", or "triple-maker") (Harding, 2004).

The length of the diagonal in a square with a one-unit side is √2 = 1.4142135… (as per the calculator). Verses I, 61-2 of Baudhāyana *Śulbasūtras*, I, 6 of Āpastamba *Śulbasūtras* and II, 13 of Kātyāyana *Śulbasūtras* state the following: "Increase the length of the side by its third, and this third by its own fourth less the thirty-fourth part of that fourth". Arithmetically this is expressed as:

$$\sqrt{2} = 1 + \frac{1}{3} + \frac{1}{4} \cdot \frac{1}{3} - \frac{1}{34} \cdot \frac{1}{4} \cdot \frac{1}{3}.$$
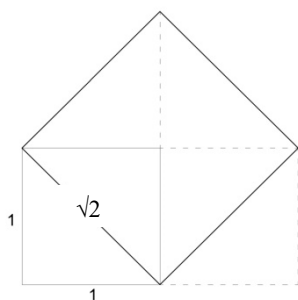
Fig. 5. *Dvi-karaṇī* (drawn by the author)

The value is √2 = 1.4142156…, which is very close to √2 = 1.4142135… (as per the calculator). The geometrical construction corresponding to the √2 calculations described in the *Śulbasūtras* is shown in Fig. 6.

Verse I, 54 of Baudhāyana *Śulbasūtras* says, "If you wish to turn a rectangle into a square, use the shorter side of the rectangle as the side of the square, divide the remaining two parts, invert them, and join them into two sides of the square". This geometrical construction is explained in Fig. 7.

Thus, the *Śulbasūtras* provide the geometrical and arithmetical solution for using the fundamental shapes of the circle and square in construction, and also give an idea of how to convert a rectangle into a square. The square root concepts can be derived from the sūtras as well.

Converting a square into a circle

Verse I, 58 of Baudhāyana *Śulbasūtras* states, "If one desires to transform a square into a circle, (a cord of length) half the diagonal (of the square) is stretched from the center to the east (with a part of it lying outside the eastern side of the square); with one-third (of the part lying outside) added to the remainder (of the half diagonal), the (required) circle is drawn" (Sen and Bag, 1983).
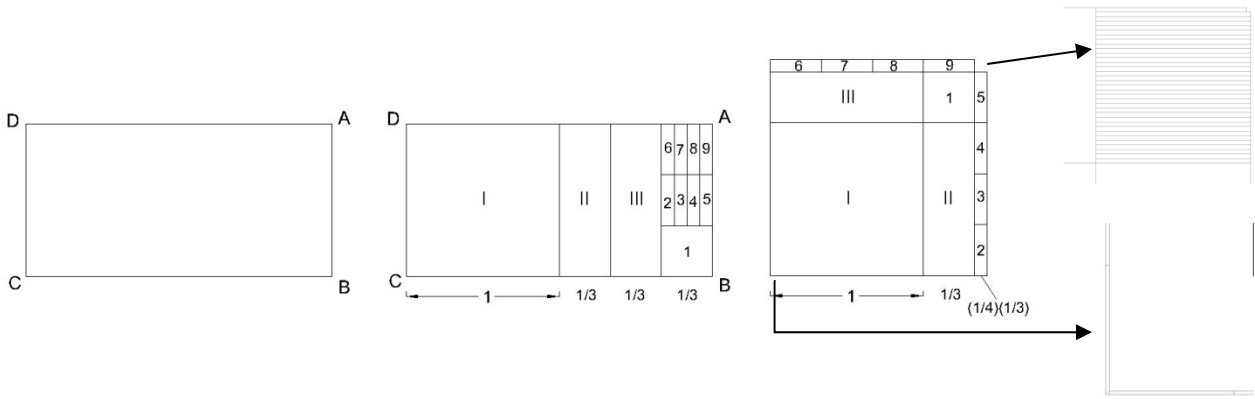
Fig. 6. Deriving the value of √2 (drawn by the author)
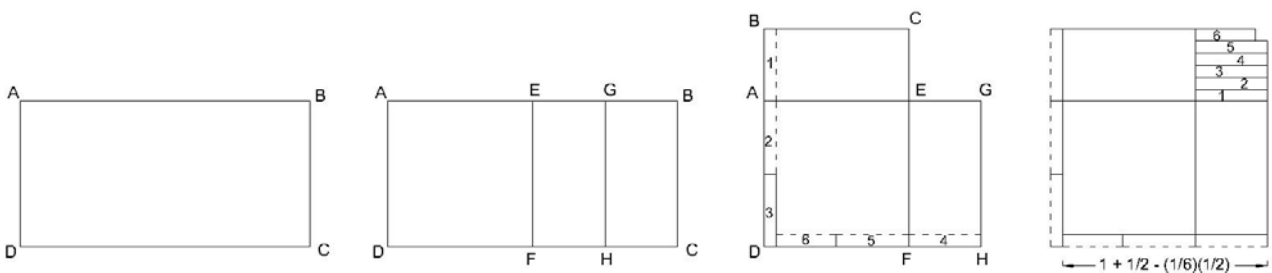
Fig. 7. Converting a rectangle into a square (drawn by the author)
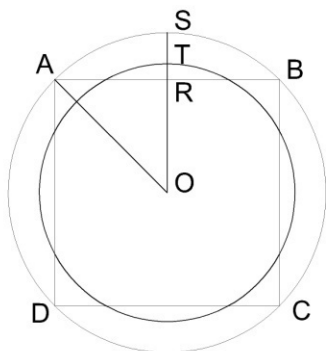
Fig. 8. Converting a square into a circle (drawn by the author)

Fig. 8 demonstrates how this is done:

Let ABCD be a square with a center in point O. Draw an arc, AS, with its center being O and radius being OA, so that OS is parallel to AD. Let us suppose OS intersects AB at point R.

Let T be the point on RS at 1/3 of the distance from R to S. Then OT is the radius of the required circle.

Let 2a be the side of the square and r be the radius of the constructed circle. Then:

$$r = OT = OR + RT = OR + \tfrac{1}{3}(OS - OR) =$$

$$= a + \tfrac{1}{3}\left(a\sqrt{2} - a\right).$$

Hence:

$$r = \tfrac{a}{3}\left(2 + \sqrt{2}\right).$$

Now, the area of the constructed circle is as follows:

$$Area = \pi r^2 = \pi \left(\tfrac{a}{3}\left(2 + \sqrt{2}\right)\right)^2.$$

If we substitute the value of π = 3.141593 and $\sqrt{2}$ = 1.414214, we get the area of the constructed circle:

$$Area = \pi r^2 = 4.069009\, a^2,$$

which is within about 1.7 % of the correct value for the area of the square = 4 (Price, 2000).

Converting a circle into a square

To continue, verse I, 59 of Baudhāyana *Śulbasūtras* states that to transform a circle into a square, the diameter is divided into eight parts; one such part is also divided into twenty-nine parts, then twenty-eight of them are removed, and the last part left is further reduced by one sixth and then one eighth (of the sixth) (Sen and Bag, 1983)

This equation can be solved as follows:

Let the diameter of the circle be *d*, then the length (*a*) of the required square is as follows:

$$length\ a = d - \frac{d}{8} + \frac{d}{8 \times 29} - \frac{d}{8 \times 29}\left(\frac{1}{6} - \frac{1}{6 \times 8}\right)$$

$$= \frac{9785}{11136}d.$$

Now, the area of the square = the area of the circle.

Therefore: $\dfrac{Area\ of\ the\ square}{Area\ of\ the\ circle} = \dfrac{a^2}{\pi r^2} =$

$$= \frac{\left(\frac{9785}{11136}\right)^2 d^2}{\frac{\pi}{4} d^2} = = 0.983045.$$

The ratio should be 1, and so the result is accurate with a margin of approximately 1.7%, same as in the previous section (Price, 2000).

Circle-circle intersection geometry

According to Euclidean geometry, to construct an equilateral triangle with a line segment as one of the sides (Fig. 9), we need to do the following:

Let AB be the finite line segment. Then we draw a circle (D), with its center being in point A and radius being AB. Similarly, another circle (E) is drawn with its center in point B. Let the two circles intersect at point C. These points are joined to form lines AC and BC. This results in an equilateral triangle, ABC.

The following proves that the constructed triangle is an equilateral triangle:

A is the center of circle CDB.

Thus, AC = AB ---------------- 1

B is the center of circle ACE.

Thus, AB = BC ------------------ 2

From 1 and 2, we conclude that AC = AB = BC.

Therefore, ABC is an equilateral triangle (Srinivasan, 2010).

Thus, the simple, complex, and advanced geometrical shapes can be derived from points, lines, and planes with the help of advanced techniques.

When any two circles intersect, this produces an almond shape, but when two circles of identical size intersect in such a way that the center of one lies on the circumference of the other, this produces Vesica Piscis (Fletcher, 2004). Vesica Piscis is a Latin term, where *Vesica* means "bladder" and *Piscis* means "fish" (Fletcher, 2004). Barrallo et el. (2015) stated that this geometric form can be expanded to construct two contiguous equilateral triangles with opposite orientation in the intersection between the circles. From this, it can be easily demonstrated that the ratio between the vertical and horizontal proportions of Vesica Piscis is the square root of various proportional systems (Fletcher, 2004).

Fletcher (2004) mentioned that Vesica Piscis can also signify the womb — in Christianity, that would be the womb of the Virgin from which Christ emerges. Additionally, Vesica Piscis proportions appear in the

Gothic arch and underlie rectangular floor plans of numerous churches and chapels (Fletcher, 2004).

Proportional systems in Vesica Piscis

Starting from the two circumferences, γ1 and γ2, we want to compute the lengths of AB and CD for the respective segments. Let r1 and r2 denote, respectively, the radii of the γ1 and γ2 circumferences. We thus have r1 = r2 = 1. Segment AB is, by construction, the radius of both circumferences, and its length equals one unit. Since O is the midpoint of segment AB, segment AO has a length of 1/2 unit. Similarly, by construction, AC is the radius of circumference γ1, and its length equals 1. This results in an equilateral triangle, ABC. Triangle AOC is rectangular, with segment CO being perpendicular to AB (Sparavigna and Baldi, 2016).

a. Equilateral triangle and the ratio of √3:1

Therefore, we can apply Pythagoras' Theorem to triangle AOC (Figs. 10 and 11) and calculate the length of segment CO. We obtain the following:

$$CO = \sqrt{(AC^2 - AO^2)} = \sqrt{[1^2 - (\tfrac{1}{2})^2]} = \frac{\sqrt{3}}{2}. \quad (1)$$

According to the symmetry in Fig. 11:

$$CD = 2CO = 2\left(\frac{\sqrt{3}}{2}\right) = \sqrt{3}. \quad (2)$$

The ratio of the two main segments is:

$$CD/AB = \frac{\sqrt{3}}{1} = \sqrt{3}. \quad (3)$$

We thus have geometrically obtained the square root of 3, which is an irrational number. However, since we referred to Pythagoras' Theorem, let us consider Eq. (3), written as follows:

$$CD^2/AB^2 = 3. \quad (4)$$
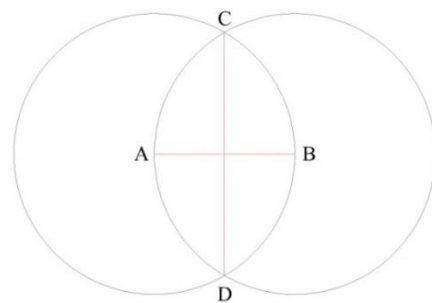
Fig. 10. CD:AB : √3:1 (drawn by the author)
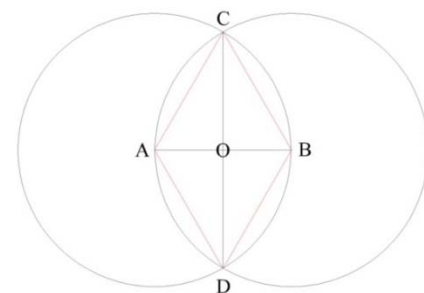
Fig. 11. OC:OB : √3:1 (drawn by the author)
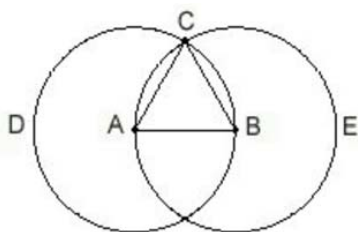

Fig. 9. An example of a metrical theorem (Victor Katz, A History of Mathematics: An Introduction, 1998) (Srinivasan, 2010)

b. Square and the ratio of √2:1

We draw two circles with radius AB = 1 (Fig. 12).

We then locate the vertical diameters, EF and GH, of the generating circles (EF = GH = 2).

We connect points ABGE and ABHF. This results in two squares.

We draw diagonal BE through square ABGE.

Thus, by applying Pythagoras' Theorem to triangle ABE, we have

$$EB^2 = \sqrt{\left(AB^2 + AE^2\right)} = \sqrt{\left(1^2 + 1^2\right)} = \sqrt{2}. \qquad (5)$$

Similarly, we connect points EFHG (Fig. 13), to create rectangle EFHG.

We then draw diagonal EH through rectangle EFHG.

Now, by applying Pythagoras' Theorem to triangle FHE, we obtain:

$$EH^2 = \sqrt{\left(FH^2 + EF^2\right)} = \sqrt{\left(1^2 + 2^2\right)} = \sqrt{5}. \qquad (6)$$
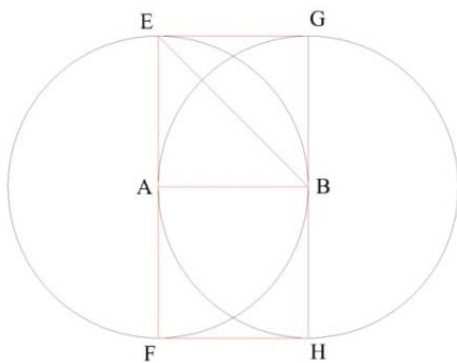
Fig. 12. BE:AB : √2:1 (drawn by the author)
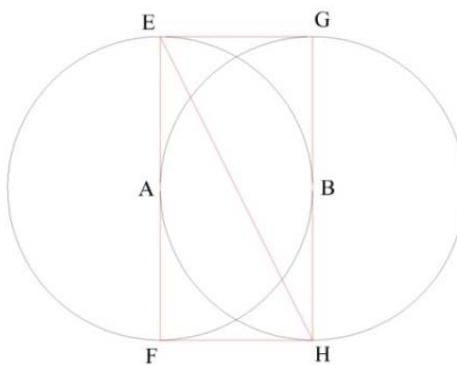
Fig. 13. EH:HF : √5:1 (drawn by the author)

Circle-circle intersection geometry in architecture

Barrallo et al. (2015) mentioned that during the Gothic period, many structural and ornamental elements utilized a geometry based on circle-circle intersections: the arches, windows, vaults, porches, and traceries that form the distinctive features of Gothic cathedrals contain Vesica Piscis forms.

In modern architecture, Vesica Piscis, or circle-circle intersection geometry, can be seen in the designs and works of Norman Foster and Santiago Calatrava. Repeatedly using the Vesica Piscis construction technique, with spheres spread out across three dimensions, is a way to create a complex building design. Probably the most important building of this category is the Sydney Opera House, designed by the Danish architect Jørn Utzon in 1957 (Barrallo et al., 2015). The Lotus Temple (Bahai house of worship) in Delhi, designed by the architect Fariborz Sahba in 1986, can also be categorized under the Vesica Piscis complex construction technique.

Square-circle intersection

Baudhāyana *Śulbasūtras* provide the geometrical methods for constructing altars in rectilinear shapes and converting them into other shapes. Thus, the square and the circle are considered to be the fundamental shapes for constructing any geometrical figures. They can also be adopted as geometrical tools for determining the various geometries in a building.

The *Bṛhat Saṁhitā* part of Varāhmihira (dating back to 6th century AD) says in chapter LIII, "House Building" that residential buildings are to be built in a square grid of 9 x 9 = 81 squares and that temple buildings are to be built in a square grid of 8 x 8 = 64 squares, as per the *Vāstūpūrūshamaṇdala*. The *Mayamata* by Dagens (1985) records thirty-two types of square *maṇdala*, which create *maṇdala* arrangements suitable for all construction sites. These range from *sakala*, consisting of just one square, to *indrakānta*, consisting of 1024 squares. Rian *et al.* (2007) adopted two types of square *maṇdala* — *yugma maṇdala* (even number of square grids) and *ayugma maṇdala* (odd number of square grids) — to analyze the constructional planning of the Kandariya Mahadev Temple in Khajuraho, which is a *fractal iteration of maṇdala (*Fig. 14*)*.
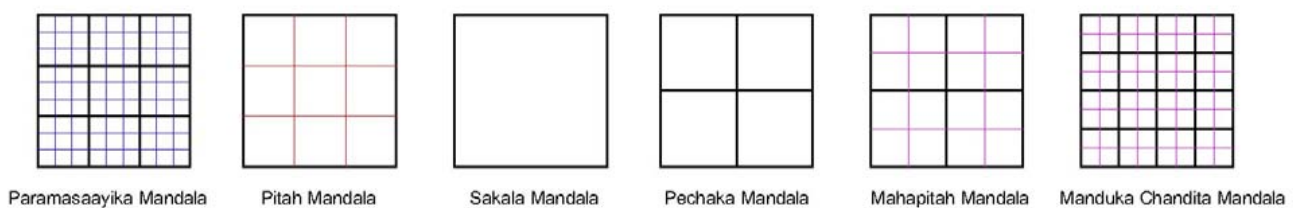
Fig. 14. Fractal iteration of *maṇdala* (Rian *et al.* 2007) (drawn by the author)

The inherent geometry of Indian temples, governing their planning and overall form, has been studied and documented widely by researchers. One of the methodologies developed by Gandotra (2011) is the *Square-Circle Sequence* (SCS). The method is based on a simple sequence of squares and circles (Gandotra, 2011). The author explained that "the squares are rotated at 22.5º to form a 16-point star (the 16 points can be equated to the 16 petals of the *Sri Yantra*) (Fig. 15).

The intersection points (*marmas*) of this 16-point figure, when projected, provide all the key locations of the temple plan". Notably, depending on the deity in the temple's sanctuary (*garbhagriha*), the SCS starts with either a circle (if the deity is a *linga*) or a square (if the deity is on a pedestal) (Fig. 16).

Proportional system of the SCS

The SCS is a generic figure that will have the following sequence for its side of the square: 1x, 1.4x, 2x, 2.8x, 4x, 5.6x, 8x, 11.3x, 16x… (Gandotra, 2011). We can see that every alternate dimension is doubling.
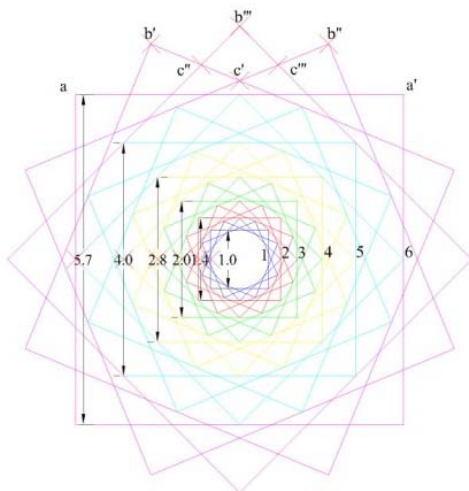
Fig. 15. Constructing a Square-Circle Sequence (SCS) to form a 16-point star (*mamra*) (drawn by the author)
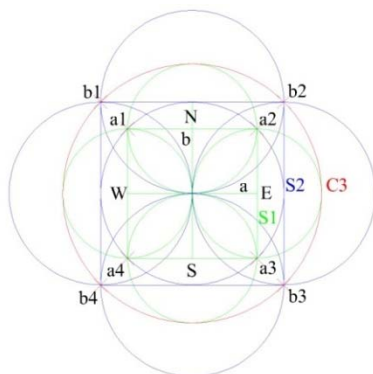
Fig. 16. Development of the Square-Circle Sequence (SCS) diagram (drawn by the author)

For instance, the first square side is 1x, while the next square is 1.4x. The first square is rotated at 22.5º thrice to obtain the second square, forming a *marmas* shape (a 16 point-star). If subsequent squares are drawn through these intersection points, the sides we get are 1.1x and 1.2x (Gandotra, 2011) (Fig. 17).

Square-circle interaction in architecture

Gandotra (2011) applied the Square-Circle Sequence (SCS) geometry when reviewing the plan, elevation and roof form of the Hindu temples in India. The researcher used the *Nāgara* style in North India for validating the SCS theory. The cases selected for the study are the square temple of Brahmeshvara in Bhubaneshwar, built in ca. 1060 AD, and the stellate temples of Chennakeshava in Nagalapura, Tumkur District, Karnataka, ca. 1200 AD, and in Jagdamba Devi, Kokamthan, Maharashtra, ca. 14th century AD. In turn, the cases selected for the analysis of the *rekha*, or the curved profile, included the *Latina* style temples of Gujarat and Madhya Pradesh, dating back to the 10th and 11th century.

Meister (1981–1982) mentioned that "the construction of the outer walls of the stellate temples (from 11th century) depends entirely on a constructional geometry using circles to produce turned squares". The researcher studied the Gargaj Mahādeva Temple in Indor, Madhya Pradesh, constructed in ca. mid-8th century. For study purposes, he created sets of circles to locate the squares and *bhadras* projections. Their constructional geometry is shown in Fig. 18.

Application of the square-circle geometry at the Lakshman Temple in Sirpur

The old city of Sirpur, or *Sirpura*, is located in the Central Province of India, on the east bank of River Māhānadī. Cunningham (1884) reported that there are several temples about half a mile to the north-east of the Gandheswar Temple, including a large one called the Lakshman Temple, with a fairly well-preserved *garbhagṛiha* tower. The inscription found at the temple dates it back to the reign of Siva Gupta, around 475 to 500 AD (Cunningham, 1884). The temple is
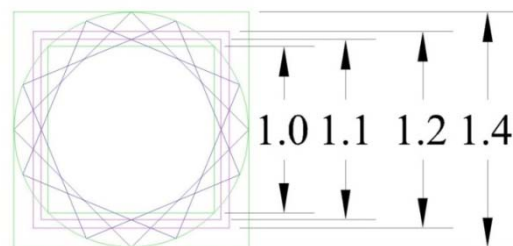
Fig. 17. Ratios (1:1.1:1.2:1.4) between the first square (1x), the second square (1.4x), and the two intermediate squares, generated with the help of the 16-point star shape in the first SCS square (1.1 and 1.2) (drawn by the author)

9
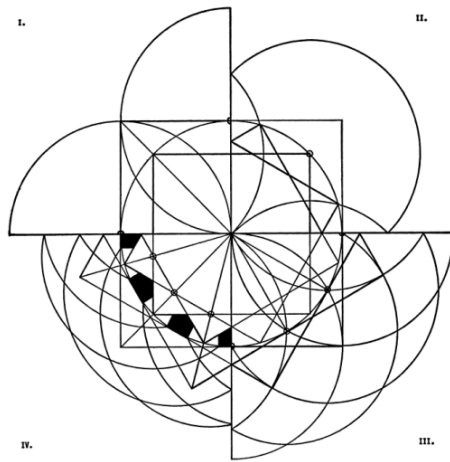
Fig. 18. Sequence showing the circles used for the construction of the outer wall in the Gargaj Mahādeva Temple plan (Meister, 1981–1982).

I: circles at the corners of inscribed and circumscribed squares;

II: circles at the corners of inner turned squares;

III: circles at the corners of outer turned squares;

IV: circles along the width of the *bhadra* projections

dedicated to Lord Vishnu. The sanctum stands on a stone platform: 77 feet long, 39 feet wide, and 7 feet tall. The temple is built up of red brick, with a *garbhagṛiha* and a *maṇḍapa* (which is currently in ruins). The sanctum's area is 22½ square feet outside and 9 square feet 9 square inches inside. It rises 45 feet above the platform.

An attempt was made to apply the geometry of circle-circle intersection (Vesica Piscis) to the proportionate elevation of the Lakshman Temple. The study found that the *Rekha* curvature of the tower, or *Shikhar*, follows the circular arcs of Vesica Piscis. Furthermore, the space between the top of the entablature (*varaṇdika*) to the bottom of the socle (*vedibandha*) forms a square, which corresponds to the lower part of Vesica Piscis, with a proportion of √2 (Fig. 19).

Result

Now the question arises: what would be the radius of the Vesica Piscis circles used for deriving the *Rekha* curvature of the tower *(Shikhar)*?

To answer it, we apply the geometry of squares and circles (Square-Circle Sequence, or SCS) to the plan of the Lakshman Temple. It starts with a square, which is the inner dimension of the *garbhagṛiha*. Further rotating this square thrice at 22.5º generates the *marma* points (intersection points of the rotating squares). The first square and the circumscribed circle intersect at the *antaral*. The radius of the *fourth* circumscribed circle is used as the radius of circles for Vesica Piscis.

In addition, the dimensions of the square used in the lower part of the temple façade equal the *third* square, whose *marma* points intersect with the outer peripheral wall of the *garbhagṛiha* (Fig. 20). Thus, the *Rekha* curvature of the tower *(Shikhar)* is derived from the radius of the *fourth* circumscribed circle.

Conclusion

Vesica Piscis is the geometry of circle-circle intersection, when two circles of the same radius are drawn with the center of one lying on the circumference of the other. Mostly, this geometry was applied in research when examining building elevation or façade. However, the origin of the circles' radius remained unknown.

Gandotra (2011) introduced a type of square-circle intersection geometry titled the Square-Circle Sequence
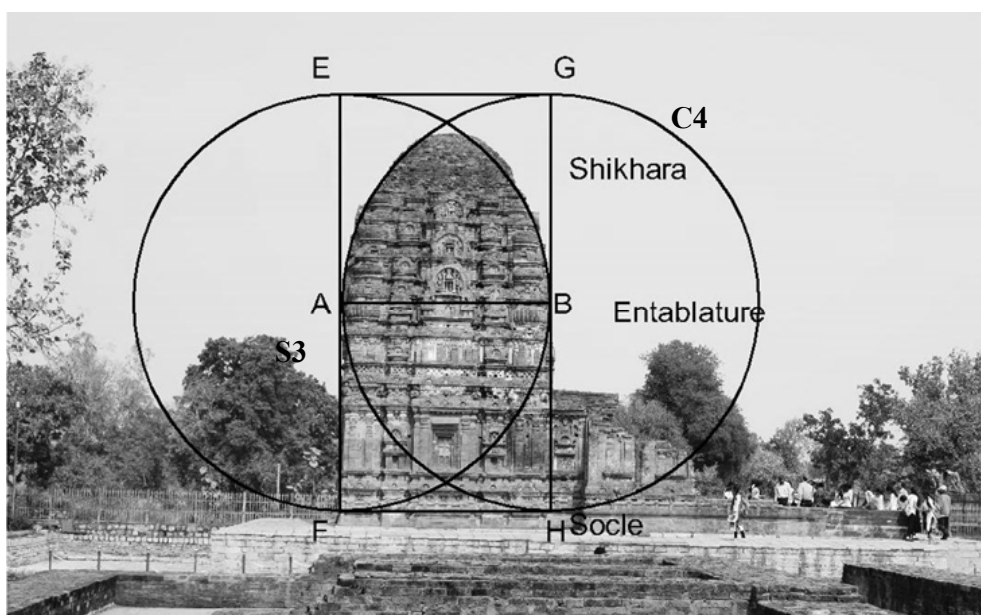
Fig. 19. Geometry of Vesica Piscis applied to the elevation of the Lakshman Temple in Sirpur, Chhattisgarh (photographed and drawn by the author)
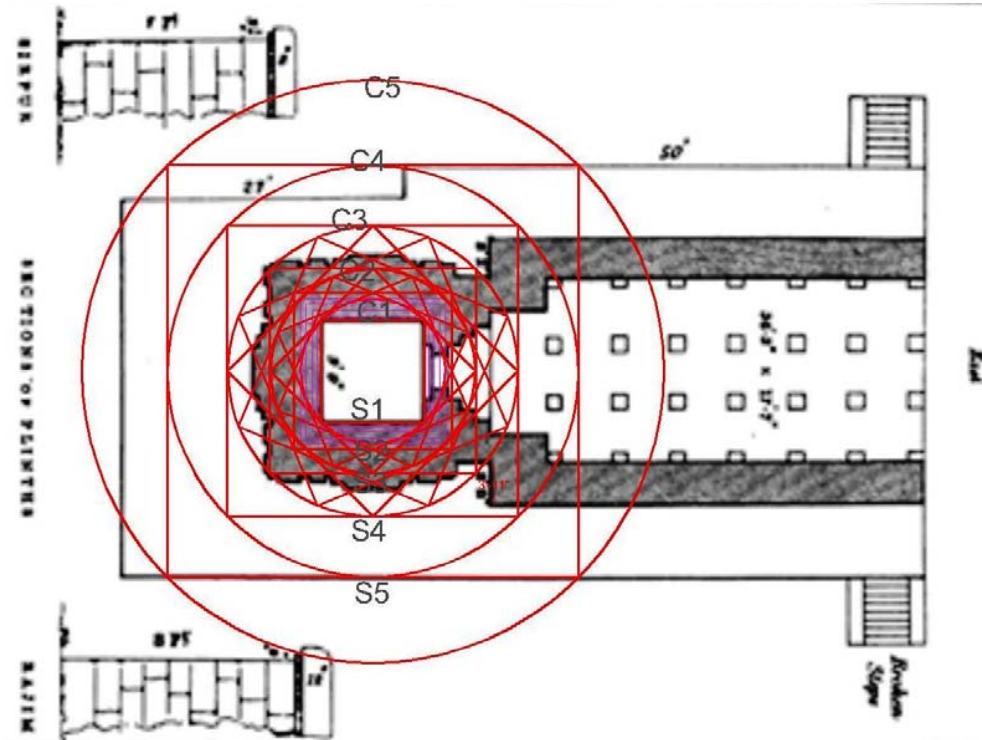
Fig. 20. Applying the Square-Circle Sequence geometry to the plan of the Lakshman Temple in Sirpur, Chhattisgarh (plan sourced from (Cunningham, 1884); the SCS drawn by the author)

(SCS), and applied it to studying the plan and elevation of temples in North India. In her work, the researcher used the circles (obtained from the sequence applied to solving the temple plan geometry) to examine the curvature of the temple's *Shikhara*.

In attempting to derive the constructional geometry behind the elevational form of *Lakshman* Temple in *Sirpur*, we apply the geometries of Vesica Piscis and Square-Circle Sequence. Our study attempts to find a link between these two geometries. Thus, the radius of circles in Vesica Piscis (applied to the curvature of the *Shikhara*) can be obtained by applying the SCS to the temple plan. Also, the square's proportion system and the √2 ratio for Vesica Piscis, as applied to *prāsāda*, can be derived from the SCS in the temple plan.

References

Acharya, P. K. (1994). *Architecture of Mansara*. New Delhi: Munshiram Manoharlal Publishers Pvt Ltd. Pp. 23–32.

Barrallo, J., González-Quintial, F., and Sánchez-Beitia, S. (2015). An introduction to the Vesica Piscis, the Reuleaux Triangle and related geometric constructions in modern architecture. *Nexus Network Journal*, Vol. 17, Issue 2, pp. 671–684. DOI: 10.1007/s00004-015-0253-9.

Cunningham, A. (1884). *Report of a tour in the Central Provinces and lower Gangetic Doab in 1881-82 (Vol. 17)*. Calcutta: Office of the Superintendent of Government printing, 160 p.

Dagens, B. (1985). *Mayamata: An Indian treatise on housing architecture and iconography*. New Delhi: Sitaram Bhartia Institute of Scientific Research, 389 p.

Fletcher, R. (2004). Musings on the Vesica Piscis. *Nexus Network Journal*, Vol. 6, Issue 2, pp. 95–110. DOI: 10.1007/s00004-004-0021-8.

Gandotra, A. (2011). *Indian temple architecture: Analysis of plans, elevations and roof forms*. Vol. 1. Gurgaon: Shubhi Publications, 58 p.

Gandotra, A. (2011). *Indian temple architecture: Analysis of plans, elevations and roof forms*. Vol. 2. Gurgaon: Shubhi Publications, 75 p.

Gandotra, A. (2011). *Indian temple architecture: Analysis of plans, elevations and roof forms*. Vol. 3. Gurgaon: Shubhi Publications, 145 p.

Harding, P. E. (2004). *The proportions of sacred space: South Asian temple geometry and the Durga Temple of Aihole*. MSc Thesis in Arts. Ohio State University.

Henderson, D. W. (2000). Square roots in the Sulbasutra. In: Gorini, C. A. (ed.) *Geometry at work, Papers in Applied Geometry, MAA NOTES*. Washington, DC: Mathematical Association of America, No. 53, pp. 39–45.

Joseph, G. G. (1997). What is a square root? A study of geometrical representation in different mathematical traditions. *Mathematics in School*, Vol. 26, No. 3, pp. 4–9.

Meister, M. W. (1981–1982). Analysis of temple plans: Indor. *Artibus Asiae*, Vol. 43, No. 4, pp. 302–320. DOI: 10.2307/3249846.

Meister, M. W. (1985). Measurement and proportion in Hindu temple architecture. *InterdisciplinaryScience Reviews*, Vol. 10, Issue 3, pp. 248–258. DOI: 10.1179/isr.1985.10.3.248.

Price, J. F. (2000). Applied Geometry of the Sulba Sutras. In: Gorini, C. A. (ed.) *Geometry at work, Papers in Applied Geometry, MAA NOTES*. Washington, DC: Mathematical Association of America, No. 53, 46–55.

Rian, I. M., Park, J.-H., Ahn, H. U., and Chang, D. (2007). Fractal geometry as the synthesis of Hindu cosmology in Kandariya Mahadev temple, Khajuraho. *Building and Environment*, Vol. 42, Issue 12, pp. 4093–4107. DOI: 10.1016/j.buildenv.2007.01.028.

Seidenberg, A. (1961). The ritual origin of geometry. *Archive for History of Exact Sciences*, Vol. 1, Issue 5. pp. 488–527. DOI: 10.1007/BF00327767.

Sen, S. N. and Bag, A. K. (1983). *The Sulbasutras of Baudhayana, Apastamba, Katyayana and Manava*. New Delhi: Indian National Science Academy, 293 p.

Sinha, S., Yadav, N., Vahia, M. N. (2011). In Square Circle: geometric knowledge of the Indus civilization. In: Sujatha, R., Ramaswamy, H. N., and Yogananda, C. S. (eds.) *Math Unlimited: Essays in Mathematics*. Boca Raton: CRC Press, pp. 451–462. DOI: 10.48550/arXiv.1112.6232.

Sparavigna, A. C. and Baldi, M. M. (2016). A mathematical study of a symbol: the Vesica Piscis of sacred geometry. *PHILICA*, Article 560.

Srinivasan, U. (2010). *Approaches to the use of geometry in architecture: A study of the works of Andrea Palladio, Frank Lloyd Wright, and Frank Gehry*. MSc Thesis in Architecture. Texas A&M University.

ИНТЕРПРЕТАЦИЯ ГЕОМЕТРИИ КВАДРАТОВ И КРУГОВ В АРХИТЕКТУРНОЙ ФОРМЕ ХРАМА ЛАКШМАН В г. СИРПУР (ИНДИЯ)

Мамта Деванган (Mamta Dewangan)[1*], Вандана Агравал (Vandana Agrawal)[2]

[1] Кафедра архитектуры, Государственное женское политехническое училище, г. Райпур, Чхаттисгарх, Индия

[2] Кафедра архитектуры, Национальный технологический институт, г. Райпур, Чхаттисгарх, Индия

*E-mail: mamta.dew01@gmail.com

Аннотация

Использование базовых фигур, круга и квадрата — один из фундаментальных методов построения конструктивной геометрии любого здания. Круг символизирует жизненную энергию, а квадрат — силу. В мировой истории концепция геометрии восходит к строительным работам в Египте и Вавилоне, где системы пропорций описывались с помощью математических уравнений. Впоследствии они стали известны как теорема Пифагора. В Древней Индии концепция геометрии берет начало от возведения алтарей для ведических жертвоприношений в соответствии с учениями Шульба-сутр. Процесс включал в себя создание кругов и квадратов, преобразование квадратов в круги и наоборот, а его результатом становились алтари различных форм и пропорций. Пересечение основных фигур, квадрата и круга — ключ к конструктивной геометрии зданий. Так, Vesica Piscis, или «рыбий пузырь» — это геометрический элемент, получаемый при пересечении кругов. Исследователи опираются на «рыбий пузырь» при изучении геометрии как древних, так и современных зданий. Аналогичным образом, последовательность «квадрат-круг» (Square-Circle Sequence, SCS) — это метод, где за основу берется пересечение кругов и квадратов. С помощью данного метода Gandotra (2011) исследует конструктивную геометрию индуистских святилищ на севере Индии (нагарских храмов). В работе Meister (1981) пересечение квадрата и круга также используется как конструктивно-геометрический метод для определения системы пропорций индуистских храмов в Индии. Наконец, в настоящем исследовании предпринимается попытка соотнести данные типы конструктивной геометрии с храмом Лакшман в индийском городе Сирпур. В ходе исследования установлено, что конструктивная геометрия здания основана на базовых фигурах: круге и квадрате.

Ключевые слова: геометрия, Шульба-сутры, Vesica Piscis, последовательность «квадрат-круг» (SCS), пересечение кругов, пересечение круга и квадрата, храм Лакшман в Сирпуре.

THE IMPACT OF THE JAVA MONARCHY INVOLVEMENT IN THE COLONIAL RAILWAY NETWORK ESTABLISHMENT ON CONTEMPORARY URBAN DEVELOPMENT

Harmilyanti Sulistyani

Institut Seni Indonesia Surakarta, Surakarta, Indonesia

Corresponding author's e-mail: hrmillistya@isi-ska.ac.id

Abstract

Introduction: This paper discusses the role of the monarchy in Java in establishing railways in the colonial period. How did the rulers of the Principalities (Surakarta and Yogyakarta) become involved in and grant their land for the development of a new type of transportation infrastructure in the 19th century? **Purpose of the study**: We aimed to reveal the impact of the colonial-era railway network as an urban artifact and the monarchs' participation in railway building on the contemporary urban morphology of Java. **Methods**: The conceptual framing is based on Aldo Rossi's theory of the evolution of urban artifacts, which emphasizes the urban artifact as the main element of the city's morphological and cultural evolution. **Results:** Java's contemporary urban morphology demonstrates the power of the monarchy to shape its cityscapes and how some aspects of city layouts today are related to railway development in colonial times, which adds significance from the perspective of the engineering component.

Keywords: *Vorstenlanden*, history, infrastructure, heritage, architecture

Introduction

Both physical and non-physical aspects of cities evolve over time. A city's architecture, which Rossi calls an urban artifact, is the most obvious observable manifestation of urban morphology (Rossi, 1982). Rossi sees it as two different things: a very large man-made object, growing over time, and an urban artifact characterized by its own history and form.

The interrelationship between urban growth and transportation cannot be severed. Such an inseparable association is the influence of railways established in the 19th century on present-day urban development. The impact of railways on cities has been and continues to be significant (Roth and Van Heesvelde, 2022). Their influence on Victorian cities can be traced through topography, the character of the city center, the condition of poor neighborhoods, the sewerage system, suburbs, the direction and character of growth, and the market price of land in the 19th century (Kellet, 2006). Examples can be seen in London, Manchester, Liverpool, Glasgow, and Birmingham. In their study of major cities of the world, Okamoto and Tadakoshi (2000) stated that urban railways encourage intensive development around stations and are highly important as a means of reducing the dependence on cars and protecting the urban environment. At the end of the 20th century, many countries made major investments to improve the quality and increase the size of their rail networks as an alternative to feeder flights, thereby linking the railways to international travel and trade (Bruinsma et al., 2008). According to Bruinsma et al. (2008), the development of railways offers new opportunities to cities that are experiencing a period of decline. Based on the authors' discussions, it can be concluded that the city and the railways are interrelated and continue to interact even today.

The railway system was first developed in Europe and later introduced to Asia to support the exploitation of the colonies. No study to date has attempted to understand the involvement of the monarchy, especially in Java, Indonesia, in the construction of railways during the colonial period, although those rulers had little political power. The current discussion of the railways in Indonesia is largely limited to engineering aspects. Their historical value and impact on modern life are only partially considered, with the focus tending to be on the role of the Dutch colonial government. In contrast, the part played by the monarchs of the Principalities (*Vorstenlanden*) in the establishment of railways in Java has not received any attention. In any consideration of contemporary urban development, it is necessary to understand urban artifacts by examining the morphology and cultural evolution of the city.

Methods

In this study, Rossi's view of urban artifacts is used to understand the role of the monarchy in the establishment of railways during the colonial period. The presence of railways in the Principalities in the last 150 years must have influenced their urban and cultural evolution. This study of the monarchs' involvement in the establishment of railways in Java will fill a gap, and the results should provide a guide to understand the urban artifacts of the

Harmilyanti Sulistyani — Pages 14–24

THE IMPACT OF THE JAVA MONARCHY INVOLVEMENT IN THE COLONIAL RAILWAY NETWORK ESTABLISHMENT ON CONTEMPORARY URBAN DEVELOPMENT

island. This study investigates the involvement of the monarchs of the Principalities in the establishment of railways during the colonial period and its impact on contemporary urban development.

The paper consists of two parts. The first part, which is the result, addresses the development of the railways during the colonial period in the Principalities. The political conditions as well as the management and exploitation of the area under the monarchs' rule were slightly different from those in the area directly under the administration of the Dutch colonial government. Nonetheless, all parties supported the efforts to bring railways to Java. The discussion in the second part of the paper considers the railways and urban morphologies of Surakarta and Yogyakarta. The impact of the monarchs' involvement more than a century ago in the construction of the railway network is evident in today's urban development. The relationship between the railway network and the city poses a challenge to the development of the city. The cityscape cannot avoid changes due to the presence of railway infrastructure, such as level crossings.

Results

The local rulers of the Principalities, located in the heart of Java, also appeared to have a desire to develop a railway system in their territories. Their involvement in the construction of the railway network cannot be underestimated although the monarchs had little power and few opportunities to exert their authority in the 19th century to the same extent as they had been able to in previous centuries. The presence of a railway system, which was supported by local rulers, certainly affected the urban evolution of the island during the colonial period and still has an impact on today's urban morphology.

The railway network has undeniably had an impact on the city. The network of railway tracks and stations that have existed since the early 19th century has clearly been part of urban evolution. In the mid-19th century, European cities placed their main stations on the outskirts of the city. By the end of the 19th century, this trend changed, and stations were located as close as possible to the city center. In the early 20th century, the United Kingdom, France, Germany, Austria, and Sweden began to build stations in the city center (Bataviaasch Nieuwsblad, 1916), so that changes to the cityscape became inevitable.

The Dutch presence in Java began with the establishment of trading posts by the *Vereenigde Oostindische Compagnie* (VOC), which was replaced in 1800 by the colonial government, headquartered in Batavia, that politically controlled Java. A series of actions were taken by the Dutch colonial government in Batavia to control and exploit the island, including economic activities in the coastal area (Lombard, 2008). However, the monarchy in Java still possessed land needed to construct a rail network.

Monarchs of the Principalities and the Plantation System

In order to discuss the monarchs' involvement in the construction of the railways in Java, it is necessary to describe the conditions that existed on the island as the background to the emergence of the need for a rail network. The island of Java is part of the Pacific Ring of Fire and has a chain of volcanoes stretching from the east to the west that dominates the southern part of the island. The ash from volcanic eruptions provides abundant fertility in the interior, making the area ideal for rice cultivation. The rice fields of Java are among the most productive in the world (Lombard, 2008).

The population of Java is mostly rural and the island has a relatively small number of cities along the north coast (Van Zanden and Marks, 2012). Historically, Java largely consisted of rural areas, with cities arising on the northern coast and at the center of the Mataram Kingdom. Prior to 1800, the state structure that developed in Java was dominated by elite groups who had authority over land and labor, meaning that these groups controlled the productive land and most of the peasants were subjected to forced labor (Van Zanden and Marks, 2012).

The urban area in the interior of Java was at the center of the Mataram Kingdom called *Vorstenlanden*, which was dominated by the cities of Yogyakarta and Surakarta (Van Zanden and Marks, 2012). The *Vorstenlanden* region was made up of Yogyakarta, which was the domain of Sultan Hamengkubuwono and Prince Pakualam, and Surakarta, which encompassed the domains of Susuhunan/Sunan Pakubuwono and Prince Mangkunegoro. *Vorstenlanden*, which literally means Prince's Land and is generally translated as the Kingdom, is more correctly translated as the Principalities (Rouffaer, 1931). The term was introduced by Dirk van Hogendorp in the *Bericht*, or the Report on the Present State of Batavia's Assets in the Dutch East Indies, in 1800. Both geographically and culturally, this region is different from other areas in Java. In his work Historical Atlas of Indonesia, Cribb (2000) compared the territory of the Mataram Kingdom at the height of its power in the early 17th century, the expansion of Dutch control in Java, 1705–1768, and Java after the Treaty of Giyanti.

The strengthening of Dutch colonial power in Java in the early 19th century led to the diminishment of the powers of the local rulers. From 1830 onward, most areas of Java were subjected to a forced Cultivation System (*cultuurstelsel*) introduced by Governor-General Johannes van den Bosch in 1830, plantations and agricultural crop cultivation were developed more widely in the eastern and western regions of Java in the next 40 years (Bosma and

Raben, 2008). Under the Cultivation System, each village was obliged to surrender the yield of one-fifth of the land cultivated to the government, and each adult farmer had to spend one-fifth of his working time cultivating this land.

Meanwhile, land in the Principalities in Central Java was managed under land lease of the apanage *(tanah lungguh)* system existing in this area (Bosma and Raben, 2008). Under this system, the princes rented out land with *tanah lungguh* status to foreign entrepreneurs for the purpose of establishing plantations. Although the systems prevailing in the Principalities and Dutch-ruled areas were different, there was an abundance of plantations in both areas to produce commodities for sale in the European market (Figs. 1-2). This then demanded a means of transportation of plantation products from the interior of Java to the ports.

Monarchs of the Principalities and the Colonial Railway Network

The conditions underlying the need for mass and fast modes of transportation indicated that a rail network was the most appropriate choice to solve transport problems in Java. However, not all of the land was within the territory of the Dutch colonial government. Some of the land that

had to be traversed by the railway network was part of the territories of the rulers of Surakarta and Yogyakarta (Samarang-Joana Stoomtram-Maatschappij, Oost-Java Stoomtram-Maatschappij, Serajoedal Stoomtram Maatschappij, Semarang-Cheribon Stoomtram-Maatschappij, 1913). Since the monarchs also had interests that required transportation (Tweede Kamer der Staten-Generaal, 1863), it was understandable that they would grant permission to build the railway network on land in their territory. At the celebrations for the issuance of the concession to construct the Semarang–*Vorstenlanden* Line in 1862, Pakubuwono IX of Surakarta stated that the presence of the railway would increase the prosperity of his domain and his people (Samarangsch Advertentie-blad, 1862).

According to Rossi's concept, the railways in the Principalities can be regarded as urban artifacts embodied in the city's architecture. The planning of the Semarang–*Vorstenlanden* Line to transport tropical products from the Java hinterland to the port of Semarang was a fairly long process. After taking into account various considerations, the route chosen traversed the colonial government land (*gouvernement ground*) in the Semarang Residency and the territories of the rulers of Surakarta
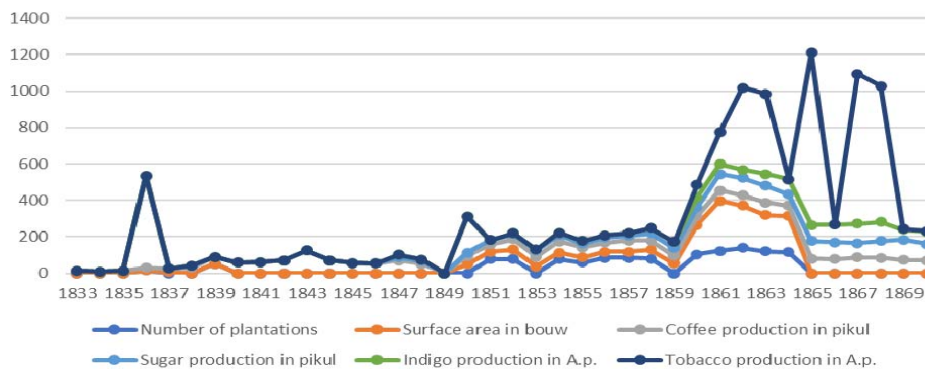
Fig. 1. Production on private plantation in Surakarta 1833-1870 (Houben, 1994)
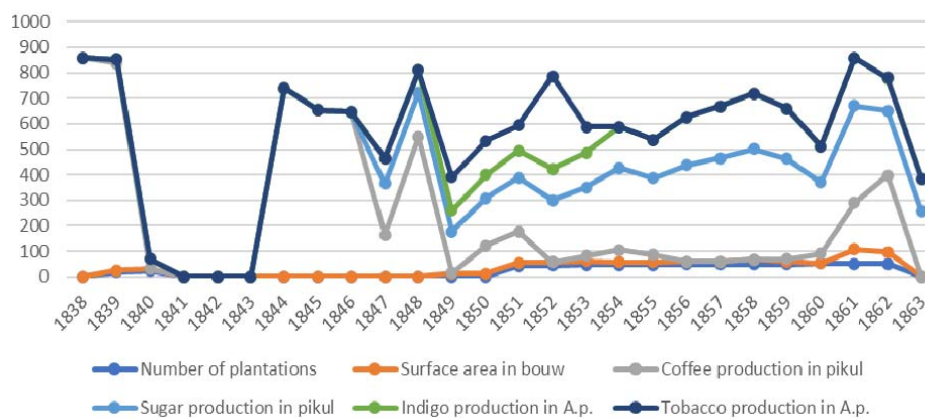
Fig. 2. Production on private plantation in Yogyakarta 1838–1863 (Houben, 1994)

and Yogyakarta. Susuhunan Pakubuwono IX of Surakarta and Sultan Hamengkubuwono VI of Yogyakarta gave permission to route the railway through their territories (De Bordes, 1870). Thus, stations and railroads became a new part of the urban architecture of Surakarta and Yogyakarta.

In accordance with the Javanese cosmological concept, an imaginary axis passes through the traditional city structure of Surakarta and Yogyakarta. The north–south and east–west axes of the four cardinal points meet at the *kraton* (palace), with the north–south axis being the stronger one (Behrend, 1989; Purwani, 2014). At the time of its initial construction, the railway lines running through Surakarta and Yogyakarta did not intersect the imaginary north–south axis. However, the need for an integrated rail network meant that the railway line from Solo Jebres Station to Solo Balapan Station had to cut across the imaginary axis of Surakarta (Fig. 3). Likewise, the imaginary axis of the city of Yogyakarta was bisected by the railway line from Tugu Yogyakarta Station to Lempuyangan Station (Fig. 4). In other words, the presence of the railway is proof that Surakarta and Yogyakarta were growing. Although the imaginary axis was not initially intersected, it was eventually interrupted during the later stages of the development of the railway network. This shift is evidence of Rossi's view that city architecture is a man-made object that grows over time.

On the other hand, Rossi sees an inseparable relationship between urban history and geographical conditions (Rossi, 1982). Parts of the city display their form, way of life, and traces of their memories, and become urban artifacts. The second section of the Semarang–*Vorstenlanden* Line, which was laid

in the territories of the Principalities, exemplifies this notion. The main station in this section is Solo Balapan Station. According to the report sent to the *Koninklijk Instituut van Ingenieurs* — KIVI (the Royal Dutch Institute for Engineers) in 1871 by J. P. de Bordes, the engineer of the first railway company in Java, which was the *Nederlandsch Indische Spoorweg Maatschappij* — NISM (Netherlands Indies Railway Company), Solo Balapan Station was located between the Pepe River and the road to Malang Jiwan because of the need for cost savings and efforts to avoid floods. The original plan was for the station to be located in the eastern part of the Solo city on the banks of the Solo River (Lang, 1869; Smulders & Co., 1868). However, the area was regularly flooded; the station and the rail line would have had to be raised, adding to the costs of the venture. The second alternative was on the west side of the city, which would have meant shifting several princely houses and relocating royal families, inevitably imposing high compensation costs. Another risk of building a railway and a station in this section was that some parts of the property belonging to Kasunanan Surakarta Palace would have been destroyed or moved to make way for the railway infrastructure (De Bordes, 1870). The problem of finding a suitable location for the station was resolved by the intervention of Mangkunegoro IV, the ruler of Mangkunegaran, who allowed the NISM to establish a station at the site of his cavalry barracks to the north of the Mangkunegaran Palace. It is difficult to find a map of Surakarta with the location of the cavalry barracks before it was replaced by the station. However, it can be traced from the name *Balapan*, which means "horse racing"

a) Before Solo Balapan Station and Solo Jebres Station were connected
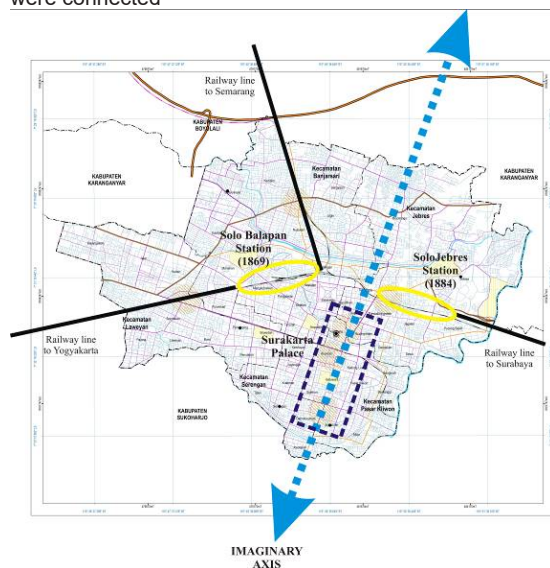
b) After Solo Balapan Station and Solo Jebres Station were connected in 1899
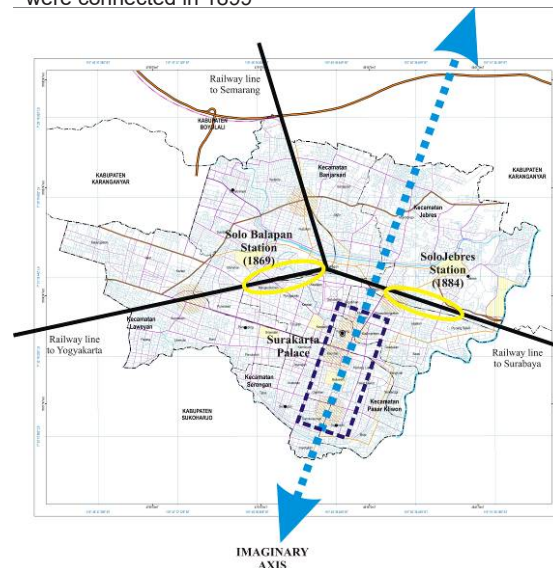
Fig. 3. Railway connection cutting across the imaginary axis of Surakarta
(adapted from https://intip.surakarta.go.id/album-peta)

a) Before Lempuyangan Station and Yogya Tugu Station were connected
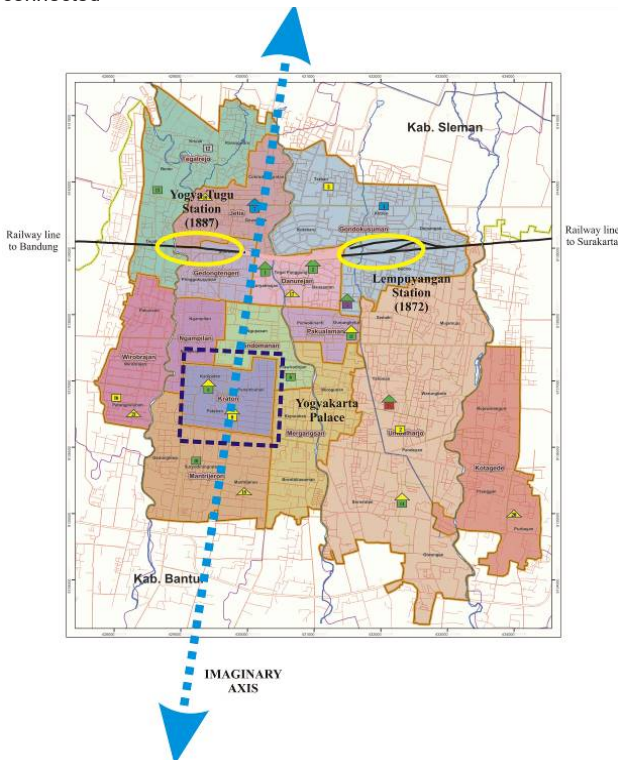
b) After Lempuyangan Station and Yogya Tugu Station were connected in 1894
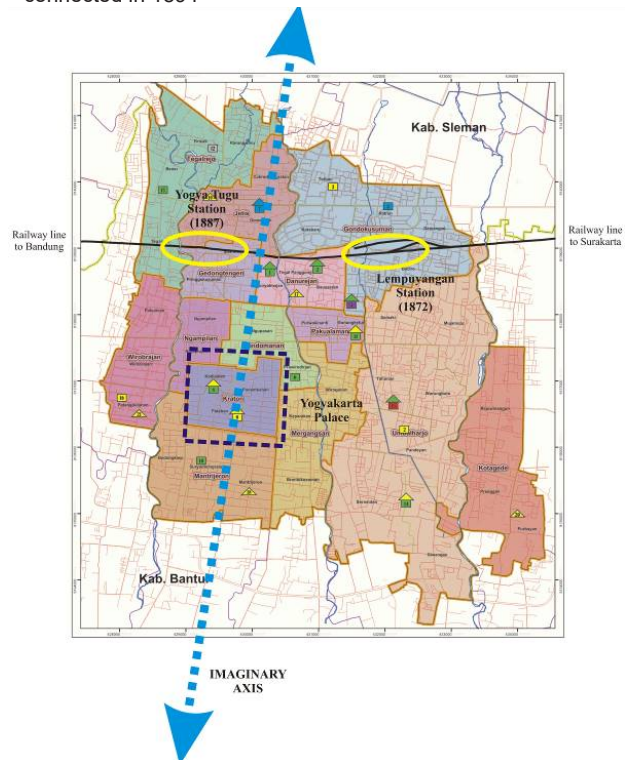
Fig. 4. Railway connection cutting across the imaginary axis of Yogyakarta
(adapted from https://bakung16.files.wordpress.com/2011/08/peta_penyebaran_pendidikan.jpg)

(*balap* = racing), and the *kestalan* area located southeast of Solo Balapan Station. The word *kestalan* is derived from the Dutch *stal* (pl. *stallen*), which means "stable for horses", providing evidence that the area was part of the cavalry *stallen* (cavalry stables). Although it is somewhat far from the center of Surakarta, the NISM accepted the location because the main road in Surakarta was accessible from it. In addition, the company did not have to pay Mangkunegoro IV for the land (De Bordes, 1870). It is possible that Mangkunegoro IV gave his land for the station because he considered the future of his sugar factory in Malang Jiwan. The road to Malang Jiwan and the postal road to Ngawi were accessible from the location (De Bordes, 1870). Mangkunegoro IV appears to have considered the time and cost savings obtained for sugar transportation by the construction of the railway. It took 20 hours to transport sugar from Surakarta to the port of Semarang in horse-drawn carts (*cikar*), while the same journey would have taken only three hours by train (Wasino et al., 2019). The selection of the location and the name of the station (Solo Balapan) confirm Rossi's view that a city's history cannot be separated from its geography; the flood proneness of the banks of the Solo River encouraged the selection of flood-free land in the north of the city of Surakarta even though it was a little far from the city center. The name Balapan is a reminder that

the location was previously a horse racing venue belonging to Mangkunegoro IV.

Urban artifacts, as manifestations of the form and way of life of parts of cities, are also evident in the Sewu Galur–Yogyakarta light-train network. The development of the sugar industry in Sewu Galur, which was within the territory of the ruler of Pakualaman, encouraged the construction of a light-train network as a means of transporting industrial products to Yogyakarta and to the port (Murdiyastomo and Darini, 2020). The sugar industry would not exist in Sewu Galur if Pakualam had not allowed his *tanah lungguh* land to be leased by European planters and used for the construction of waterways to irrigate sugarcane fields in the Sewu Galur Plantation (Murdiyastomo and Darini, 2020). The plantation and sugarcane industry changed the social life in the area around Sewu Galur Station and Brosot Station due to new economic activities, which led to the emergence of small towns (Murdiyastomo and Darini, 2020). Thus, the role of the ruler of Pakualaman in the construction of railways, especially the light train in Yogya, was intended to support the sugar industry. Sugarcane plantations and the sugar industry have specific characteristics so that the artifacts of the city they formed are also different from those that existed before.

Discussion

Javanese society had been a target of European colonization longer than other Southeast Asian

Harmilyanti Sulistyani — Pages 14–24

THE IMPACT OF THE JAVA MONARCHY INVOLVEMENT IN THE COLONIAL RAILWAY NETWORK ESTABLISHMENT
ON CONTEMPORARY URBAN DEVELOPMENT

communities; consequently, the monarchical power in Java was reduced and local rulers were forced into an indirect form of rule (Kershaw, 2001). Currently, the railway network and several locations around the stations are facing problems that date back to the development of the railways more than a hundred years ago. The problems are varied and range from conflicts of land ownership and economic conflicts related to traffic flow to social conflicts due to the development of cities and the railway network. The monarchy's role in the construction of railways in the colonial period influenced the condition of urban morphology. The following discussion considers the impact of the monarchy's involvement in the construction of the railway network during the colonial period on the morphology of the cities.

The Railway Network and the City

The railway network in Java has become an urban artifact. Its existence influences the transformation and cultural evolution of cities on the island. The railway network has become an important contributor to transportation of people and goods. Rail transportation in Java experienced a period of decline due to the increased adoption of motor vehicles. Some railway networks were decommissioned because they were no longer profitable or even considered loss-making. However, at the beginning of the 21st century, the Indonesian government took an interest in supporting the redevelopment of train transportation. The year 2009 was an important moment for Indonesian railways because they began to show service improvements (Djuraid, 2013). In Surakarta and Yogyakarta, the authorities have facilitated better integration of the railway network and stations with improved connections to airports and bus terminals. The idea of the railway station as a transit space, as well as a gateway to the city, was revived by equipping it with service facilities with adequate standards. It is hoped that the railway network will also support the central business district.

The morphology of the cities of Surakarta and Yogyakarta is influenced by the presence of the railways, which supported trade and industrialization and propelled Surakarta and Yogyakarta into becoming modern cities. Distance was no longer a problem in Surakarta and Yogyakarta after the basic infrastructure of roads and rail networks was established. Due to the presence of this infrastructure, the trajectory of development changed. Initially, the *kraton* (palace) was the focal point of development, but roads and railways encouraged the growth of the city outside the palace. The stations, like the ancient "urban gates", are sites of access to the city, as well as symbols of the identities of the places where they are situated (Somma, 2018). The Principalities rulers realized the importance of the railway network. By allowing a part of their territory to be developed as

the station they might have envisaged the possibility of the station becoming a new gateway to the Principalities.

As gateways to the city, stations provide the first experiences of the city to visitors and become identity-formers (Richards and MacKenzie, 1986; Schivelbusch, 1986). That means that railway stations become identity-forming places. For example, we can consider the transformation of Solo Balapan Station in 1927, with the addition of a building that functions as a reception hall, which was an effort to create an identity-forming place. The new building, which was designed with a square shape, was topped with a prism-shaped roof (Fig. 5). *Tajug* is the Javanese term for a prism-shaped roof. *Tajug* roofs were traditionally used in Javanese architecture for sacred places such as mosques and cemeteries (Rujivacharakul *et al.*, 2013) (Fig. 6). The adoption of a *tajug* roof for a public space seems to be an endeavor to form an identity. The *tajug* roof was deliberately chosen to emphasize the status of Solo Balapan Station as the main gateway to the Principalities. Moreover, the designer, architect Herman Thomas Karsten, from the architecture firm Karsten and Schouten, took into account the station's relationship with urban planning. Thus, relocating the village in front of the station and turning it into a park was an attempt to provide visitors with a vista of the *Sunansveste* (the seat of the Sunan/Susuhunan).

As a geographical entity, the railway station has two basic identities: as a node and as a place (Bertolini and Spit, 1998). According to Bertolini and Spit (1998), the railway station's identity as a node means that it is a gateway, and its identity as a place means that it is a specific area of the city with a concentration of infrastructure and a diverse collection of buildings and open spaces. The station's identity as a node is evident in the development of Solo Balapan Station. The railway network in Surakarta is still functioning as a means of transportation of goods and passengers. The

Fig. 5. *Tajug* roof emphasizing the status of Solo Balapan Station as the Principalities main gateway Photo by author, 2010

19
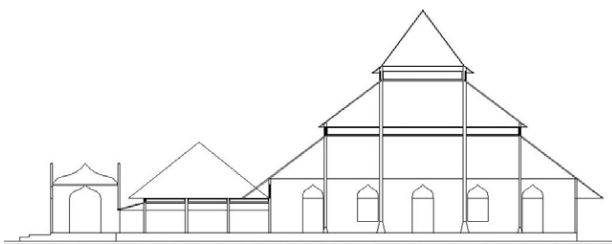
Fig. 6. *Tajug* roof on the Al Wustho Mosque Photo by author, 2006

Surakarta City Government has developed an integrated transportation system that connects Surakarta to other areas by making Solo Balapan Station the central station. Solo Balapan Station is also part of the integrated transportation development of Surakarta and Yogyakarta areas, linking it with the international airport and bus terminal. The double track, which was officially inaugurated in 2007, facilitates the connection of Solo Balapan Station to Adisutjipto International Airport in Yogyakarta. To help pedestrians, Solo Balapan Station was connected to Tirtonadi Terminal via a skybridge in 2019. The connection between Solo Balapan Station and Adisumarmo International Airport in Boyolali is supported by the Airport Rail Link inaugurated in 2020. Recently, PT. Kereta Api Indonesia (PT. KAI), the train operator in Indonesia, began improving the railway connections to Semarang. The project to regenerate the Solo–Semarang railway line started in 2022.

The power possessed by the city has consequences for the evolution of the city itself, and the management of different forces will lead to different changes (Rossi, 1982). The power in question can be economic or political. Economic power may manifest as expropriation and land ownership. Some of the obstacles to land acquisition for the construction of a passenger network, especially to cater to commuters, are a consequence of the involvement of the monarchy in the development of the railways in the mid-19th century. Today, the railway network

is an asset of PT. KAI, the sole train operator in the country. As described in previous sections, historically, the railways were not built solely on land belonging to the Dutch administration; some of the land was part of the Javanese rulers' territories. At the time of nationalization of the company in 1958, not much attention was paid to the ownership of the land used for the construction of the railway network. The nationalization process was based on implementation of Law No. 86 of 1958 concerning the nationalization of Dutch-owned companies. Article 1 of Law No. 86 of 1958 states that Dutch-owned companies located in the territory of the Republic of Indonesia, which will be specified by a government regulation, are subject to nationalization and declared to be the full and free property of the Republic of Indonesia (Wasino, 2016).

The power ascribed to land ownership can force the evolution of cities (Rossi, 1982), a problem that is often faced in the development of the railway network in Java. The problem of land ownership was articulated as early as in the second decade of the 20th century in a letter sent to the NISM by the Prince of Mangkunegaran. The Prince questioned the use of land that had been handed over to the NISM and the *Staatsspoorwegen* — SS (The State Railways) and stated that transfer of the rental of the property to a third party was a breach of contract. The letter was sent on October 7, 1928, by the *Patih* (vizier) of Mangkunegoro VII. The Resident of Surakarta, on behalf of NISM and SS, responded by letter dated November 21, 1928, stating that NISM had used the land in accordance with the terms of the concession (Sulistyani, 2022). Mangkunegoro VII was a descendant of Mangkunegoro IV who donated his cavalry barracks to NISM to build a station in Surakarta at the beginning of railway construction in the city. The problem continued until 1931 when Mangkunegoro VII revoked the status of the land. This act underlines the fact that the rulers of the Principalities gave permission to the Dutch railway company only to use the land, not to transfer the right of use to a third party. This suggests that the land rights were not properly defined, a problem that remains to this day. The issue of ownership status of the land, which is an asset of PT. KAI, is one of the roots of the difficulties faced by the organization in developing the railway network. The nationalization of the company after independence transformed the land that was originally an asset of the monarch into an asset of PT. KAI. The problem became more complicated when the land was occupied by people and social conflicts arose with the community when PT. KAI took over the company's property.

Today, the existing railway line in Yogyakarta is the only main line connected to the Surabaya–Bandung and Surabaya–Jakarta railway network. The local railway network within the city of Yogyakarta and

Harmilyanti Sulistyani — Pages 14–24

THE IMPACT OF THE JAVA MONARCHY INVOLVEMENT IN THE COLONIAL RAILWAY NETWORK ESTABLISHMENT ON CONTEMPORARY URBAN DEVELOPMENT

its surroundings ceased to operate in 1970. The Yogyakarta–Sewu Galur line, built to support the sugar plantations and industry during the colonial period with the support of the rulers of Pakualaman, was decommissioned. Due to problems of land ownership, there are numerous barriers to activating or revitalizing this route. A part of the infrastructure of the Yogyakarta–Sewu Galur railway line is not an asset of PT. KAI, the line and station belong to the Yogyakarta City Government and the Bantul Regency Government (PT. Kereta Api (Persero), 2000).

Collective Memory

Rossi sees collective memory as a communal connection to a place that helps to understand the urban structure and its architecture. The union between the past and the future lies in the idea that the city must be formed, which becomes a permanent aspect of the artifacts and monuments of the city (Rossi, 1982). To the Javanese, the arrival of the train was foretold. The railway network is the monument to the myth about the arrival of the iron serpent in Java, a prediction that came true. The transformations brought by the railways in Java marked a faster and farther movement. The railways, an easy mode of mass transportation because the station is located in or close to the inner city, became a collective memory. The station is the gateway to the city, and the collective memory of the railways is one of the drivers for improving services to attract passengers.

The Morphology of the Cityscape

Some aspects of today's urban planning also relate to station planning of the past. The city, according to Rossi (1982), is a man-made object, a work of engineering and architecture. Currently, the conditions for crossing railway lines and highways is the city government's homework. According to the Regulation of the Minister of Transportation No. PM 36 of 2011 concerning the Intersection and/or Intersection between Railroad Tracks and Other Buildings Article 6 verse 1, trains receive traffic priority (Kementerian Perhubungan, 2011). This becomes a problem in urban development. Before Surakarta decided to build bridges at several level crossings in the city, Yogyakarta had already taken steps to solve the problem of congestion due to the intersection of railway and roadway lines. Three flyovers, Lempuyangan, Janti, and Jombor, were built to relieve congestion due to level crossings. However, not all level crossings can be engineered with flyovers. The crossing east of Tugu Yogyakarta Station cannot be negotiated by a bridge. Rotation of the flow of motor vehicles to the east to pass under the railroad tracks was the traffic engineering solution applied to this crossing point. In Surakarta, the level crossings in Palur, Manahan, Purwosari, i.e., the Joglo level crossings from the direction of Semarang, are handled by flyovers, which are still under construction. The problem of the Ledok Sari crossing has not yet been resolved. Does the construction of flyovers in Ledok Sari-Surakarta and Yogyakarta Tugu Station have something to do with the imaginary axis of the city (Figs. 3-4)? Is it part of the cultural evolution of the cities? These questions suggest new avenues of research.

The current development of Solo Balapan Station is also an example of a man-made object. At the end of the 19th century, Solo Balapan Station became a hub for the railway network from three directions: Eastline from Surabaya, Westline from Bandung, and Semarang from the north. Initially the three lines met at Solo Balapan Station, but the rails were not connected. SS developed the Eastline and Westline network from the beginning and planned to build a main line connecting the east and west sides of the island of Java (Perquin, 1921). However, the plan had to be delayed several times because of the difference in gauge of the tracks at Solo Balapan Station. The SS railway line to Eastline and Westline were narrow gauge, but the NISM railway tracks in the Principalities were broad (standard) gauge. The plan that emerged in 1913 involved turning Solo Balapan Station into a common station for both NISM and SS. The new station building complex would be elevated toward Purwosari Station, so that pedestrians could pass under the bridge. The plans have never been implemented. For more than a hundred years, the problem of the dangerous level crossing near Solo Balapan Station has remained unsolved. In 2018 and 2021, the Surakarta City Government built a bridge at the intersection of the roadway and railway line in Manahan and Purwosari, which is to the west of Solo Balapan Station. The bridge built to accommodate motor vehicles brought a significant change to Surakarta's cityscape. Pedestrians and cyclists are accommodated by a tunnel. Mangkunegoro IV's intervention by donating his cavalry barracks 150 years ago to build a station influenced the urban morphology of the city of Surakarta. Meanwhile, in Yogyakarta, the government persists in its attempts to solve the congestion problem by planning the construction of two new flyovers, one on Jalan Kaliurang, around the Universitas Gadjah Mada campus, and one on Jalan Gejayan. However, there is also a discussion about overcoming the problem of crossing a plot with an underground tunnel (underpass). Surakarta has implemented the construction of an underpass at the Makam Haji crossing (Figs. 7-8).

Conclusion

Several city artifacts in Surakarta and Yogyakarta still existing today are directly related to the construction of the railway network in Java, which was begun in the mid-19th century. At that time, the political power of the monarchs of the Principalities

Fig. 7. Manahan-Surakarta Level Crossing, 2020 (Kementerian PUPR, 2020)

Fig. 8. Purwosari Surakarta Level Crossing, 2021 (Kementerian PUPR, 2021)

was diminished under the control of Dutch colonial rule. However, it is undeniable that these rulers in Java played an active role in the construction of the railway network and became part of the spatial history of Java. The railway network, including its stations, in Surakarta and Yogyakarta is still largely functioning, although some parts are neglected or even forgotten. Understanding its presence and its stakeholders during its development will help in planning future developments in the city within the context of urban morphology.

The main factor driving the establishment of Java's railway network was the increase in plantation products. The land lease system in Surakarta and Yogyakarta and the Cultivation System in West Java and East Java led to the growth in plantation yields

and industrialization. The monarchs of Surakarta and Yogyakarta were aware of the changes taking place during their reign, and their openness to supporting and facilitating the arrival of the railways illustrates their drive to bring modernity to their territories. The monarchs were actively involved in establishing the railways and thus became agents of modernism.

The impact of the monarchs' involvement in the establishment of railways in Surakarta and Yogyakarta on today's urban development is quite diverse. Examples include the influence on transportation arrangements within the city, mobility between regions, settlements, and economic activities. All these aspects required traffic engineering which brought changes to the cityscape. Another challenging element is the impact of the railway network on land ownership, which is often followed by long-lasting social conflicts due to neglect of or unclear land rights. It is difficult to solve these problems without understanding the role of the monarchs because it was they who granted permission for the railways to cross their territories and formulated the relevant conditions for land use. With the establishment of the railways, changes in the cityscape are inevitable due to the infrastructure such as level crossings, as well as at a spiritual level. In Java, the architecture of the railway network, including its stations, intervenes in the imaginary axes of the cities of Surakarta and Yogyakarta, a crucial aspect of Javanese mysticism. The development of the railway network transforms the city, and the evolution of the city brings changes to the railway network. Built as part of the colonial infrastructure for exploitation of the colonies, the railways are a testament to the involvement of the Javanese monarchs in catalyzing modernity. The railway network in Java has become one of the most important elements that make up the urban artifact. Aspects of urban development today cannot be separated from the existence of the railways. This study emphasizes that the monarchs' involvement in ensuring the existence of the railways in Java had an impact on urban development.

References

Bataviaasch Nieuwsblad (1916). Nogmaals de Nieuwe spoorplannen voor Batavia. *Bataviaasch Nieuwsblad*, July 27, *1916, Tweede Blad, 1 p*. https://resolver.kb.nl/resolve?urn=ddd:011037470:mpeg21:p005 [Date accessed 5 August 2022].

Behrend, T. E. (1989). Kraton and Cosmos in Traditional Java. *Archipel*, Vol. 37, pp. 173–187. DOI: 10.3406/arch.1989.2569.

Bertolini, L. and Spit, T. (1998). *Cities on rails: the redevelopment of railway stations and their surroundings*. London: E & FN Spon*, 256 p.*

Bosma, U. and Raben, R. (2008). *Being "Dutch" in the Indies: a history of creolisation and empire, 1500–1920*. Singapore: NUS Press*, 439 p.*

Bruinsma, F., Pels, E., Rietveld, P., Priemus, H., and van Wee, B. (2008*). The impact of railway development on urban dynamics.* In: Bruinsma, F., Pels, E., Rietveld, P., Priemus, H., and van Wee, B. (eds.) *Railway Development*. Heidelberg: Physica-Verlag, pp. 1–11. DOI: 10.1007/978-3-7908-1972-4_1.

Cribb, R. (2000). *Historical atlas of Indonesia*. Richmond: Curzon Press, 256 p.

De Bordes, J. P. (1870). *De Spoorweg Samarang-Vorstenlanden*. Den Haag: De Gebroeders van Cleef, *41 p.*

Djuraid, H. M. (2013). *Jonan & Evolusi Kereta Api Indonesia*. Jakarta: PT Mediasuara Shakti - BUMN Track, 336 p.

Houben, V. J. H. (1994). *Kraton and Kumpeni: Surakarta and Yogyakarta, 1830–1870.*. Leiden: KITLV Press, *396 p.*

Kellet, J. R. (2006). *The impact of railways on Victorian cities*. London: Routledge*, 514 p.*

Kementerian Perhubungan (2011). *Peraturan Menteri Perhubungan No. PM. 36 Tahun 2011 tentang Perpotongan dan/atau Persinggungan antara Jalur Kereta Api dengan Bangunan Lain.* [online] Available at: https://peraturan.bpk.go.id/Home/Details/106888/permenhub-no-36-tahun-2011 [Date accessed August 2, 2022].

Kementerian PUPR (2020). *Manahan Flyover*. [online] Available at: https://twitter.com/KemenPU/status/1307639172115521536/photo/1 [Date accessed August 23, 2022].

Kementerian PUPR (2021). *Purwosari Flyover*. [online] Available at: https://binamarga.pu.go.id/index.php/berita/jadi-ikon-baru-kota-surakarta-ini-sejumlah-hal-unik-flyover-purwosari [Date accessed August 7, 2022].

Kershaw, R. (2001). *Monarchy in South-East Asia : the faces of tradition in transition*. London: Routledge*, 304 p.*

Lang, C. (1869). *Kaart van den Spoorweg van Samarang naar de Vorstenlanden*. *Leiden University Libraries. Digital Collections*. [online] Available at: http://hdl.handle.net/1887.1/item:811882%0A [Date accessed July 28, 2022].

Lombard, D. (2008). *Nusa Jawa: Silang Budaya. Bagian 2: Jaringan Asia*. Jakarta: PT Gramedia Pustaka Utama, 498 p.

Murdiyastomo, H. Y. A. and Darini, R. (2020). Kebijakan Sosial Ekonomi Pada Masa Pemerintahan K.G.P.A.A. Paku Alam IV – K.G.P.A.A. Paku Alam VIII Tahun 1864–1950. *Mozaik: Kajian Ilmu Sejarah*, Vol. 11, No. 1, pp. 34–51. DOI: 10.21831/moz.v11i1.45204.

Okamoto, T. and Tadakoshi, N. (2000). Rail transport in the world's major cities. *Japan Railway & Transport Review*, No. 25, pp. 4–17.

Perquin, B. L. M. C. (1921). *Nederlandsch Indische Staatsspoor- en Tramwegen*. Amsterdam: Bureau Industria, 6-7 p.

PT. Kereta Api (Persero) (2000). *Tanah Kereta Api Suatu Tinjauan Historis, Hukum Agraria/Pertanahan dan Hukum Perbendaharaan Negara*. Semarang: Seksi Hukum PT. Kereta Api (Persero)*, 67 p.*

Purwani, O. (2014). *Javanese power: silent ideology and built environment of Yogyakarta and Surakarta. University of Edinburgh*. [online] Available at: http://hdl.handle.net/1842/9885 [Date accessed July 2, 2022].

Richards, J. and MacKenzie, J. M. (1986). *The railway station: a social history*. Oxford: Oxford University Press, 460 p.

Rossi, A. (1982). *The architecture of the city*. Cambridge: The MIT Press, 163 p.

Roth, R. and Van Heesvelde, P. (2022). *The city and the railway in the world from the nineteenth century to the present*. London: Routledge, 520 p.

Rouffaer, G. P. (1931). *Vorstenlanden*. 's-Gravenhage: Martinus Nijhoff, 146 p.

Rujivacharakul, V., Hazel Hahn, H., Tadashi, O. K., and Christensen, P. (eds.) (2013). *Architecturalized Asia: mapping a continent through history.* Honolulu: Hong Kong University Press, University of Hawai'i Press, 344 p.

Samarang-Joana Stoomtram-Maatschappij, Oost-Java Stoomtram-Maatschappij, Serajoedal Stoomtram Maatschappij, Semarang-Cheribon Stoomtram-Maatschappij (1913). *Handleiding voor de Verwerving en Verzekering van Rechten op Grond*. [online] Available at: https://resolver.kb.nl/resolve?urn=MMUBL07:000001523:00005 [Date accessed July 15, 2022].

Samarangsch Advertentie-blad (1862). *De Spoorweg-Feesten te Soerakarta den 2den Nov 1862. Samarangsch Advertentie-blad 7 November 1862, 3 p.* Available at: http://resolver.kb.nl/resolve?urn=ddd:011089375:mpeg21:p003 [Date accessed July 10, 2022].

Schivelbusch, W. (1986). *The railway journey: the industrialization of time and space in the 19th century*. Leamington Spa: Berg*, 203 p.*

Smulders & Co. (1868). *Spoorweg Samarang-Vorstenlanden*. *Leiden University Libraries. Digital Collections*. [online] Available at: http://hdl.handle.net/1887.1/item:815534%0A [Date accessed December 26, 2022].

Somma, L. M. (2018). Railway transport and "city gates" in the development of the city: the case of matera. In: Amoruso, G. (ed.). *Putting Tradition into Practice: Heritage, Place and Design. INTBAU 2017. Lecture Notes in Civil Engineering*, Vol. 3. Cham: Springer, pp. 1209–1217. DOI: 10.1007/978-3-319-57937-5_125.

Sulistyani, H. (2022). *The railway station In Java: creation of the new power structure 1862–1942*. [online] Available at: https://research.vu.nl/en/publications/the-railway-station-in-java-creation-of-the-new-power-structure-1 [Date accessed July 30, 2022].

Tweede Kamer der Staten-Generaal (1863). *Tweede Kamer der Staten-Generaal 92ste 1863*, pp. 1019–1023. Available at: SGD_18621863_0000194.pdf (overheid.nl) [Date accessed July 5, 2022].

Van Zanden, J. L. and Marks, D. (2012). *Ekonomi Indonesia 1800–2010: Antara Drama dan Keajaiban Pertumbuhan*. Jakarta: Penerbit Buku Kompas, 491 p.

Wasino (2016). Nasionalisasi Perusahaan-Perusahaan Asing Menuju Ekonomi Berdikari. *Paramita*, Vol. 26, No. 1, pp. 62–71. DOI: 10.15294/paramita.v26i1.5146.

Wasino, Hartatik, E. S., and Nawiyanto (2019). From royal family-based ownership to state business management: Mangkunegara's sugar industry in Java from the middle of the 19th to early 20th century. *Management & Organizational History*, Vol. 14, Issue 2, pp. 167–183. DOI: 10.1080/17449359.2019.1614462.

ВЛИЯНИЕ УЧАСТИЯ ЯВАНСКОЙ МОНАРХИИ В ФОРМИРОВАНИИ СЕТИ ЖЕЛЕЗНЫХ ДОРОГ В КОЛОНИАЛЬНЫЙ ПЕРИОД НА СОВРЕМЕННОЕ ГОРОДСКОЕ РАЗВИТИЕ

Хармильянти Сулистьяни (Harmilyanti Sulistyani)

Институт искусств Индонезии, Суракарта, Индонезия

E-mail: hrmillistya@isi-ska.ac.id

Аннотация
Введение: В данной статье рассматривается роль монархии на Яве в устройстве железных дорог в колониальный период. Каким образом правители княжеств (Суракарты и Джокьякарты) оказались вовлечены в процесс и передали свои земли под формирование нового вида транспортной инфраструктуры в XIX веке? **Цель исследования** заключалась в том, чтобы дать оценку влиянию участия монархов в устройстве сети железных дорог в колониальный период, ставшей городским артефактом, на современную городскую морфологию Явы. **Методы**: Понятийный аппарат базируется на теории Альдо Росси о развитии городских артефактов, которая придает особое значение городскому артефакту как основному элементу морфологического и культурного развития города. **Результаты**: Современная городская морфология Явы указывает на влияние монархии на формирование городского ландшафта, а также на то, что некоторые аспекты городской планировки имеют отношение к развитию железных дорог в колониальный период, что придает определенную значимость с точки зрения инженерной составляющей.

Ключевые слова: *Форстенланден (княжеские земли)*, история, инфраструктура, наследие, архитектура.

Civil Engineering

ANALYTICAL DESIGN OF COMPOSITES IN TERMS OF SYSTEMS ANALYSIS

Irina Garkina*, Alexander Danilov

Penza State University of Architecture and Civil Engineering, Penza, Russia

*Corresponding author's e-mail: fmatem@pguas.ru

Abstract

Introduction. The development of composite materials is considered with account for the shifts of paradigms based on the basic models of the continuous self-developing environment towards paradigms based on the models of the structured self-developing environment using the ideas and methods of the system approach and synergetics. The system approach can: reduce or even eliminate the uncertainty inherent to the problem to be solved; reconstruct it in models meeting the objectives of the study; identify objects, properties, and relationships in the system under consideration, taking into account the mutual influence of the external environment. **Methods.** It is shown that the structural organization of the material determines the design of the product or structure and largely determines the functional properties of the entire system. Composite materials are considered as large, complex systems formed based on a modular principle; material properties are determined on the basis of autonomous studies of individual subsystems. **Results**. It is assumed that individual subsystems have a certain degree of autonomy; it is possible to introduce customizable reference models with the simultaneous decentralization of modules by inputs; the conditions for transferring the results of autonomous studies to the system as a whole are determined by the completeness of understanding the processes of the formation of the structure and properties of the system. In the development of composites, the relative importance, the mutual utility of the quality criteria, a reasonable balance between the internal logic of science and its practical significance are taken into account. Partial criteria are analyzed, and a generalized quality criterion for the building material is formalized. The following is considered: the complexity of the object of study (multi-dimensionality, multi-connectedness, incompleteness of diagnostic information), diagnostic interpretation of the analyzed factors, the probabilistic nature of diagnostic information (using methods of both concrete and abstract-logical cognition; each new logical stage continues the previous one and serves as a prerequisite for the previous one).

Keywords: composite materials, complex systems, system approach, systems analysis, mathematical modeling, quality assessment, functionals.

Introduction

There are several dozen definitions of the "system" concept. L. von Bertalanffy (Bertalanffy L. Von., 1973) defined a system as "a complex of interacting elements" or "a set of elements standing in interrelation among themselves and with the environment". In a philosophical dictionary, a system is defined as a set of elements standing in interrelation and interconnection among themselves and forming some coherent unity. V. N. Volkova (Volkova V. N., Denisov A. A., 1997) suggests considering a technical system as "a set of enlarged components, essentially necessary for the existence and functioning of each other":

$$S = \{A, B, C, D\},$$

where A — the set or structure of the goals; B — the set of structures implementing the goals (formulation, technological, production, organizational, etc.); C — the set of technologies implementing the system; D — the conditions for the existence of the system or the factors affecting its creation

and functioning. As can be seen, the definitions of complex technical systems available in the systems theory are applicable to the description of composite building materials. Therefore, it is fair to consider the construction composite as a complex technical system (Korolev E. V., 2020) and apply the optimal control theory and methods of systems analysis to the synthesis of such composites.

Mathematical modeling of the structure and properties of new-generation materials

Materials are presented as systems, which makes it possible to apply the system approach to the full extent in solving problems of their synthesis, identification, management, the use of an information-computing environment, including the conceptual aspects of modeling. When the problems of identification are solved, based on the application of a particular mathematical apparatus and the degree of its development, a preliminary analysis of a priori information is performed. The main efforts are directed at structuring and absolute

formalization. It is assumed that the human has an unconditional priority over the results of the analysis: the construction of fully automatic quality management systems is not considered.

When building materials with controllable structure and properties are developed and their quality is managed, methods of vector optimization are used (lexicographic problem; method of successive concessions; scalarization of quality criteria based on linear convolution and introduction of benchmarks; construction of Pareto sets, etc.). The target function is determined by the required types of the kinetic processes for the formation of the main physical and mechanical characteristics of composites (Figure) based on solving at first the general and then the partial problem of identification (Budylina et al., 2021; Garkina et al., 2017).

Curve 1 (a particular case of curve 2; $x_0 = 0$) represents a solution to the Cauchy problem:

$$\ddot{z} + 2n\dot{z} + \omega_0^2 z = 0; \ z = x - x_m; \ z(0) = -x_m; \dot{z}(0) = x(0)$$

and has the following form:

$$x = c_1 e^{-\lambda_1 t} + c_2 e^{-\lambda_2 t} + x_m \quad (\lambda_1 > \lambda_2).$$

The parametric identification of kinetic processes of this type can be easily carried out by sequentially determining l2, d, l1, $\left(-\dfrac{c_1}{c_2}\right)$, $\dot{x}_0$ (e.g., for epoxy composite, the $\dot{x}_0$ value determines the initial polymerization rate). The identification of a process of parametric type 2 (e.g., heating of epoxy composites during initial structure formation) is carried out in a similar manner:

$$\ddot{z} + 2n\dot{z} + \omega_0^2 = 0, \ (z = x - x_m; \ x = z + x_m);$$

$$z(0) = x_0 - x_m; \ \dot{z}(0) = \dot{x}_0; \ (x(0) = x_0).$$

The determination is based on the known values of λ_1, λ_2, x_m, $\left(-\dfrac{c_1}{c_2}\right)$, x_0.

The possibility of establishing a connection between the composite structure and changes in macroscopic characteristics is taken into account. Considering the complexity of establishing the influence of formulation and technological parameters on the characteristics of materials, a special methodology for controlling the output characteristics of the material is developed, cross-links (synergy) between the material properties are determined, mathematical models of subsystems are specified with the subsequent identification of parameters (for individual systems — based on the conditions for obtaining extrema of target functions).

The use of the Pareto principle and diagrams (where the initial 20% determine the subsequent 80% of the time for the controlled parameter to reach its operating value) proved effective in the quality management of composites: it facilitates formulation development with the allocation of elements that determine the performance characteristics of the material. For instance, for epoxy composites used for radiation protection, strength and density were mainly determined by the degree of filling and type of modifier. An iterative method of improving the quality of the material was also used, based on the sequential construction of corresponding Pareto diagrams at each stage.

Cognitive modeling

Cognitive modeling is one of the ways to study complex weakly structured systems with many contradictory goals and criteria ((Tolman E. C.,1948); structuring, involves formulating and clarifying a hypothesis about the object functioning). At the preliminary stage of studies, most complex systems can be considered as weakly structured. Cognitive modeling is based on a cognitive map (an oriented graph; incomplete, fuzzy and even contradictory information can be used). The vertices of the oriented
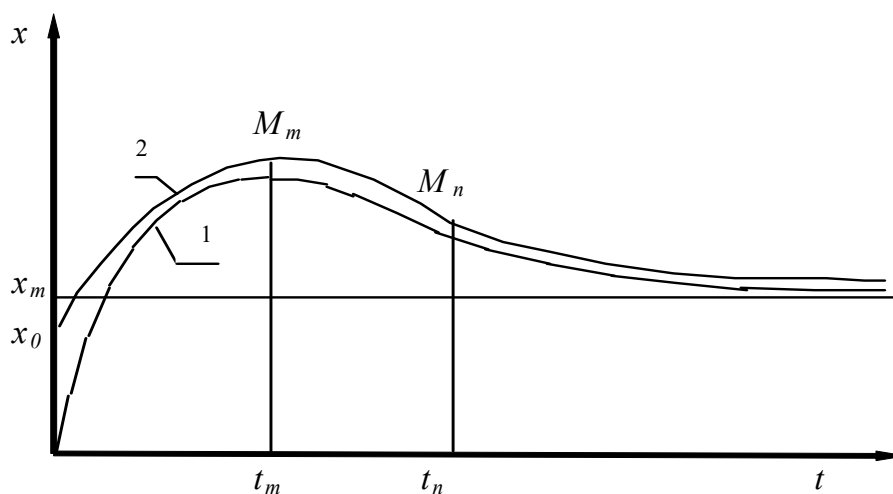
Standard types of kinetic dependences for changes in material stability ("overshoot" phenomenon (Bobryshev A.N. et al., 1994)

graph are the factors (concepts), while its arcs indicate the causal connections between the factors (the weights determine the degrees of influence). Various modifications of models (corresponding to various interpretations of vertices, arcs, and weights) are studied using the formal apparatus. Substantial human participation in the formalization of the primary representations by subject-formal methods does not make it possible to guarantee the reliability of the obtained solutions (e.g., the risk of inadequate application of a formalized model to a specific problem situation due to misunderstanding of the mathematical meaning of structures by specialists in the problem area). It is reasonable to represent the factor in a normal form (a variable on a particular rating scale). In terms of linguistics, the normality of the factor makes it possible to use such verbal contexts as: "more – less", "growth – decline" (it is often difficult even to choose contexts "worse – better" similar in meaning), etc. Cognitive clarity of the "factor" concept as a variable of the required type is necessary. In modeling, the same causal relationships can be represented in a cognitive map with the use of different concepts. The validity of the principle of transitivity of causal concepts (from the fact that A causes B, and B causes C, it follows that A causes C), which is usually assumed, is not true in many cases (false transitivity is possible). As can be seen, a cognitive map reflects subjective ideas about the system functioning and development (the strategic step $S^i \rightarrow S^{i+1}$ means taking the system from the state S^i to the state S^{i+1}). When building a hierarchical structure of quality criteria, as well as a hierarchical structure of the system itself (if possible) with its help, we can further consider the system as a structured one. The target state of the system is considered to be achieved if the assessment of the targeted development of the system, specified in the form of a goal achievement functional, almost does not change.

The system complexity requires: interdisciplinary studies and involvement of specialists competent in various narrow subject areas in the construction of a cognitive map; formalization of the primary representations of a weakly structured problem in the form of a collective cognitive map (to generalize and coordinate different representations). It is possible to solve this problem to some extent with the use of the methods of conceptual structuring, criteria and special technologies for the formation and coordination of collective concepts.

The above approach has been successfully used in the synthesis of radiation protective composite as a complex system, its identification, formation and formalization of goals, a set of alternatives for their achievement, and, finally, multi-criteria optimization (Garkina and Danilov, 2019; Smirnov and Korolev, 2019).

Principal component analysis in quality management of materials used for protection against ionizing radiation

The chemometric approach is based on the use of projective mathematical methods, which make it possible to isolate latent variables in big data and analyze the relationships in a system under consideration. Unfortunately, despite the simplicity and efficiency of such an approach (which is often visual) to the analysis of experimental data, it is almost not used in construction materials science. By using the principal component analysis (PCA), we ranked the quality criteria $q_i, i = \overline{1, p}$ according to the obtained values for n experimental prototypes. The first principal component was defined as the direction of the largest change (scattering along some central axis — a new variable) in the data $\mathbf{q} = \left\| q_{ij} \right\|, i = \overline{1, p}, j = \overline{1, n}$ in the Cartesian coordinate system $Oq_1 q_2 \ldots q_p$ (approximated — purely geometrically; clarified — based on the best linear approximation of all the initial points q_{ij} by the least squares method). The second principal component was assumed (by definition) to be orthogonal to the direction of the first component (along it, the next largest change in the values q_{ij} occurs), and the third component was assumed to be perpendicular to both the first and second components (lying in the direction in which the third largest change in the data occurs). The subsequent principal directions were determined in a similar manner. The resulting system of the principal components provides a set of orthogonal axes, each of which lies in the direction of the maximum change in the data in descending order of these values. Due to the orthogonality of the principal components in the new resulting set, the variables (linear combinations of the initial variables) no longer correlate with each other. The transition from the initial Cartesian coordinate system to the new set of orthogonal axes makes it possible to get rid of the dependence between the criteria. The upper limit of the number of the principal components does not exceed $\max \{n-1, p\}$. The effective dimension of the principal component space is determined by the $\mathbf{q} = \left\| q_{ij} \right\|$ matrix rank. The last principal component lies in the direction in which the difference between the prototypes will be minimal (in fact, it is impossible to distinguish the prototypes here, since all these differences are just random noise). The principal components with large numbers were considered as directions in which the principal component is noise. Thus, the PCA made it possible to decompose the initial data matrix into a structural part (several first principal components lying in the directions of maximum changes) and noise (directions in which the difference between the positions of the points is small and can be neglected)

(Danilov et al., 2009). Each of the properties (quality criteria) is an integral characteristic of the material, depending on the properties of the components, composition, preparation conditions, curing, etc. The assessment of the composite quality is made by the set of both dependent and contradictory criteria (chemical resistance, frost and heat resistance, impact and abrasion resistance, radiation heating, adhesion properties, protective properties in relation to the steel reinforcement, etc.). With the help of the PCA, a set of linear combinations of the initial criteria (practically independent) was distinguished, which subsequently, using methods of experimental design and multi-criteria optimization, made it possible to develop radiation protection and corrosion-resistant materials. Dimensionality reduction (separation of the initial data into the substantial part and noise) within the principal component analysis is achieved by neglecting the directions corresponding to small eigenvalues. There are no common rules for choosing the number of significant principal components (determined by the eigenvalues of the covariance matrix, the research tasks (visualization on the plane or in space), the intuition of the researcher, etc.).

Among the priority criteria were the following: strength, density, and porosity of the material. The dependences of porosity $q_1(x_1, x_2)$, %, compressive strength $q_2(x_1, x_2)$, MPa, and density $q_3(x_1, x_2)$, kg/m3, obtained by methods of mathematical experimental design, on the encoded volume fractions of the aggregate (lead pellets with a diameter of 4–5 mm) $x_1 \in [0,5;0,6]$ and filler (barite, $S_{sp} = 250$ m²/kg) $x_2 \in [0,35;0,4]$ were used:

$$q_1(x_1, x_2) = 5.18 + 3.44x_1 + 0.96x_2 - 1.33x_1x_2 + 3.83x_1^2;$$

$$q_2(x_1, x_2) = 22.5 - 3.72x_1 + 1.43x_2 - 2.87x_1^2;$$

$$q_3(x_1, x_2) = 7143 - 147x_1 - 181.7x_1^2.$$

The covariance matrix obtained based on the experimental values ξ_{ui} of the listed indicators has the following form:

$$C = \frac{1}{N-1}(\xi_{ui})^T(\xi_{ui}) = \begin{pmatrix} 0.169 & 0.023 & -1.35 \\ 0.023 & 0.220 & 0.149 \\ -1.35 & 0.149 & 21.5 \end{pmatrix}.$$

The eigenvalues λi and eigenvectors $\mathbf{v}i$ of the covariance matrix:

$$\lambda_1 = 0.226, \ \mathbf{v}_1 = (0.221; 0.975; 0);$$

$$\lambda_2 = 0.077, \ \mathbf{v}_2 = (0.973; -0.221; 0.063);$$

$$\lambda_3 = 21.6, \ \mathbf{v}_3 = (-0.063; 0; 0.998).$$

The matrix of transition to the principal components G_1, G_2, G_3 has the following form:

$$L = \begin{pmatrix} -0.063 & 0 & 0.998 \\ 0.221 & 0.975 & 0 \\ 0.973 & -0.021 & 0.063 \end{pmatrix}.$$

The principal components are linearly related to the initial indicators q_1, q_2, q_3:

$$G_1 = -0.063q_1 + 0.990q_3;$$

$$G_2 = 0.221q_1 - 0.975q_2;$$

$$G_3 = 0.973q_1 - 0.021q_2 + 0.063q_3.$$

By virtue of $\lambda_3 >> \lambda_1$ and $\lambda_3 >> \lambda_2$, the significant principal component is unique and corresponds to the principal direction $\mathbf{v}_3$; the vector of the first principal direction forms a small angle with the axis of the third principal variable. The dominant indicator is the average density (the third indicator).

Industrial applications of system methodologies, system identification and control theory

The relevance of the studies is conditioned by the need to ensure the environmental safety of nuclear power facilities, extremely hazardous chemical production facilities, bases, and arsenals; bunkers, burial sites, and storage facilities for low-level radioactive waste, etc. The prerequisites in the synthesis include the principle of 100 % mathematics efficiency, the hierarchy of quality criteria, and the hierarchical structure of the radiation protection composite material, developed with account for the following:

- the paradox of integrity (a holistic description of a system is possible only when it is "holistically" broken down into parts; when a given system is described as some unity; cognition of a system as a unity is impossible without analysis of its parts);

- the paradox of hierarchy (description of a system is possible only if it is described as an element of a supersystem (a broader system) and vice versa, description of a system as an element of a supersystem is possible only if there is a description of this system (subsystems are systems for their subsystems; each system is part of some supersystem)); in the synthesis of building material (system), the supersystem is represented by building materials suitable for use in the given operating conditions;

- system-forming properties (integrative; formed with the coordinated interaction of the elements combined in a structure, which the elements did not possess before) (Chernyshov and Makeev, 2022; Selyaev et al. 2016).

Based on the classification of the main kinetic processes for the formation of the structure and properties of special-purpose composite materials (radiation resistance coefficient, linear coefficient of gamma-radiation attenuation, strength gain, change in the elastic modulus, contraction and shrinkage, increase in internal stresses, heat emission, chemical resistance, water absorption, water resistance, etc.), their generalized model is built in a class of ordinary differential equations with constant coefficients up to the fourth order inclusive.

Each of the kinetic processes is a special case of the generalized model and can be represented as a solution to the Cauchy problem:

$$z^{(4)} + a_1 z^{(3)} + a_2 z^{(2)} + a_3 z^{(1)} + a_4 z = 0;$$

$$z = x - x_m; \; x(0) = x_0, \; \dot{x}(0) = \dot{x}_0, \; \ddot{x}(0) = \ddot{x}_0, \; \dddot{x}(0) = \dddot{x}_0;$$

$x_0, \; \dot{x}_0, \ddot{x}_0, \dddot{x}_0$ are determined by the required type of kinetic process and given operating value x_m of the material characteristic under study (aperiodicity of the processes is assumed; sufficient conditions are specified). The parametric identification, formalized quality assessment, and one-dimensional optimization of each of the kinetic processes are carried out (functionals of the form $\Phi(S) = f \lambda_m + a \dfrac{1}{\lambda_m} + b\,r + c \dfrac{1}{r}$ are used, which allow for considering the formation of the composite structure and properties in time;

$$\lambda_m = \min_i \{\lambda_i\}, \; r = \max_i \left\{ \frac{\lambda_i}{\lambda_m} \right\}; \; k_i = -\lambda_i \text{ — the roots}$$

of the characteristic polynomial, $\lambda_i > 0, \; i = \overline{1, \; n}$). The multi-criteria synthesis of radiation protection composite is carried out using vector optimization methods (solution of the lexicographic problem, narrowing of the search area by the method of successive concessions, scalarization by introduction of metrics in the space of target functions (strength, porosity, density), construction of Pareto sets) (Smirnov and Korolev, 2019).

Portable implementation of an image processing language

Tools and methods of digital image processing are currently used in various fields. In construction materials science, these applications are used in the study of the material structure: when determining the distribution of the structural objects under study (air cavities, particles of dispersed aggregates, etc.), determining the fractal dimensionality of cracks, hardness, etc. Each of these methods involves several stages, where the discretization of the continuous color-brightness field and the transformation of the resulting image are mandatory. Discretization is carried out by the hardware of a receiving device. The resulting two-dimensional array of chromatic coordinates serves as the input data, and it is also a result of most operations. There are software environments available that make it possible to perform matrix calculations. Many of them are driven by high-level languages (being in fact *interpreters* from those languages). The standard is the MATLAB package with its features available through tool chains including one intended for image processing. In particular, the tools make it possible to perform the two-dimensional Fourier transform and calculate convolution. However, no functions of image processing in different color spaces are implemented. The image processing tools are also contained in software packages for working with raster graphics. For example, GIMP has advanced tools for switching between color spaces, performing statistical analysis, calculating convolution in the spatial domain, and working in batch mode (the input language is a superset of LISP). However, most packages use single-byte integer values for internal data representation, which leads to loss of information.

To describe image processing tasks, we suggest a specialized image processing language — the IPL language. In the IPL-interpreter implementation, the following requirements are taken into account: support for batch mode, use of floating point values for internal representation, support for tools of convolution in the inverse length domain. The emphasis is on openness (understood as the capability to maintain and extend features) as well as portability between heterogeneous computing platforms (WinAPI and POSIX).

The fundamental language types are vector, matrix and binary decomposition. In the structure of the interpreter, two levels are distinguished: application and service ones (implemented in ANSIC). The first one encapsulates parsing and basic processing algorithms. The second one involves the implementation of abstract types of data and objects that isolate system calls to the target platform.

The functionality of the proposed language and the operation of the interpreter were tested when solving a number of applied problems: assessment (calculation of scalar criteria) of the quality of protective-decorative coatings, recognition of features in the spatial domain and inverse length domain, comparison of digital filtering means (Gusev et al., 2018).

Analytical methods for the synthesis of materials: experience in application

Based on the experience of developing and managing the quality of special-purpose materials, we determined the approach and methodological principles of creating materials using the methods of systems analysis and modeling of kinetic processes. First, the material is considered as a weakly structured multi-purpose system. As a result of interdisciplinary studies (incomplete, fuzzy and even contradictory information is used), the interaction of the basic relationships existing in the system that determine its functioning is formalized. Hierarchical structures of quality criteria and the system itself are built using a cognitive map (including a collective map), which makes it possible to view the system as already structured. During the qualitative assessment of material properties and determination of relationships between them, methods of rank correlation were used (in particular, stress-strain properties (14 indicators were taken into account) and the relationships between them were studied for 10 types of epoxy composites)

29

(Garkina and Danilov, 2018). It was shown that some properties (e.g., compressive strength or hardness) do not need to be determined due to the availability of significant relationships between them. Based on the statistical significance of the sample value of the concordance coefficient, the lack of consistency within the entire set of indicators was shown in the presence of pairwise consistency between some of the indicators. Considering the compressive strength as a resultant variable, the problem of regression on ordinal variables was solved.

The kinetic processes (in particular, the residual strength by years of operation) were considered as time series, and autoregressive models with a moving average were developed:

$$x_t = a_1\, x_{t-1} + \ldots + a_p\, x_{t-p} + b_0 e_t + b_1\, e_{t-1} + \ldots + b_q\, e_{t-q}.$$

The Markov, Yule, and Yule–Walker processes were considered. The Levinson–Durbin algorithm was used to determine the model coefficients. The formalization of processes for the formation of physical and mechanical characteristics of the material was carried out as a solution of the general identification problem in the class of ordinary differential equations (for radiation protective composites — not higher than the fourth order); the parametric identification of kinetic processes was performed. In the optimization of formulation and technological parameters and material quality management, the problem of multi-criteria optimization with the preliminary minimization of the dimensionality of the criteria space was solved. The Pareto principle, diagram and sets were used (the analytical dependences of properties on the points of the factor space were determined in advance by methods of experimental design; nonlinear programming methods were used). The multi-criteria optimization under contradictory criteria was performed using the method of sequential concessions; methods of criteria scalarization based on the results of solving single-criterion problems (as benchmarks) were considered.

The effectiveness and prospectivity of using the proposed methods are confirmed by the results of the multi-criteria synthesis of radiation protective materials (Budylina et al., 2021; Garkina et al., 2017; Korolev and Smirnov, 2013).

Conclusions

1. The methods for mathematical modeling of the structure and properties of new-generation materials were developed based on cognitive modeling.

2. The partial criteria and the formation of a generalized criterion for the quality of the material with a hierarchical structure were proposed.

3. The effectiveness of using the principal component analysis to minimize the dimensionality of the criteria space and manage quality was shown by the example of materials with special properties.

4. The specialized image processing language was proposed (IPL) for solving a number of applied problems (calculation of scalar criteria; assessment of the quality of protective-decorative coatings).

The common approach to industrial applications of system methodologies, system identification and control theory was presented.

References

Bertalanffy, L. Von. (1973). General System Theory (Foundations, Development, Application) *N.Y.: G.Brazillier*, 295 p.

Bobryshev, A.N. et al. (1994). Synergetics of composite materials. *Lipetsk: NPO ORIUS*, 152 p.

Budylina, E., Garkina, I., and Danilov, A. (2021). Approximation of functions in multi-criterial synthesis of composite materials. *IOP Conference Series: Materials Science and Engineering*, Vol. 1203, 022010. DOI: 10.1088/1757-899X/1203/2/022010.

Chernyshov, E. M. and Makeev, A. I. (2022). Problem of complexity, system qualitative description and statistical reliability of the building characteristics composites. *Expert: Theory and Practice*, No. 2 (17), pp. 75–80. DOI: 10.51608/26867818_2022_2_75.

Danilov, A. M., Loganina, V. I., and Smirnov, V. A. (2009). Principal component analysis: evaluation of the quality of coatings. *Regional Architecture and Engineering*, No. 1, pp. 31–32.

Garkina, I, and Danilov, A. (2018). Experience of Development of epoxy composites: Appendix of methods of rank correlation. *Key Engineering Materials*, Vol. 777, pp. 8–12. DOI: 10.4028/www.scientific.net/KEM.777.8.

Garkina, I. and Danilov, A. (2019). Composite materials: identification, control, synthesis. *IOP Conference Series: Materials Science and Engineering*, Vol. 471, Issue 3, 032005. DOI: 10.1088/1757-899X/471/3/032005.

Garkina, I., Danilov, A., and Skachkov, Yu. (2017). Modeling of building materials as complex systems. *Key Engineering Materials*, Vol. 730, pp. 412–417. DOI: 10.4028/www.scientific.net/KEM.730.412.

Gusev, B. V., Korolev, E. V., and Grishina, A. N. (2018). Models of polydisperse systems: evaluation criteria and analysis of performance indicators. *Industrial and Civil Engineering*, No. 8, pp. 31–39.

Korolev, E. V. (2020). Prospects for the development of construction materials science. *Academia. Architecture and Construction*, No. 3, pp. 143–159. DOI: 10.22337/2077-9038-2020-3-143-159.

Korolev, E. V. and Smirnov, V. A. (2013). Using particle systems to model the building materials. *Advanced Materials Research*, Vol. 746, pp. 277–280. DOI: 10.4028/www.scientific.net/AMR.746.277.

Selyaev, V. P., Selyaev, P. V., and Kechutkina, E. L. (2016). Evolution of the theory of concrete strength. From simple to complex. *Construction Materials*, No. 12, pp. 70–79.

Smirnov, V. A. and Korolev, E. V. (2019). Building materials as disperse systems: multiscale modeling with dedicated software. *Construction Materials*, No. 1–2, pp. 43–53. DOI: 10.31659/0585-430X-2019-767-1-2-43-53.

Tolman, E. C. (1948). Cognitive maps in rats and men. *Psychological Review, 55*(4), 189–208. DOI:10.1037/h0061626

Volkova, V.N., Denisov, A.A. (1997). Fundamentals of systems theory and system analysis. *St. Petersburg: St.PSTU*, 510 p.

АНАЛИТИЧЕСКОЕ КОНСТРУИРОВАНИЕ КОМПОЗИТОВ С ПОЗИЦИЙ СИСТЕМНОГО АНАЛИЗА

Гарькина Ирина Александровна*, Данилов Александр Максимович

[1]Пензенский государственный университет архитектуры и строительства,
г. Пенза, Россия

*E-mail: fmatem@pguas.ru

Аннотация
Введение. Разработка композиционных материалов рассматривается с учетом смены парадигм, основанных на базовых моделях непрерывной саморазвивающейся среды, в сторону парадигм, основанных на моделях структурированной саморазвивающейся среды на идеях и методах системного подхода и синергетики. Системный подход может уменьшить или даже устранить неопределенность, присущую решаемой задаче; реконструировать ее в моделях, отвечающих задачам исследования; выявлять объекты, свойства и отношения исследуемой системы с учетом взаимного влияния внешней среды. **Методы.** Показано, что структурная организация материала определяет исполнение изделия или конструкции и во многом определяет функциональные свойства всей системы. Композитные материалы рассматриваются как большие сложные системы, образованные по модульному принципу; свойства материалов определяются на основе автономных исследований отдельных подсистем. **Результаты.** Предполагается, что отдельные подсистемы обладают определенной степенью автономии; возможно внедрение пользовательских эталонных моделей с одновременной децентрализацией модулей по входам; условия переноса результатов автономных исследований на систему в целом определяются полнотой понимания процессов формирования структуры и свойств системы. При разработке композитов учитываются относительная важность, взаимная полезность критериев качества, разумный баланс между внутренней логикой науки и ее практическая значимость. Анализируются частные критерии, и формализуется обобщенный критерий качества строительного материала. Учитывается сложность объекта исследования (многомерность, многосвязность, неполнота диагностической информации), диагностическая интерпретация анализируемых факторов, вероятностный характер диагностической информации (использование методов как конкретного, так и абстрактно-логического познания; каждый новый логический этап продолжает предыдущий и служит исходной предпосылкой для предыдущего).

Ключевые слова: композиционные материалы, сложные системы, системный подход, системный анализ, математическое моделирование, оценка качества, функционалы.

CALCULATION AND TESTING OF A REINFORCED CONICAL BRIDGE BEAM

Assylkhan Jalairov[1], Dauren Kumar[2]*, Nurzhan Dosaev[3], Gulzhan Nuruldaeva[4],
Khaini-Kamal Kassymkanova[4], Gulshat Murzalina[4]

[1]Department of Transport Construction, Bridges and Tunnels,
International University of Transportation and Humanities, Almaty, Republic of Kazakhstan

[2]Department of Cartography and Geoinformatics, Al-Farabi Kazakh National University,
Almaty, Republic of Kazakhstan

[3]Department of Science and Introduction of New Technologies,
National Center for Quality of Road Assets, Astana, Republic of Kazakhstan

[4]Satbayev University, Almaty, Republic of Kazakhstan

*Corresponding author's e-mail: daurendkb@gmail.com

Abstract
Introduction: The paper addresses the compliance of the actual strength and deformation properties of the standard precast block (hereinafter — UPB 185.25) with the design data. **Purpose of the study**: We aimed to check convergence of the experimental data for a reinforced concrete beam with variable outline of the bottom chord with the design assumptions. **Methods:** In the course of the study, the moments of inertia at each section of the unit were taken averaged, in steps. Each section was calculated separately. The results were then summed up. In addition, the calculated values were verified using the finite element method in MIDAS. **Results:** The adopted design assumptions based on the test results showed high convergence of the results and confirmed the compliance of the beam in terms of stiffness, crack resistance, and strength. The control crack opening width a_{cr} = 0.2 mm was achieved at a load of 503.2 kg, which is 22.7 % higher than the design load.

Keywords: beam deflection, control loads, crack resistance, graph-analytic method, UPB 185, FEM analysis.

Introduction

Beams of variable cross-section, characterized by variable geometric and physical parameters, have a number of particular features as compared to beams of constant cross-section. Specifically, reinforced concrete bridge beams ensure the architectural expressiveness of the assembled superstructure, are characterized by lower weight, and involve bench assembly in the manufacture of units without prestressed reinforcement. The latter makes it possible to simplify the manufacturing technology due to the lack of special channels for the use of high-strength reinforcement ropes, and the injection of specially selected solutions for grouting these channels. Processes for anchoring high-strength reinforcement ropes with subsequent prestressing of bridge beams were discussed, in particular, in papers by Jalairov et al. (2022a, 2022b). Besides, the joints of beams of variable cross-section require high-quality filling with cast-in-situ concrete, ensuring tight jointing and adhesion of cast-in-situ and precast concrete.

The design of beams of variable cross-section was earlier studied by Timoshenko (1965), Smirnov (1961), and Ruditsyn — using the method of breaking loads (Ruditsyn, 1940).

The variety of shapes and sections of such heterogenous beams poses the problem of determining their characteristics by various methods. For instance, in the works of the Russian researchers Gusev and Saurin (2017, 2018), the vibrations of heterogeneous beams and variational approaches to finding the eigen frequencies of such beams were described in detail following the analysis of publications based on materials from foreign press. The classical variational formulations, the method of integro-differential relations, energy estimates of the quality of the solution, a family of variational formulations, and a connection with classical variational principles were presented. It was shown that the proposed two-sided quality criteria for an approximate solution make it possible to obtain high-precision solutions for mathematical models of conventional concrete beams of small size.

The minimization of the weight of thin curved beams, the stress state of which is described by the Saint–Venant theory, was considered by Petukhov (1980). The effect of the cross-sectional shape on

the stress state was studied. It was assumed that each point of the beam must satisfy some condition for the strength of the material, and the optimal design of the conical beams must satisfy the critical load in bending (Wang et al., 1986). The cantilever and hinged beams were considered under the action of a uniformly distributed and concentrated load. The solution to the problem was achieved by two independent approaches: 1) using the energy method of Timoshenko; 2) using the Lagrange multiplier and the gradient expression of the problem.

Balduzzi et al. (2016) presented equations of compatibility, equilibrium and governing equations, including those for conical beams. It was shown that the shear distribution depends not only on the resultant vertical stress but also on the horizontal resultant stress and bending moment. The complex geometry of non-prismatic beams leads to the fact that each generalized deformation depends on all generalized stresses, in contrast to prismatic beams.

The spline method for the numerical calculation of the natural vibration frequency of a beam with a variable cross-section was also discussed by researchers (Cazzani et al., 2016; Zhernakov et al., 2017). The second order of convergence makes it possible to increase the calculation accuracy with almost six significant digits for the first ten forms of natural frequencies of beams with an exponentially changing width of a rectangular section.

Barham and Idris (2021) described the large increment method for the nonlinear analysis of Timoshenko beam structures. The essence of the method is to separate the linear equations of global equilibrium and compatibility from local nonlinear equations. This makes it possible to reduce errors in the step-by-step solution of nonlinear structural problems, which is typical for the finite element method (FEM). The final Timoshenko beam version formulated for solving beam structures with a rectangular and wide flange section, based on two numerical examples, showed a more accurate result with less computational algorithms.

A solution of Timoshenko–Ehrenfest beam problems using the theory of functional connections was given by Yassopoulos et al. (2021). This method is an alternative one, and under certain boundary conditions, in comparison with the finite element method, the design prerequisites of the theory of functional relationships may not work. But when solving some problems, the application of the theory of functional relationships allows you to quickly solve differential equations in comparison with FEM.

An analytical solution for the flat behavior of conical monosymmetric I-beams was considered by Chockalingam et al. (2020, 2021). An analytical formulation of the Timoshenko beam was proposed, which included the relationship of axial bending in basic differential equations. This approach allows

us to consider a cone-shaped I-beam with a monosymmetric section as a straight line segment along the central line of the wall. This solution can be used within the FEM to design an accurate one-dimensional tapered beam element.

An analysis of the shear characteristics of a reinforced concrete conical beam with corrugated steel inclusions in the wall was presented by Zhou et al. (2019a, 2019b, 2021). It was shown that in conical beams, the lateral force near the supports is perceived not only by trapezoidal corrugated steel walls, as in the case of prismatic beams, but also by reinforced concrete walls. These theoretical assumptions are confirmed with experimental results and FEM calculations.

Zhong et al. (2021) presented an experimental and numerical analysis of crack propagation in reinforced concrete structures on a three-phase concrete model. In reinforced concrete structures, including conical beams, the Weibull distribution model can be used to describe microcracks in concrete. To study the behavior of cracks in the structure, a numerical program written in the parametric design language ANSYS and the tool control language was used. The simulation results showed good agreement with the experimental data.

Tayfur et al. (2021) presented an approach to determining the crack resistance of non-prismatic reinforced concrete beams based on the elastic and plastic behavior of reinforced concrete under static load. Two non-prismatic beams with hinged supports were tested with the construction of the deformation diagrams of reinforced concrete.

Resan and Zamel (2021a, 2021b) provided results of bending tests involving models of T-shaped reinforced concrete beams. As a way of control, the behavior of a prismatic beam was analyzed. The T-shaped beams differed in the height of the ribs in the longitudinal direction at the ends and middle of the beam, as well as the ribs in the transverse direction. The results generally confirm the effectiveness of T-beams in terms of material consumption with a single concrete strength and percentage of reinforcement.

From the analysis of the above sources, it follows that a significant number of works cover various methods for finding the modes and frequencies of vibrations of non-prismatic beams. There are also laboratory studies to clarify the strength and deformation characteristics and the process of cracking of such beams. However, there is very little information on the testing of full-scale reinforced concrete beams and their simplified calculation. In this paper, as an object of research, the results of tests of a conical reinforced concrete bridge beam and the beam calculation according to the standards of the Republic of Kazakhstan are considered.

The research was aimed at identifying the compliance of the calculated positions of the beam by the method of strength of materials and finite elements of the real operation of the beam under load.

The novelty of the research presented in this paper consists in proving the convergence of the design and experimental data in the calculation of the variable section of the beam with ledges, assuming an elastic stage of behavior.

Materials and Methods

Preparation for beam testing

Fig. 1 shows the front and cross-sections of the UPB 185.25 unit at its ends. The unit height in the support area is 2087 mm, and at the opposite end — 515 mm. The unit length is 18.5 m. Table 1 presents data on the

dimensions of the UPB 185.25 unit along its length. The unit reinforcement with rods was earlier considered by Shalkarov et al. (2018).

The compressive strength class of concrete in the UPB 185.25 unit was taken as B35. The volume of concrete in the beam was 8.77 m³. The concrete unit was at the age of 54 days as of the time of testing.

Rods with a diameter of 32 and 36 mm, class A400 (A-III), grade 25Mn2Si in accordance with GOST 5781-82 (SP RK 3.03-112-2013) were used as main longitudinal reinforcement in the upper and lower chords of the unit. In the support area of the unit, bends were installed from rebars with a diameter of 28 mm, class A400 (A-III), grade 25Mn2Si in accordance with GOST 5781-82. Reinforcement consumption in the beam was
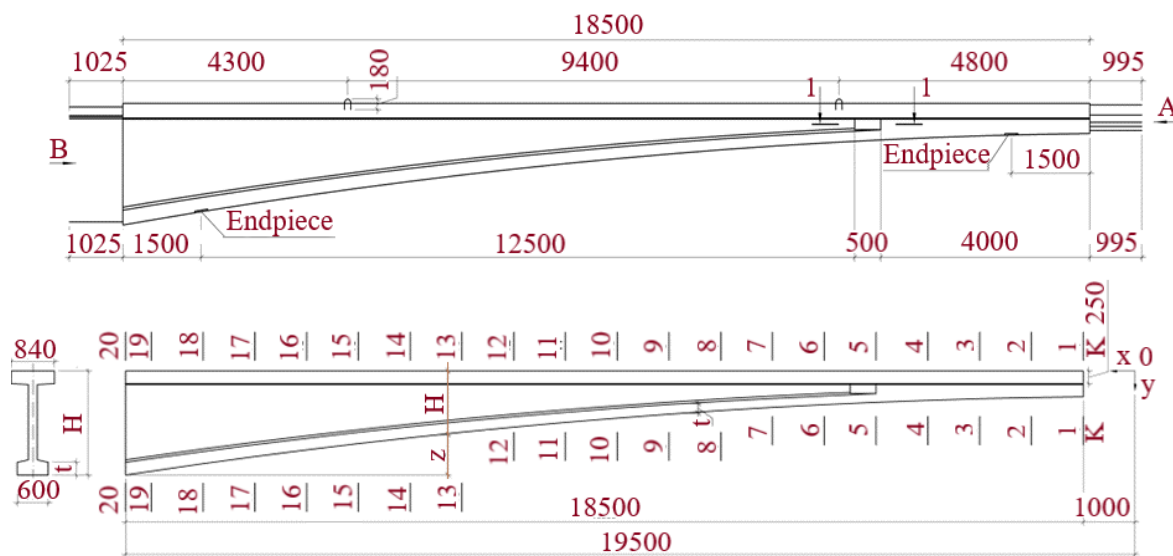
$$H = 0.507 + 0.003952(x+1)x, \text{ m}; \quad z = 2.087 - H, \text{ m}; \quad t = 0.138 + 0.006x, \text{ m}.$$

(a) Front
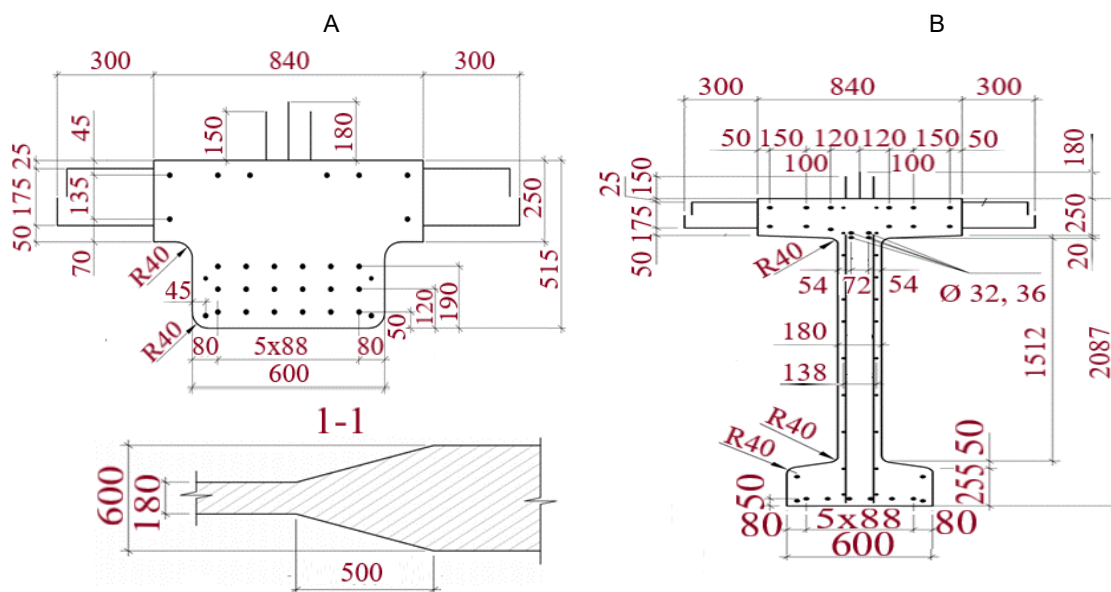
Fig. 1. Front and cross-sections of the UPB 185.25 unit

Table 1. **Data on the dimensions of the UPB 185.25 unit along its length**

Section No.	20	19	18	17	16	15	14	13	12	11	10	9	8	7	6	5	4	3	2	1	0
x, mm	19,500	19,000	18,000	17,000	16,000	15,000	14,000	13,000	12,000	11,000	10,000	9000	8000	7000	6000	5000	4000	3000	2000	1000	0
H, mm	2087	2009	1859	1716	1582	1455	1337	1226	1123	1029	942	863	791	728	643	626	586	554	531	515	507
z, mm	0	78	228	371	505	632	750	861	964	1058	1145	1224	1296	1359	1414	1461	1501	1553	1556	1572	1580
t, mm	255	252	246	240	234	228	222	216	210	204	198	192	186	180	174	168					

as follows: class A-III — 563 kg/m³, class A-I — 8.6 kg/m³. The weight of the embedded parts was 142.5 kg, and the total weight of the beam, taking into account the reinforcement, was 25.15 t.

As a rule, the diagrams of bending moments show that their greatest values can be found in the places where the blocks are joined together on intermediate supports and in the middle of the middle span structures (Smirnov, 1961). Accordingly, in the sections of the UPB 185.25 unit, between sections 20-20 and 19-19 and between sections 2-2 and 1-1 (see Fig. 2), a diagram of bending moments with different signs should be obtained in tests. Control loading tests are recommended to be carried out according to the schemes provided in the design documentation. Table 2 shows the geometric characteristics of the beam.

The creation of such a test scheme would require the development of a special power bench and significant tangible costs. In this regard, by
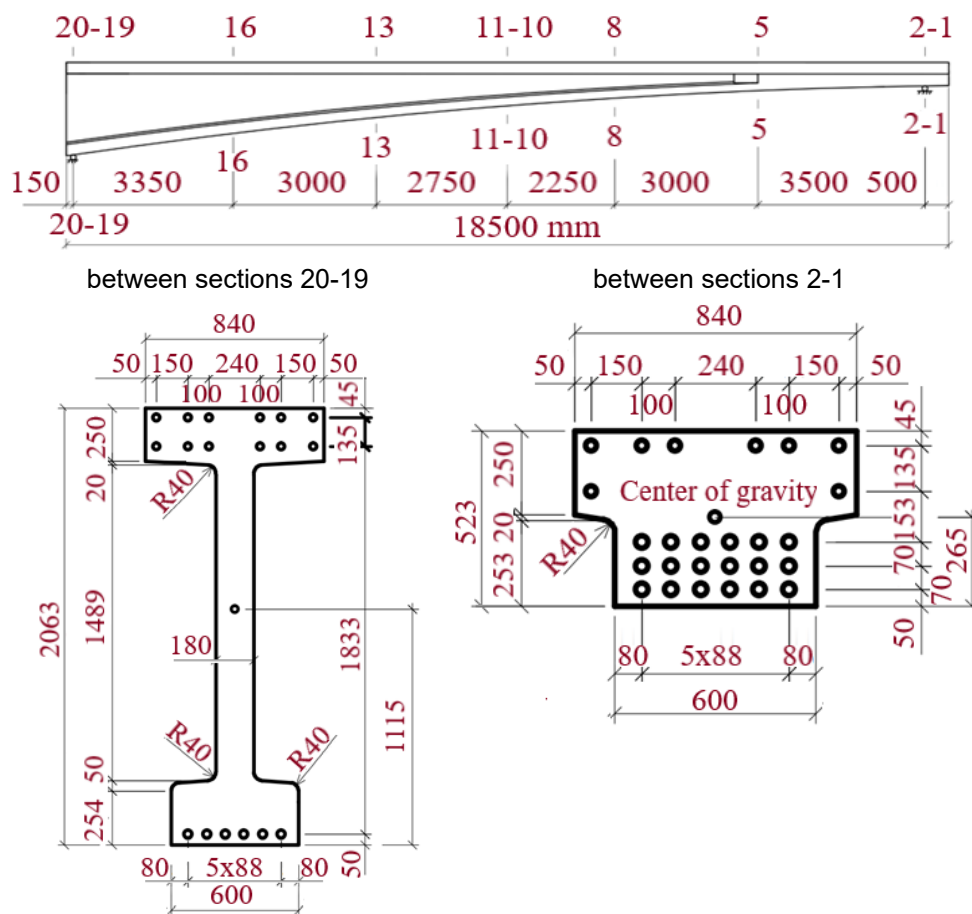
Fig. 2. Diagram of the UPB 185.25 unit, cross-sections and geometric characteristics of the unit

agreement with the design organization, another test scheme for the unit was adopted, which also makes it possible to assess its operational reliability. The process of preparing the unit for testing is shown in Fig. 3a.

The design model of the unit adopted for testing represented a freely supported single-span beam loaded in the middle of the span with a concentrated force P. In accordance with this design model, control loads were also determined in terms of strength, stiffness and crack resistance (see Fig. 3b).

To create and control the load when testing the UPB 185.25 unit, a power installation was used, which included two hydraulic jacks with a load capacity of 500 kN each, a pressure gauge, high-pressure hoses, and an electric pumping station.

The design length of the UPB 185.25 prototype was 17.85 m, and the axes of the supporting parts were located at a distance of 0.15 m from the elevated end of the unit, and 0.5 m from the lowered end. The test scheme of the UPB 185.25 unit corresponded to the design diagram shown in Fig. 2. Fig. 3c shows mechanical devices — deflectometers installed on the unit, which had a scale division of 0.1 mm, and the deflectometers under load P, which had a scale division of 0.01 mm. The test took into account the weight of the loading devices, which was 5.65 kN.

To load the unit, a power bench design was developed, which made it possible to transfer the load to the test specimen. As a counterweight, an anchor was made of cast-in-situ reinforced concrete with its anchoring in rocky ground. The length and number of the anchors embedded in rocky ground were selected in such a way that they could withstand the maximum load created by two hydraulic jacks.

During the tests, the deflections of the unit in the considered middle section under the jacks were determined, at a distance of 2.75 m and 2.25 m in each direction from the considered section and at a distance of 3.35 m and 3.50 m from the axes of the unit support. The settlement of the supports was also monitored using dial indicators with a scale division of 0.01 mm. Crack opening was determined using a Brinell microscope with a scale of 0.05 mm (Fig. 3c).

The load was applied to the unit in stages. After each stage of loading, readings were taken from deflectometers and indicators. Based on the test results, the stiffness, crack resistance and strength of the experimental structure were evaluated. The process of preparing the unit for testing is shown in Fig. 3a.

According to Table 40 of Regulations SP RK 3.03-112-2013 (Committee for Construction, Housing and Communal Services and Land Management of the Ministry of National Economy of the Republic of Kazakhstan, 2015), the category of crack resistance requirements for the UPB 185.25 unit is 3c, allowing cracking under the action of standard loads.

Control load for strength, crack resistance and stiffness testing

Control load for strength testing

The control load for strength testing is determined in accordance with the provisions set out in SP RK 3.03-112-2013 and GOST 8829-94 (Gosstroy of Russia, 1998).

Hereinafter, the calculations of the geometric characteristics and the calculated values are omitted, and only the resulting values are given.

The test load P_{test} is taken to be 682 kN.

According to clause B.1 of Appendix B (GOST 8829-94), the value of the control load Pc for testing the strength of the UPB 185.25 unit is determined by multiplying the value of the test load P_{test} corresponding to the bearing capacity of the unit, determined by calculation taking into account the design resistance of concrete and reinforcement and the adopted loading diagram in Fig. 4, by the safety factor C.

The value of the safety factor C for the 1st case of failure along the normal section due to reaching the yield point in longitudinal tensile reinforcement is determined according to Table B.1 of Appendix B (GOST 8829-94). For A400 class reinforcement, the safety factor C is assumed to be C = 1.3. Taking into account the adopted safety factor, the control breaking strength load is taken equal to:

$$P_k = C \cdot P_{test} = 1,3 \cdot 682 = 887 \text{ kN.} \qquad (1)$$

Control load for crack resistance testing

According to Table 40 of Regulations SP RK 3.03-112-2013, in beams with non-tensioned reinforcement to which the category of crack resistance requirements 3c applies, under the action of standard loads, crack opening normal to the longitudinal axis of the element with a width of up to 0.3 mm is allowed. Taking into account the safety factor C = 0.7 and the correction factor (Section B.12 of SP RK 3.03-112-2013), the revised control crack opening width is taken to be $a_{cr} = 0.2$ mm.

In the Technical Regulations of the Republic of Kazakhstan "Safety requirements for buildings and structures, building materials and products" (Government of the Republic of Kazakhstan, 2010),

Table 2. **Geometric characteristics of the beam**
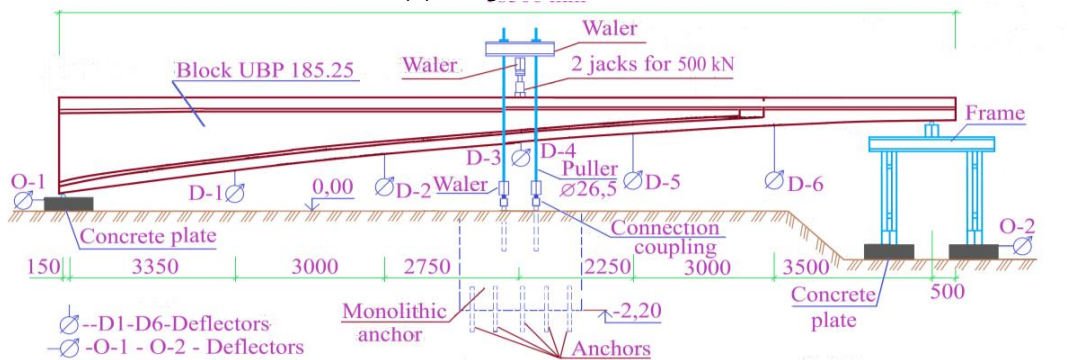
Cross-sectional area, A_{red}	$7415.1 \cdot 10^2$ cm^2
Distance from the bottom of the unit to the center of gravity of the section, U_{bot}	1115 cm
Inertia moment of the section, I_{red}	$43,118,818 \cdot 10^4$ cm^4

(a) the process of preparing the unit for testing

(b) design test scheme

(c) power bench for the placement of mechanical devices

Fig. 3. Test scheme of the UPB 185.25 unit

it is noted that building structures can be designed and manufactured according to other regulatory documents, provided that their requirements are not lower than the requirements specified in the regulatory documents of the national level. The calculation of the control load for crack resistance testing is carried out according to the Regulations of the Russian Federation (SP 63.13330.2018 "Concrete and reinforced concrete structures"), in which the crack opening width is limited to 0.3 mm as in SP RK 3.03-112-2013.

The control load for crack resistance testing according to the calculation is taken equal to $P_c = 410$ kN at the control crack opening width $a_{cr} = 0.2$ mm.

Control load for stiffness testing

The control load for stiffness testing of the UPB 185.25 unit is determined from the condition for assessing the state of the unit at the moment preceding the crack formation in the lower fiber of the concrete unit and is taken equal to $P_c = 178$ kN.

To determine the control deflection of the UPB 185.25 unit in the middle of its span from the action of the control load $P_c = 178$ kN, we use the graph-analytical method (Smirnov, 1961), which makes it possible to determine displacements in beams of variable cross-section, assuming that at this stage of testing, the unit behaves practically in elastic stages.

Fig. 4a shows a design diagram of the unit loaded with the concentrated force P, which in our case is a control load for stiffness. In Fig. 4b, a diagram of bending moments M is shown, where in the considered sections 2 ÷ 6 their values are given in general form from the action of the control load for stiffness.

a) unit loaded with the concentrated force P

b) bending moments M

c) the averaged values of the moments of inertia in unit sections 2-3, 3-4, 4-5, 5-6, and 6-7 in fractions of the value I_0

d) separate areas in the center of gravity of which weights W_i are applied

e) the effect of fictitious loads W_i
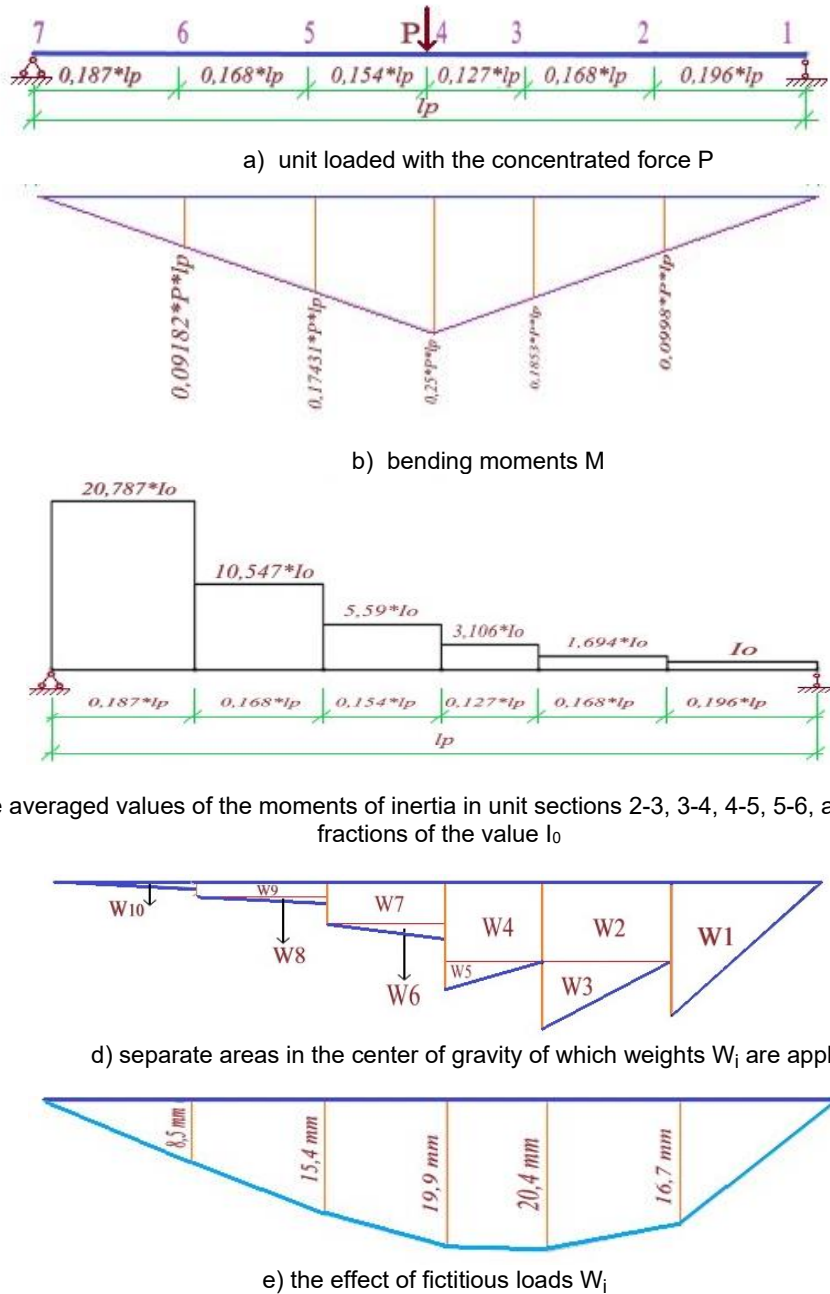
Fig. 4. Determining the deflection of the beam

Since the stiffness of the unit along its length changes according to a curvilinear law, in this case, to simplify the calculation, the moments of inertia at each section of the unit are taken averaged, in steps. We take the averaged moment of inertia I0 of the unit section 1-2 as a basis. Fig. 4c shows the averaged values of the moments of inertia in unit sections 2-3, 3-4, 4-5, 5-6, and 6-7 in fractions of the value I_0.

The fictitious load shown in Fig. 4d changes abruptly along the unit length. This is due to the fact that the unit stiffness values are different at each of the sections, therefore, after dividing the values from the diagram of bending moments M by different stiffness values, we can obtain their own fictitious loads. Naturally, it is difficult to determine fictitious moments from such a complex load. The fictitious load shown in Fig. 4d is replaced by a lumped fictitious weight system, as shown in Fig. 4d.

Such a replacement consists in the fact that the diagram shown in Fig. 4d is divided into separate areas, in the center of gravity of which weights Wi are applied (see Fig. 4d), which are numerically equal to the corresponding areas of the diagram.

It should be borne in mind that when determining the elastic modulus of concrete, reduction factors are introduced that take into account the heat and moisture treatment of concrete (k_1 = 0.9) and the elastic-plastic properties of concrete under a short-

term action of the load P during the unit loading ($k_2 = 0.85$).

Fig. 4e shows the effect of fictitious loads Wi, determined taking into account the above-mentioned reduction factors k_1 and k_2. The values of the fictitious loads W_i, according to the calculation, are taken as follows:

$$W_1 = 0.00978 \cdot \frac{P \cdot l_p^2}{E_b \cdot I_0}; \qquad (2)$$

$$W_2 = 0.00990 \cdot \frac{P \cdot l_p^2}{E_b \cdot I_0}; \qquad (3)$$

$$W_3 = 0.00424 \cdot \frac{P \cdot l_p^2}{E_b \cdot I_0}; \qquad (4)$$

$$W_4 = 0.00758 \cdot \frac{P \cdot l_p^2}{E_b \cdot I_0}; \qquad (5)$$

$$W_5 = 0.00132 \cdot \frac{P \cdot l_p^2}{E_b \cdot I_0}; \qquad (6)$$

$$W_6 = 0.00104 \cdot \frac{P \cdot l_p^2}{E_b \cdot I_0}; \qquad (7)$$

$$W_7 = 0.00480 \cdot \frac{P \cdot l_p^2}{E_b \cdot I_0}; \qquad (8)$$

$$W_8 = 0.00066 \cdot \frac{P \cdot l_p^2}{E_b \cdot I_0}; \qquad (9)$$

$$W_9 = 0.00146 \cdot \frac{P \cdot l_p^2}{E_b \cdot I_0}; \qquad (10)$$

$$W_{10} = 0.00041 \cdot \frac{P \cdot l_p^2}{E_b \cdot I_0}. \qquad (11)$$

Plotting the diagram of the fictitious moments from the action of the weights W_i is not difficult. The diagram M in our case is a broken line. In places where the diagram is broken (q_f), i.e., in sections 2 ÷ 6, the fictitious moments M coincide with the deflections in these sections. The control deflection f_c under the load P, shown in the M diagram (see Fig. 4e), is numerically equal to 19.9 mm.

Falsone (2018) gives an explanation for the modern assumption of a concentrated external moment, interpreted as a generalized function (doublet), and shear deformation, which determines the contradictory discontinuities in deflection laws.

Thus, with the control load for stiffness $P_c = 178$ kN, the control deflection at a given load is assumed to be $f_c = 19.9$ mm.

Results and Discussion

The values of the control loads, the control deflection, and the control crack opening width for testing the UPB 185.25 unit for stiffness, crack resistance, and strength, according to the calculation results, were taken as follows:

1) by stiffness — $P_c = 178$ kN;

2) by crack resistance — $P_c = 410$ kN;
3) by strength — $P_c = 887$ kN;
4) by deflection — $f_c = 19.9$ mm;
5) by crack opening — $a_{cr} = 0.2$ mm.

The experimental value of the UPB 185.25 unit deflection in tests under the action of the control load for stiffness $P_c = 178$ kN in accordance with Clause 9.2.4 of GOST 8829-94 when testing one product should not exceed the control value of the deflection by more than 10 %.

The experimental crack opening width in tests under the action of the control crack resistance load $P_c = 410$ kN in accordance with Clause 9.3.4 of GOST 8829-94 when testing one product should not exceed the control crack opening width multiplied by a factor of 1.05.

Fig. 5 shows a diagram with the layout of deflectometers along the length of the unit and the outline of the deflections of the UPB 185.25 unit along its length during testing

The analysis of the UPB 185.25 unit deflection outline along the unit length (Fig. 5) shows that the deflections in the right part of the UPB 185.25 unit deflection outline have larger values compared to the deflections in the left part. This outline of the deflections is quite natural since the right side of the unit is less stiff compared to its left side.

Fig. 6 shows a diagram of deflections in the middle section of the UPB 185.25 unit under the load P. The analysis of the deflection diagram allows us to note the following.

At the first stage of testing, the stiffness of the unit was evaluated. With the control load for stiffness $P_c = 178$ kN, the experimental deflection of the unit should not exceed the control value $f_c = 19.9$ mm. Upon reaching this load, the experimental deflection in the considered section of the unit had a value equal to $f_{exp} = 18.3$ mm, which was 92% of the control deflection.

At the second stage of testing, the crack resistance of the unit was evaluated. With the control load for crack resistance $P_c = 410$ kN, the experimental crack opening width should not exceed the control value $a_{cr} = 0.2$ mm. At the experimental load $P_{exp} = 410$ kN, the crack opening width in the beam concrete was $a_{exp} = 0.15$ mm.

At the third (last) stage of testing, the strength of the unit was evaluated. The control load when testing the strength of the unit with the safety factor of C = 1.3 was $P_c = 887$ kN. During the control tests, the experimental load $P_{exp} = 910$ kN was achieved, which amounted to 108 %. When the experimental load $P_{max} = 910$ kN was reached, the maximum output of the hydraulic jack plunger was achieved, and in this regard, further loading was suspended. The nature of the increase in the deflections and the assessment of the stress-strain state of the UPB 185.25 unit showed that the limit state was
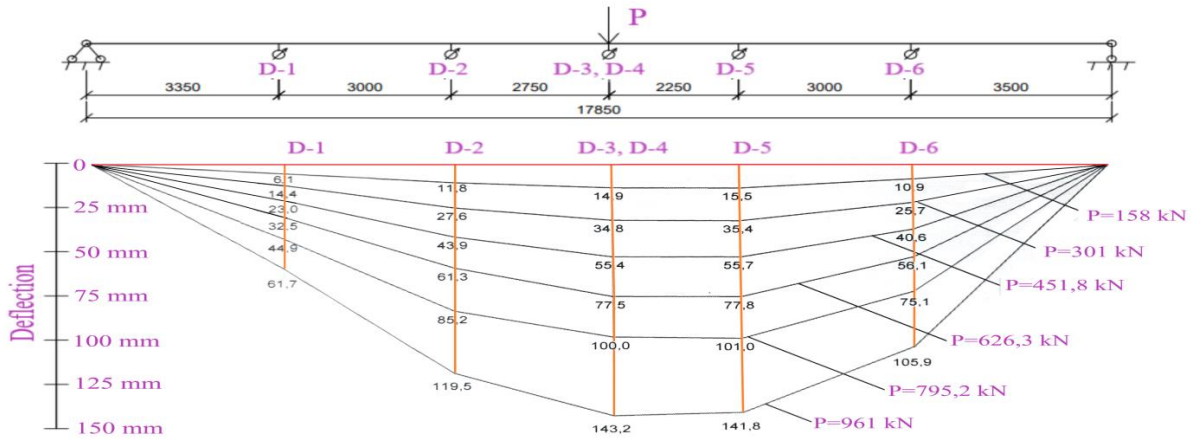
Fig. 5. Diagram with the layout of deflectometers along the length of the unit and the outline of the deflections of the UPB 185.25 unit along its length during testing
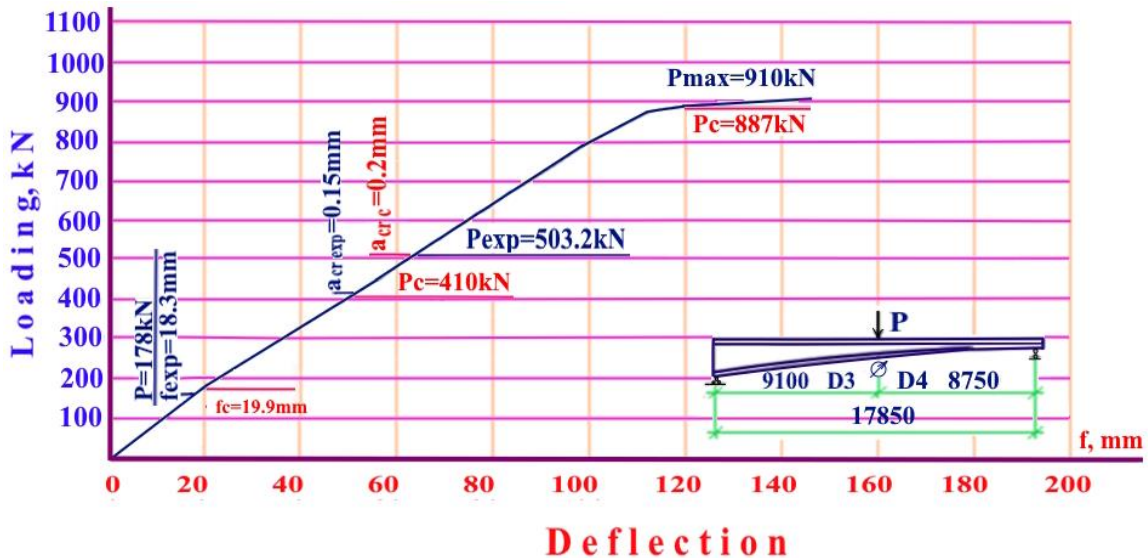
Fig. 6. Diagram of deflections in the middle section of the UPB 185.25 unit

not reached, and it had reserves in terms of bearing capacity.

Thus, the breakdown of the conical beam into separate blocks of variable cross-section confirmed the correctness of the chosen design strategy. Zheng and Ji (2011) showed that equivalent representations of beams with periodically variable cross-section in the form of several steps of variable cross-section give good convergence in calculating the displacements and the fundamental natural frequency of the beams.

4 Spatial model of the UPB unit built in MIDAS FEA NX

Three-dimensional computational modeling of a reinforced concrete beam by the finite element method was performed in MIDAS FEA NX. Fig. 7 shows a spatial model of the UPB unit built in MIDAS FEA NX. Fig. 8 shows a general view of the UPB unit reinforcement, and Fig. 9 shows a grid scheme adopted for the UPB unit 185.25.

At the first stage, the calculation of the beam and its modeling with the help of rod elements were performed.

The following parameters were used:
- element type — bending beam element;
- load type — uniaxial bending;
- maximum reinforcement percentage — 10%.

Longitudinal reinforcement consisting of A400 class rebars and transverse reinforcement consisting of A240 class rebars were taken into account in the calculation. Fig. 8 shows the adopted data for the reinforcing bars.

For concrete, the parameters specified in Figs. 10, 11 were used. In this case, the accepted diagrams of concrete deformation in tension and compression for concrete class B40 are taken for non-linear calculation at short-term loading at moisture content 40–75% according to Clause 6.1.20 of SP 63.13330.2018 "Concrete and reinforced concrete structures". Three-dimensional solid finite elements

41
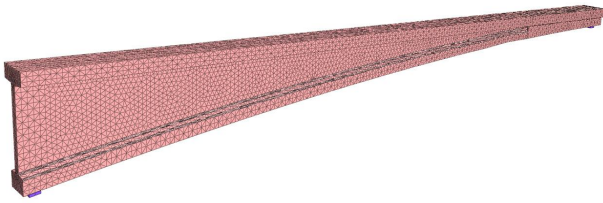
Fig. 7. Spatial model of the UPB 185.25 unit built
in MIDAS FEA NX
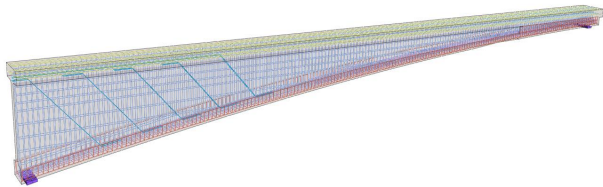
Fig. 8. General view of the UPB 185.25 unit reinforcement
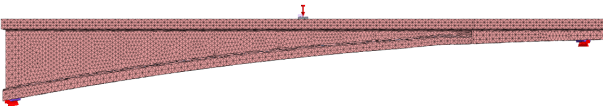
Fig. 9. Grid scheme of the UPB 185.25 unit
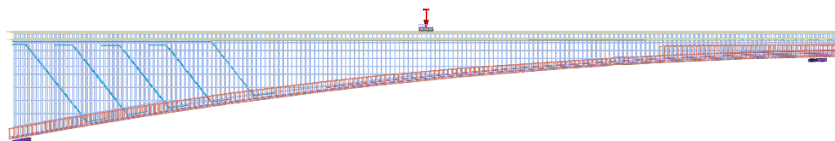
are used for concrete and three-dimensional beam elements are used for reinforcement.

According to the calculation at a vertical concentrated load of 888.85 kN, vertical displacement is 142.5 mm (Fig. 12).

The plastic stage of the reinforcement, the patterns of maximum longitudinal forces and maximum stresses in the reinforcement (Fig. 13) practically coincide with the theoretical equations for the strength of materials.

In addition, the calculation of the 3D model of the beam with cracking was performed. The crack dimensions were set in the tensile zone based on the initial calculation data.

Then the crack resistance of the beam was calculated. By iteration and compliance with the above conditions, the maximum value of crack opening equal to 0.226 mm was obtained (Fig. 14).

The maximum value of the crack opening width of 0.226 mm is significantly higher than the experimental value, which is apparently due to the failure to consider the behavior of the inclined reinforcement at the plastic stage.

Fig. 15 shows a comparative diagram of the deflections in the middle section.
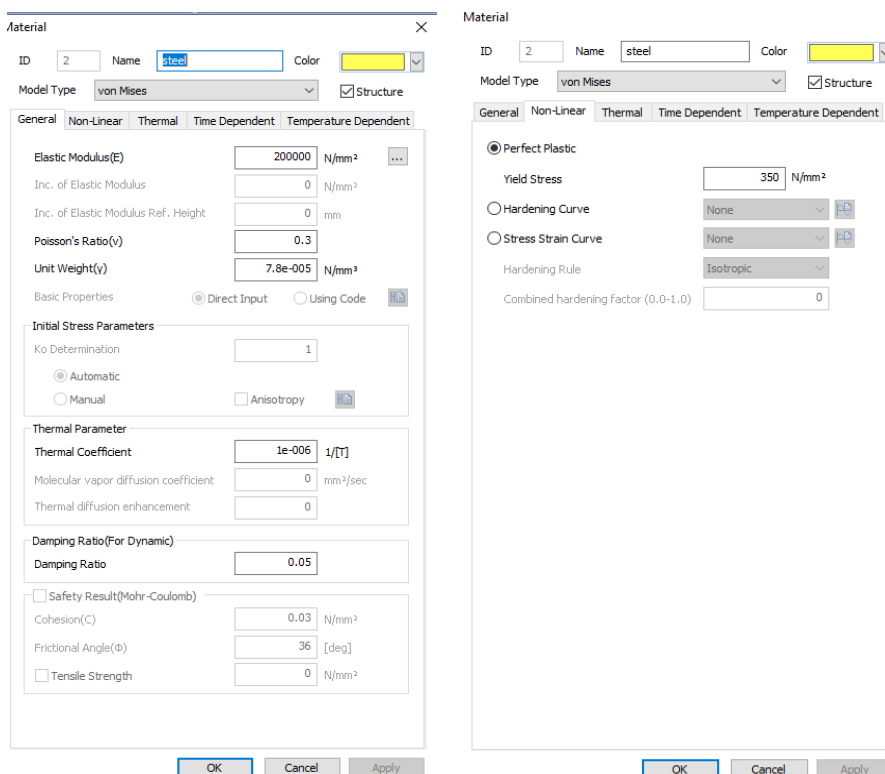
Fig. 10. Adopted data for rebars
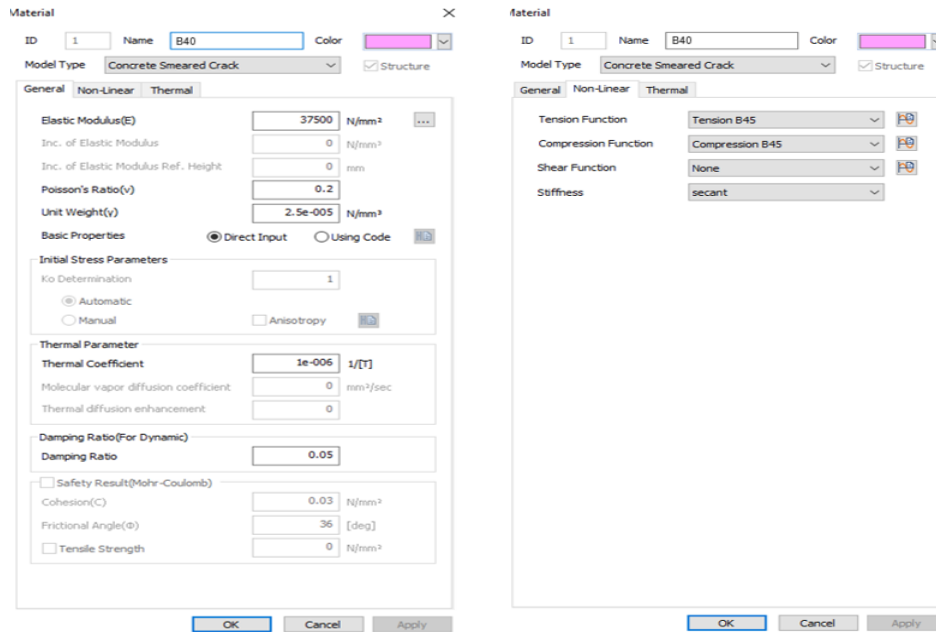
Fig. 11. Adopted data for concrete
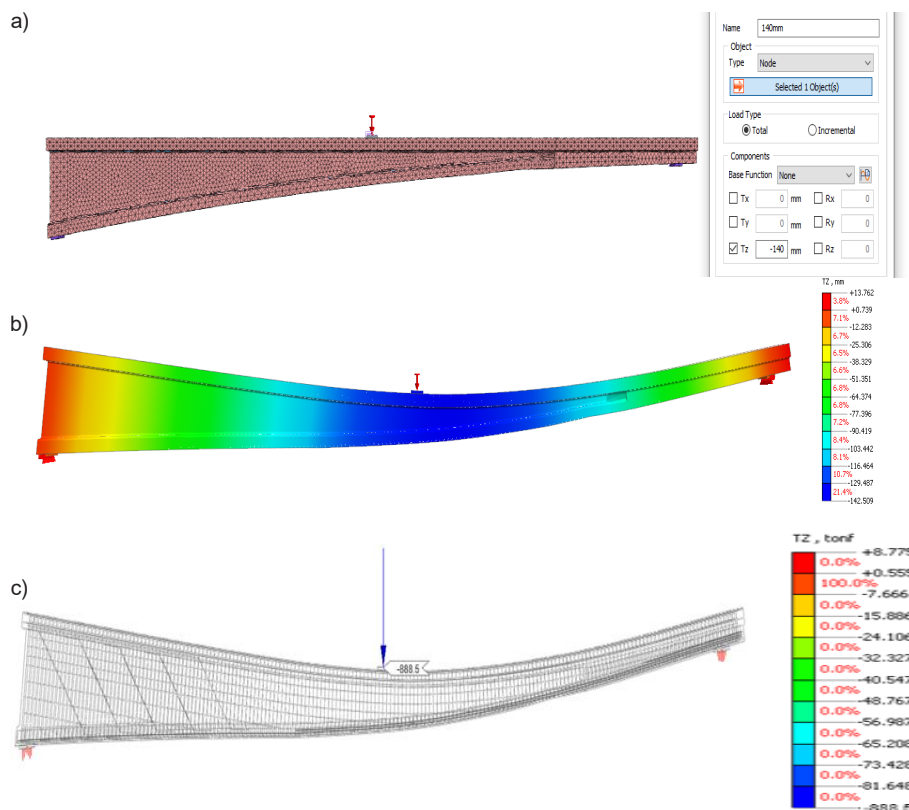
Fig. 12. Results of the beam calculation for maximum deflections: *a — deflection of 140 mm;*
b — maximum beam deflection of 142.5 mm; c — maximum load of 888.5 kN

In addition, the maximum deflections were calculated for different classes of concrete. Fig. 16 shows a comparative diagram of the deflections for different concrete classes.

If for concrete of class B40, the maximum design load P_{max} = 888.5 kN practically coincided with the

expected P_c = 887 kN, then for concretes of classes B35 and B25, there is a decrease in strength by 2.36 % and 6.7 %, respectively.

Experimental confirmation is necessary to substantiate the possibility of using concrete of class B35 in these products. The use of concrete of class B25 in these
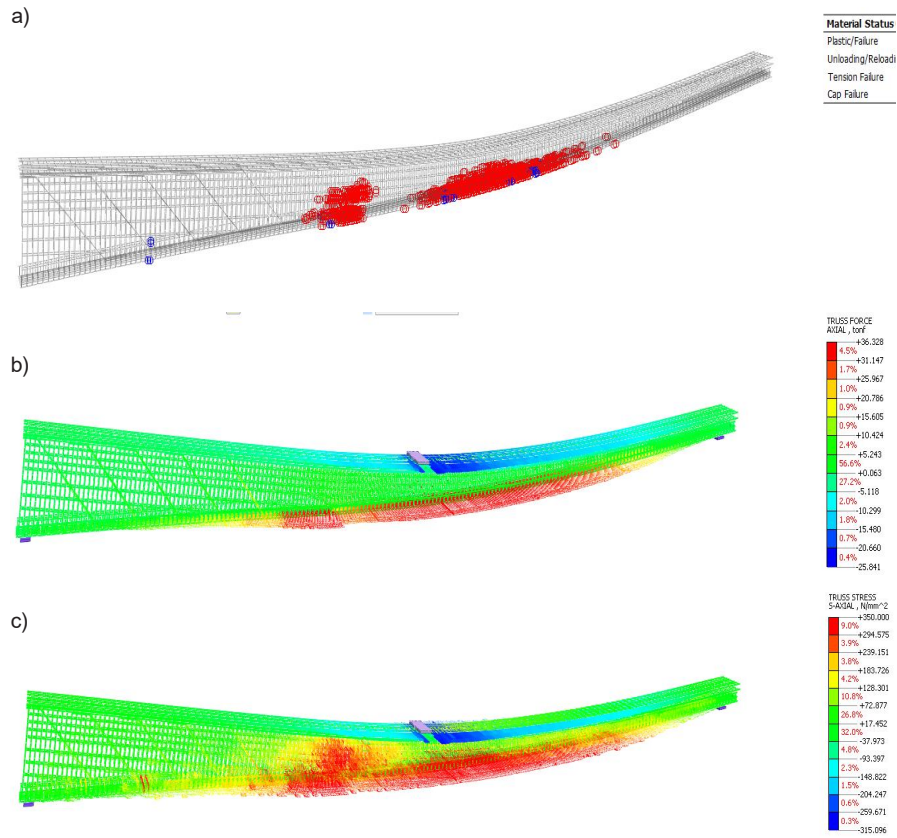
Fig. 13. Maximum deformations and stresses in the reinforcement at the limit stage:
a — "plastic status" in the UPB unit rebars; b — maximum longitudinal forces in the UPB unit rebars; c — maximum stresses in the UPB unit rebars
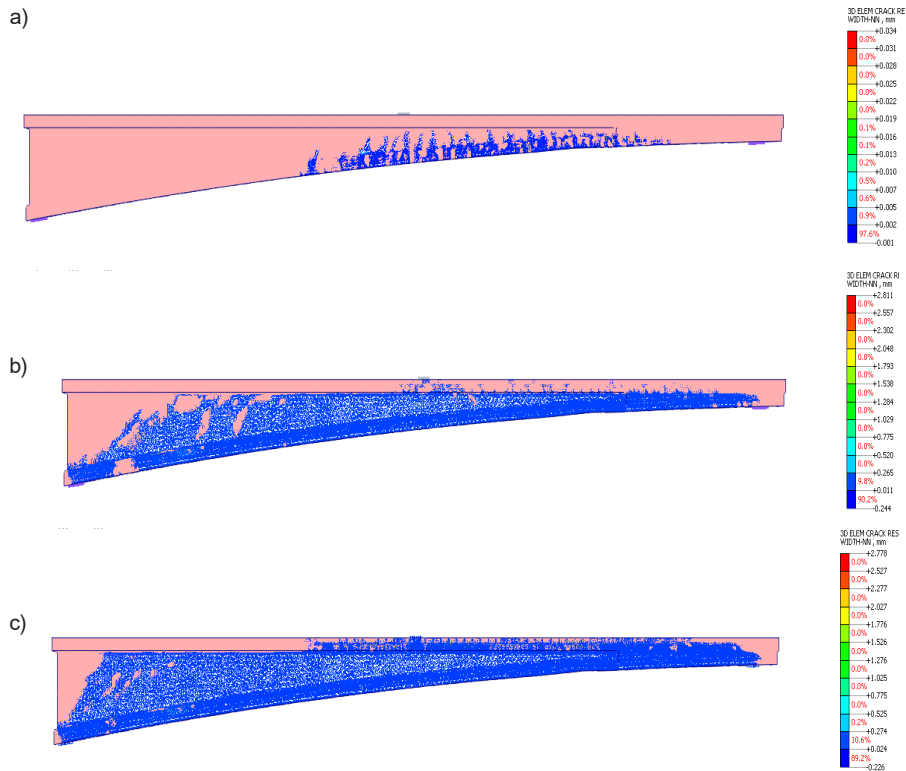
Fig. 14. Crack propagation in the concrete block: *a — at 0.05*140 mm pitch (5 % of the specified displacement); at 0.4*140 mm pitch (40% of the specified displacement); at 1.0*140 mm pitch (100 % of the specified displacement)*

1 – experimental graph, 2-calculation graph

Deflection, mm

Fig. 15. Diagram of deflections in the middle of the UPB unit

1 — experimental graph (P_{max} = 910 kN),
2 — concrete class B45 (P_{max} = 899 kN),
3 — concrete class B40 (P_{max} = 888 kN),
4 — concrete class B35 (P_{max} = 866.6 kN),
5 — concrete class B25 (P_{max} = 827.5 kN)

Fig. 16. Diagram of deflections in the middle of the UPB unit
for different classes of concrete

products is considered inexpedient due to a decrease in strength by 6.7 % in comparison with the reference beam and the absence of prestressed reinforcement.

Conclusions

• The control load for the UPB 185.25 unit stiffness testing was P_c = 178 kN, and the control deflection was taken equal to f_c = 19.9 mm. Upon reaching the experimental load equal to P_{exp} = 178 kN, the experimental deflection had a value equal to f_{exp} = 18.3 mm, which was 92% of the control deflection. In terms of stiffness, the UPB 185.25 unit meets the requirements of GOST 8829-94 and SP RK 3.03-112-2013.

• The control load for the UPB 185.25 unit crack resistance testing was P_c = 410 kN, and the control crack opening width was taken equal to a_{cr} = 0.2 mm. At the experimental load P_{exp} = 410 kN, the crack opening width in the beam concrete was a_{exp} = 0.15 mm. Only when the experimental load equal to the value of P_{exp} = 503.2 kN was reached, the experimental crack opening width was a_{exp} = 0.2 mm. In terms of crack resistance, the UPB 185.25 unit meets the requirements of GOST 8829-94 and SP RK 3.03-112-2013.

• The control load for the UPB 185.25 unit according to the strength test was P_c = 887 kN. In the tests, the experimental load equal to the value of P_{exp} = 910 kN was achieved. The nature of the increase in the deflections and the assessment of the stress-strain state of the experimental product showed that, at a given test load, the UPB 185.25 unit had reserves in terms of its bearing capacity. In terms of strength, the UPB 185.25 unit meets the requirements of GOST 8829-94 and SP RK 3.03-112-2013.

• The results of beam calculation in Midas FEA NX showed high convergence of the design (888.5 kN) and experimental load (887 kN) in terms of beam strength for concrete class B40.

The results of the beam calculation with concrete of B35 and B25 classes showed that it is inexpedient to use concrete of B25 class due to a decrease in strength by 6.7% in comparison with the reference beam and the absence of prestressed reinforcement.

References

Balduzzi, G., Aminbaghai, M., Sacco, E., Füssl, J., Eberhardsteiner, J., and Auricchio, F. (2016). Non-prismatic beams: A simple and effective Timoshenko-like model. *International Journal of Solids and Structures*, Vol. 90, pp. 236–250. DOI: 10.1016/j.ijsolstr.2016.02.017.

Barham, W. S. and Idris, A. A. (2021). Flexibility-based large increment method for nonlinear analysis of Timoshenko beam structures controlled by a bilinear material model. *Structures*, Vol. 30, pp. 678–691. DOI: 10.1016/j.istruc.2021.01.023.

Cazzani, A., Malagù, M., and Turco, E. (2016). Isogeometric analysis of plane-curved beams. *Mathematics and Mechanics of Solids*, Vol. 21, Issue 5, pp. 562–577. DOI: 10.1177/1081286514531265.

Chockalingam, S. N., Nithyadharan, M., and Pandurangan, V. (2020). Shear stress distribution in tapered I-beams: Analytical expression and finite element validation. *Thin-Walled Structures*, Vol. 157, 107152. DOI: 10.1016/j.tws.2020.107152.

Chockalingam, S. N., Pandurangan, V., and Nithyadharan, M. (2021). Timoshenko beam formulation for in-plane behaviour of tapered monosymmetric I-beams: Analytical solution and exact stiffness matrix. *Thin-Walled Structures*, Vol. 162, 107604. DOI: 10.1016/j.tws.2021.107604.

Committee for Construction, Housing and Communal Services and Land Management of the Ministry of National Economy of the Republic of Kazakhstan (2015). *Regulations SP RK 3.03-112-2013. Bridges and culverts*. Astana: Ministry of National Economy of the Republic of Kazakhstan, 717 p.

Falsone, G. (2018). The use of generalized functions modeling the concentrated loads on Timoshenko beams. *Structural Engineering and Mechanics,* Vol. 67, No. 4, pp. 385–390. DOI: 10.12989/sem.2018.67.4.385.

Gosstroy of Russia (1998). *State Standard GOST 8829-94. Reinforced concrete and prefabricated concrete building products. Loading test methods. Assessment of strength, rigidity and crack resistance*. Moscow: Gosstroy of Russia, 27 p.

Government of the Republic of Kazakhstan (2010). *Technical Regulations "Safety requirements for buildings and structures, building materials and products".* Astana: Government of the Republic of Kazakhstan, 40p.

Gusev, B. V. and Saurin, V. V. (2017). *On vibrations of inhomogeneous beams*. [online]. Available at: http://www.info-rae.ru/o-kolebaniyax-neodnorodnyx-balok/ [Date accessed March 1, 2023].

Gusev, B. V. and Saurin, V. V. (2018). Variational approaches to finding eigenvalues for beams with variable cross-section. *Innovations and Investments*, No. 3, pp. 253–264.

Jalairov, A., Kumar, D., Kassymkanova, K.-K., Nuruldaeva, G., Imankulova, A. (2022a). Structural behavior of prestressed concrete bridge girder with monolithic joint. Communications - Scientific Letters of the University of Zilina, Vol. 24, Issue 4, pp. D150–D159. DOI: 10.26552/com.C.2022.4.D150-D159.

Petukhov, L. V. (1980). Thin curvilinear beams of minimum weight. *Journal of Applied Mathematics and Mechanics*, Vol. 44, Issue 4, pp. 508–512. DOI: 10.1016/0021-8928(80)90042-8.

Jalairov, A., Kumar, D., Kassymkanova, K.-K., Sarsembekova, Z., Nuruldaeva, G., and Jangulova, G. (2022b). Structural behavior of prestressed concrete bridge girder with epoxy joint. *Communications - Scientific Letters of the University of Zilina*, Vol. 24, Issue 2, pp. D59–D71. DOI: 10.26552/com.C.2022.2.D59-D71.

Ministry of Construction, Housing and Utilities of the Russian Federation (2019). *Regulations SP.63.13330.2018. Concrete and reinforced concrete structures. General provisions.* Moscow: Standartinform, 117 p.

Resan, S. F. and Zamel, J. K. (2021a). Flexural behavior of developed reinforced concrete beams of non prismatic flanges. *Materials Today: Proceedings*, Vol. 42, Part 5, pp. 2974–2983. DOI: 10.1016/j.matpr.2020.12.808.

Resan, S. F. and Zamel, J. K. (2021b). Rotation capacity assessment in developed non prismatic flanged reinforced concrete Tee beams. *Case Studies in Construction Materials*, Vol. 14, e00517. DOI: 10.1016/j.cscm.2021.e00517.

Ruditsyn, M. N. (1940). *Calculation of beams with variable cross-section, framed and strutted systems by breaking loads*. [online] Available at: https://elib.belstu.by/bitstream/123456789/35163/1/%D0%A0%D1%83%D0%B4%D0%B8%D1%86 %D1%8B%D0%BD.pdf [Date accessed March 1, 2023].

Saurin, V. V. (2019). Analysis of dynamic behavior of beams with variable cross-section. *Lobachevskii Journal of Mathematics*, Vol. 40, Issue 3, pp. 364–374. DOI: 10.1134/S1995080219030168.

Shalkarov, A. A., Karasay, S. Sh., Tanirbergenov, A. K., and Murzalina, G. B. (2018). Monitoring the manufacture of UBS 185.14 blocks for the overhead span structure in Almaty. *Bulletin of Omsk regional Institute*, No. 4, pp. 13–26.

Smirnov, A. F. (ed.). (1961). *Strength of materials*. Moscow: Transjeldorızdat, 591 p.

Tayfur, Y., Darby, A., Ibell, T., Orr, J., and Evernden, M. (2019). Serviceability of non-prismatic concrete beams: Combined-interaction method. *Engineering Structures,* Vol. 191, pp. 766–774. DOI: 10.1016/j.engstruct.2019.04.044.

Timoshenko, S. P. (1965). Strength of materials. Part 1. Elementary Theory and Problems. Moscow: Nauka, 363 p.

Wang, C. M., Thevendran, V., Teo, K. L., and Kitipornchai, S. (1986). Optimal design of tapered beams for maximum buckling strength. *Engineering Structures*, Vol. 8, Issue 4, pp. 276–284. DOI: 10.1016/0141-0296(86)90035-0.

Yassopoulos, C., Leake, C., Reddy, J. N., and Mortari, D. (2021). Analysis of Timoshenko–Ehrenfest beam problems using the Theory of Functional Connections. *Engineering Analysis with Boundary Elements*, Vol. 132, pp. 271–280. DOI: 10.1016/j.enganabound.2021.07.011.

Zheng, T. and Ji, T. (2011). Equivalent representations of beams with periodically variable cross-sections. *Engineering Structures*, Vol. 33, Issue 3, pp. 706–719. DOI: 10.1016/j.engstruct.2010.11.007.

Zhernakov, V. S., Pavlov, V. P., and Kudoyarova, V. M. (2017). Spline-method for numerical calculation of natural-vibration frequency of beam with variable cross-section. *Procedia Engineering*, *Vol. 206*, pp. 710–715. DOI: 10.1016/j.proeng.2017.10.542.

Zhong, J., Zhuang, H., Shiyang, P., and Zhou, M. (2021). Experimental and numerical analysis of crack propagation in reinforced concrete structures using a three-phase concrete model. *Structures,* Vol. 33, pp. 1705–1714. DOI: 10.1016/j.istruc.2021.05.062.

Zhou, M., Fu, H., Su, X., and An, L. (2019a). Shear performance analysis of a tapered beam with trapezoidally corrugated steel webs considering the Resal effect. *Engineering Structures*, Vol. 196, 109295. DOI: 10.1016/j.engstruct.2019.109295.

Zhou, M., Liao, J., Zhong, J., An, L., and Wang, H. (2021). Unified calculation formula for predicting the shear stresses in prismatic and non-prismatic beams with corrugated steel web. *Structures*, Vol. 29, pp. 507–518. DOI: 10.1016/j.istruc.2020.11.060.

Zhou, M., Shang, X., Hassanein, M. F., and Zhou, L. (2019b). The differences in the mechanical performance of prismatic and non-prismatic beams with corrugated steel webs: A comparative research. *Thin-Walled Structures*, Vol. 141, pp. 402–410. DOI: 10.1016/j.tws.2019.04.049.

РАСЧЕТ И ИСПЫТАНИЯ УСИЛЕННОЙ КОНИЧЕСКОЙ МОСТОВОЙ БАЛКИ

Асылхан Джалаиров (Assylkhan Jalairov)[1], Даурен Кумар (Dauren Kumar)[2*],
Нуржан Досаев (Nurzhan Dosaev)[3], Гульжан Нурулдаева (Gulzhan Nuruldaeva)[4],
Хайни-Камаль Касымканова (Khaini-Kamal Kassymkanova)[4],
Гульшат Мурзалина (Gulshat Murzalina)[4]

[1]Кафедра «Транспортное строительство, мосты и тоннели», Международный транспортно-гуманитарный университет, Алматы, Республика Казахстан

[2]Кафедра картографии и геоинформатики, Казахский национальный университет имени Аль-Фараби, Алматы, Республика Казахстан

[3]Департамент науки и внедрения новых технологий, Национальный центр качества дорожных активов, Астана, Республика Казахстан

[4]Университет им. К. И. Сатпаева, Алматы, Республика Казахстан

*E-mail: daurendkb@gmail.com

Аннотация
Введение: в статье рассматривается соответствие фактических прочностных и деформативных свойств унифицированного сборного блока (далее — УСБ 185.25) расчетным данным. **Цель исследования** заключалась в проверке сходимости экспериментальных данных по железобетонной балке с переменным контуром нижнего пояса и расчетных допущений. **Методы:** В ходе исследования моменты инерции на каждом участке блока брались усредненными, пошагово. Каждый участок рассчитывался отдельно. Затем результаты суммировались. Кроме того, расчетные значения были проверены с помощью метода конечных элементов в MIDAS. **Результаты:** Принятые расчетные допущения, основанные на результатах испытаний, показали высокую сходимость результатов и подтвердили соответствие балки по жесткости, трещиностойкости и прочности. Контрольная ширина раскрытия трещин a_{cr} = 0,2 мм была достигнута при нагрузке 503,2 кг, что на 22,7% выше расчетной нагрузки.

Ключевые слова: прогиб балки, контрольные нагрузки, трещиностойкость, графоаналитический метод, УСБ 185, анализ МКЭ.

INFLUENCE OF THE PROBABILISTIC METHOD TO SUMMARIZE LOADS ON THE RELIABILITY AND MATERIAL CONSUMPTION OF BUILDING STRUCTURES

Dmitrii Kuligin*, Filipp Shkoliar

Peter the Great St. Petersburg Polytechnic University, Saint Petersburg, Russia

*Corresponding author's e-mail: dmitrykul17@gmail.com

Abstract

Introduction. Load rates are one of the main factors affecting the assessment of the reliability of building structures. All loads are probabilistic in nature, but short-term loads are the most representative in terms of this study since they have the most stochastic nature compared to other types of loads. According to regulatory documents, the short-term loads on a building should be summarized based on their base return period — 50 years. Due to variety of design situations, it is impossible to optimally standardize calculation methods for all types of buildings, therefore, the return period of 50 years is taken for all types of buildings regardless of their required useful life, which in some cases may lead to an excessive safety margin. **Methods.** To summarize loads on the structural schemes of buildings, two methods are used: deterministic, which is based only on data from regulatory documents, and probabilistic, which takes into account the probabilistic nature of the origin of loads. Reliability is assessed by the limit state method and Rzhanitsyn method. **Results.** In a number of cases, the use of the probabilistic method when summarizing loads makes it possible to reduce the stiffness properties of sections by equating the period of return of probabilistic loads to the required useful life of the building. Thus, reliability is guaranteed not for 50 years (as in the deterministic method) but for the useful life of a building, and, as a result, the reliability of building structures is not reduced during the entire set period of their operation. This method made it possible to reduce the total weight of the frame of an industrial building by 3 %, and that of a small-sized building — by 27 %, which indicates a more rational application of the proposed method to small-sized building schemes, since in large schemes the gains from the reduced material consumption in structures will be neutralized by the consequences of their failure and the cost of equipment inside the building.

Keywords: reliability of building structures, safety characteristics, return period, limit state method

Introduction

In the design of buildings and structures, the reliability of building structures is one of the most important factors. On the one hand, it is necessary to ensure reliability, and on the other, not to neglect the economic component of construction. Factors affecting the reliability assessment include the types of buildings, the load rates, and the calculation methods. Yet, due to variety of design situations, it is impossible to optimally standardize calculation methods for building structures, which makes this research topic extremely relevant. There have been many studies applying mathematical modeling methods to reliability assessment problems (Perelmuter and Pichugin, 2014). However, one of the related issues is the low effectiveness of those methods resulting from insufficient input data, i.e., statistical information. This may cause erroneous results and lead to even higher margin than when using regulatory methods (Kurguzov et al., 2020). Therefore, if there is not enough statistical data for a comprehensive analysis of the structural schemes of buildings by probabilistic methods of calculation, it may make sense to apply probabilistic methods locally. Load rates have a key impact on the reliability of building structures, and their representation in the

form of probabilistic models is one of the fundamental principles of the reliability theory (Spaethe, 1994). Thus, within this research, we will assess the application of the probabilistic method to summarize loads with regard to the reliability of building structures. For this purpose, we will consider snow and wind loads as the most variable types of loads. Based on comparative calculations for two structural schemes, we will assess the reliability of building structures with the application of the probabilistic and deterministic methods of calculation by the limit state method and Rzhanitsyn method.

Methods

For the analysis, we chose two structural schemes of buildings with different parameters to be used as examples to make comparative calculations of the reliability of building structures depending on the influence of various factors. The first structural scheme is large-sized, with an expected useful life of 20 years. An industrial building may serve as an example of its use. The second structural scheme is small-sized, with an expected useful life of 5 years. It can be used for construction trailers and various mobile buildings. Both frames are made of metal structures. The large-sized building is represented by a single-span building with a span of 30 m. The

general view of its design model is given in Fig. 1a. All elements of the small-sized frame are made of metal profiles of square section (Fig. 1b). The height and width of the building — 3 m, the length of the building — 9 m (Fig. 1).

Load rates represent the main comparative factor in the calculations. During the research, we will use two methods to summarize those loads. The first one is the deterministic method based exclusively on Regulations SP 20.13330 "Loads and actions". The second one is the probabilistic method, which takes into account the probabilistic nature of the loads. Let us consider in detail the probabilistic method of calculation for each type of load.

Snow load. According to Regulations SP 20.131330.2016, the regulatory value of the snow load on the horizontal surface of roofing shall be determined by the following equation:

$$S_0 = c_w \cdot c_t \cdot \mu \cdot S_g, \tag{1}$$

where: c_w — the coefficient that takes into account snow drifting from the roofing and depends on the type of terrain, the shape of the roofing, and the availability of protection from the direct effects of wind;

c_t — the thermal coefficient, which takes into account snow melting on cold roofs with high heat emissions;

μ — the roofing shape coefficient;

S_g — the regulatory value of the weight of the snow cover per 1 m² of the horizontal ground surface.

The S_g value is of the greatest interest for the research since it represents the maximum weight of the snow cover, being exceeded on average once every 50 years, which indicates the stochastic nature of this value. However, for buildings with a short required useful life, the 50-year return period suggested in the regulatory document may lead to an excessive safety margin. Therefore, it makes sense to take the S_g value for a period of time equal to the required useful life of buildings. This approach

can have a significant impact on the material consumption of structures and, therefore, reduce the cost of construction (Bulanchik and Lalin, 2021).

For further calculations, we will use the analytical method of determining S_g. First of all, it is necessary to choose a distribution function for random variables. For snow and other weather loads, it is the Gumbel distribution that is used most often (Benjamin and Cornell, 2014; Nadolsky and Veryovka, 2018):

$$S_g = u - \frac{1}{a} \cdot \ln\left\{-\ln \Phi\left(S_g\right)\right\}, \tag{2}$$

where: $u = \mu - \dfrac{0.577}{a}$; $a = \dfrac{\pi}{\sigma \cdot \sqrt{6}}$;

μ — the mathematical expectation of the annual maxima;

σ — the standard deviation of the variable;

$\Phi\left(S_g\right)$ — the maxima distribution function.

$$\Phi\left(S_g\right) = 1 - \frac{1}{\mu_T}, \tag{3}$$

where: μ_T — the mathematical expectation of the probability period (the number of years under consideration).

Let us find the values of the snow cover weight for the application of loads to the considered building frames. For the industrial building, we adopt the design period of load return equal to 20 years, and for the small-sized building — equal to 5 years.

To determine the missing statistical values, we will use the equation to determine the reliability index, which is a characteristic representing a measure of reliability in Eurocodes (CEN, 2001):

$$\beta = \frac{S_g - \mu}{\sigma}. \tag{4}$$

Using Eq. (2), we obtain the weight of the snow cover:

$$S_g = u - \frac{1}{a} \cdot \ln\left\{-\ln\left(0.98\right)\right\} = u + \frac{3.9}{a}, \tag{5}$$

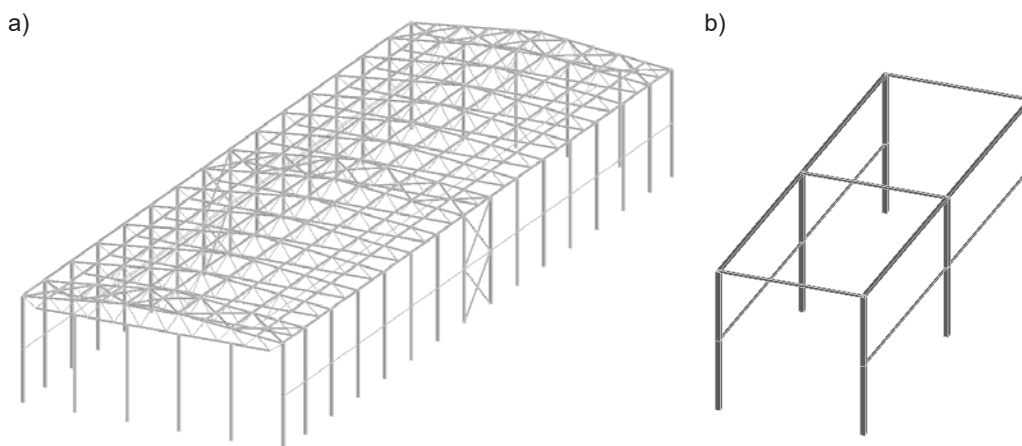a)   b)

Fig. 1. Structural schemes of the buildings

Mathematical expectation and standard deviation:

$$\mu = u + \frac{0.577}{a}; \qquad (6)$$

$$\sigma = \frac{\pi}{a \cdot \sqrt{6}} = \frac{1.282}{a}. \qquad (7)$$

Then:

$$\beta = \frac{u + \dfrac{3.9}{a} - u + \dfrac{0.577}{a}}{\dfrac{1.282}{a}} = 2.59. \qquad (8)$$

Let us express the standard deviation through the mathematical expectation and variation coefficient (which is approximately equal to 0.4 for show load):

$$\beta = \frac{S_g - \mu}{\mu \cdot f} = 2.59. \qquad (9)$$

Thus:

$$S_g = \mu \cdot (1 + 2.59 \cdot f) = \mu \cdot (1 + 2.59 \cdot 0.4) = 2.036 \cdot \mu. \quad (10)$$

As a result, we obtain an expression where we can apply the weight of the snow cover from the regulatory documents and then find the mathematical expectation, and after that, the standard deviation of the value. For snow zone III (Saint Petersburg):

$$\mu = \frac{S_g}{2.036} = \frac{1.5}{2.036} = 0.74 \ \text{kN/m}^2; \qquad (11)$$

$$\sigma = \mu \cdot f = 0.74 \cdot 0.4 = 0.296 \ \text{kN/m}^2. \qquad (12)$$

Thus, we obtain all the parameters necessary to determine the values of the snow cover weight for different return periods. Let us substitute the obtained values in Eq. (2) for the 20-year and 5-year return periods, respectively:

$$S_{g20} = u - \frac{1}{a} \cdot \ln\{-\ln(0.95)\} = u + \frac{2.97}{a} =$$
$$= \mu + \frac{2.393 \cdot \sigma}{1.282} = 1.29 \ \text{kN/m}^2; \qquad (13)$$

$$S_{g5} = u - \frac{1}{a} \cdot \ln\{-\ln(0.8)\} = u + \frac{2.97}{a} =$$
$$= \mu + \frac{2.077 \cdot \sigma}{1.282} = 1.21 \ \text{kN/m}^2. \qquad (14)$$

Thus, when going from the 50-year return period to the 20-year return period, the weight of the snow cover decreased by 14 %, and when going from the 50-year return period to the 5-year return period, the weight of the snow cover decreased by 19 %.

Wind load. Wind load is also probabilistic. Numerous studies mathematically modeling wind effects have been conducted on this topic (Krasnoschekov and Zapoleva, 2015a; Makhinko and Makhinko, 2015; Pshenichkina et al., 2019). In addition to wind speed, which is more variable than the weight of the snow cover, wind direction should be also taken into account in the calculations. This provides more complex combinations of possible wind effects for calculation and analysis.

Wind pressure at height **z** is proportional to half the square of wind speed and air density (Vrouwenvelder, 1997):

$$w(z) = \frac{1}{2} \cdot \rho \cdot v(z)^2, \qquad (15)$$

where: ρ — standard air density equal to 1.25 kg/m³ according to the JCSS;

$v(z)$ — wind speed at height **z**, m/s.

In the out-of-use Construction Rules and Regulations SNiP 2.01.07-85, wind speed and standard wind pressure were traditionally linked by the following expression:

$$w(z) = 0.61 \cdot v_5^2, \qquad (16)$$

where: v_5 — wind speed at a height of 10 meters, corresponding to the 10-minute averaging period, being exceeded on average once every 5 years, m/s.

In the latest regulatory documents, this expression was revised and modified according to Regulations SP 20.13330:

$$w(z) = 0.43 \cdot v_{50}^2. \qquad (17)$$

In this expression, v_{50} is a value similar to wind speed v_5 in Eq. (16) but for a period not exceeding 50 years.

To estimate the stochastic component of wind load and determine the value of wind pressure relative to the return period equal to the useful life of a building, we will also use the Gumbel distribution as a function of probability distribution of random variables, but in a different form:

$$F(v) = \ln\{-\ln[-a(v-u)]\}. \qquad (18)$$

In cases where there is insufficient data to determine the mathematical expectation of the values and their standard deviations, those can be expressed based on Eqs. (16) and (17).

For example, the regulatory value of wind pressure for wind zone II (Saint Petersburg) is 300 Pa. Thence, we can express v_5 and v_{50}:

$$v_5 = \sqrt{\frac{w}{0.61}} = \sqrt{\frac{300}{0.61}} = 22.18 \ \text{m/s}; \qquad (19)$$

$$v_{50} = \sqrt{\frac{w}{0.43}} = \sqrt{\frac{300}{0.43}} = 26.41 \ \text{m/s}. \qquad (20)$$

Let us compose a system of equations to determine the unknown statistical values. For this purpose, we will use the equation by Dubrovin and Semenov (2018) as the basis:

$$-\left[\frac{1.282 \cdot (v - \mu)}{\sigma(v)} + 0.577\right] = \ln\left[-\ln\left(\frac{T}{T+1}\right)\right], \quad (21)$$

where: T — the period of time under consideration, years.

Thus:

$$\begin{cases} -\left[\dfrac{1.282 \cdot (22.18 - \mu)}{\sigma(v)} + 0.577\right] = \ln\left[-\ln\left(\dfrac{5}{5+1}\right)\right] \\ -\left[\dfrac{1.282 \cdot (26.41 - \mu)}{\sigma(v)} + 0.577\right] = \ln\left[-\ln\left(\dfrac{50}{50+1}\right)\right] \end{cases} \quad (22)$$

Thence, we can find the following:

$$\sigma = 2.443 \text{ m/s} \quad \mu = 20.037 \text{ m/s}. \quad (23)$$

We will use these statistical values to find the values of wind speed for other return periods using Eq. (21). Let us find the values of wind speed and the regulatory value of wind pressure for return periods of 20 and 5 years:

$$v_{20} = \frac{\left(-\ln\left[-\ln\left(\dfrac{T}{T+1} \right) \right] \cdot \sigma + \\ +1.282 \cdot \mu - 0.577 \cdot \sigma \right)}{1.282} = 24.69 \text{ m/s}; \quad (24)$$

$$v_{5} = \frac{\left(-\ln\left[-\ln\left(\dfrac{T}{T+1} \right) \right] \cdot \sigma + \\ +1.282 \cdot \mu - 0.577 \cdot \sigma \right)}{1.282} = 22.18 \text{ m/s}. \quad (25)$$

Then we will find the regulatory values of wind pressure by Eq. (17):

$$w_{20} = 0.43 \cdot 24.69 = 262 \text{ Pa}; \quad (26)$$
$$w_{5} = 0.43 \cdot 22.18 = 212 \text{ Pa}. \quad (27)$$

Thus, when going from the 50-year return period to the 20-year return period, the regulatory value of wind pressure decreased by 13%, and when going from the 50-year return period to the 5-year return period — by 29 %.

We will perform all further calculations related to the summary of loads according to Regulations SP 20.13330.2016, substituting (when applying the probabilistic method to summarize loads) the values of wind pressure and the weight of the snow cover, obtained earlier, in the equations where they are present. As a result, two combinations of loads are applied to each of the design models: loads summarized by the deterministic method and loads summarized by the probabilistic method.

After applying loads to the design models of buildings, we will analyze the design models by the limit state method in SCAD. First, we will choose arbitrary sections for the structural elements and conduct primary calculations. To analyze the schemes for the first group of limit states, let us move on to the static calculation of the schemes. It is based on the determination of the utilization rates for various factors. In case of compressed elements, they are determined for strength, stability and flexibility. In case of tensile elements, they are determined only for strength and flexibility. The utilization rates obtained based on the calculations according to Regulations SP 16.13330.2017 "Steel structures" must be less than one but close to it. If the utilization rate is more than one, it is necessary to increase the section of the structural element or use steel with a higher design structural strength. The schemes must also meet the requirements of the second group of limit states. According to clause

15.1.1 of Regulations SP 20.133.2016 "Loads and actions", structural deflection must not exceed the limit value determined by Table E.1 depending on the span of the structure.

We can consider economic gains from reducing material consumption in building structures as the practical application of the obtained research results. Let us summarize the dimensions of the sections of the structural elements, meeting the limit state criteria for the probabilistic and deterministic methods to summarize loads, in a table, calculate the total weight of the frames of the buildings, and compare their values depending on the influence of different calculation methods.

Next, we will consider the designed models in terms of the reliability theory. There are numerous methods to assess the reliability of building structures, e.g., the method of two moments (Gordeeva, 2012; Krasnoshchekov and Zapoleva, 2015b), the Streletsky method, etc. One of such methods is the Rzhanitsyn method based mainly on the fact that the forces taken up by building structures must not exceed their load-bearing capacity (Rzhanitsyn, 1982).

Let us assume that the load forces are described by a function for random distribution of values with distribution density $f_F(F)$. The strength of a structural element is described by the deterministic value Φ_{det}, and the strength, in turn, also has its own distribution density.

It is believed that structural failure will occur when the design state represented by the shaded area w in Fig. 2 occurs. This state corresponds to the moment when the force from the applied load exceeds the load-bearing capacity of the structure. The probability of failure in such a case will be equal to the following:

$$Q = \int_{\Phi_{\text{det}}}^{F_{\text{max}}} f_F(F)\,dF. \quad (28)$$

Hence, the probability of failure-free operation can be found as follows:

$$P = 1 - Q. \quad (29)$$

In cases when the probability of failure is not zero, it is logical to assume that there is a safety margin, which can be denoted as ψ. This means that failure occurs when the safety margin is less than zero and
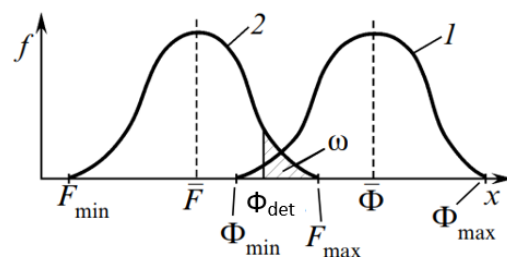

Fig. 2. Density of the load-bearing capacity and load distribution

represents the difference between the load-bearing capacity of the structure and the load applied to it (Fig. 3).
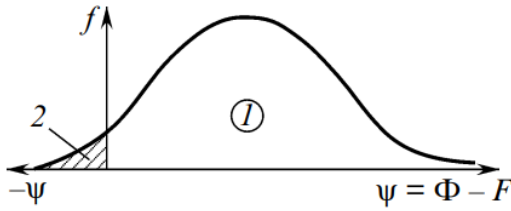

Fig. 3. Strength margin distribution density

Given that the values are distributed according to the normal law, the probability of failure can be calculated by the following equation:

$$Q = 0.5 - \Phi(\gamma), \qquad (30)$$

where: γ — the safety characteristic similar to the reliability index β, which was discussed earlier.

$$\gamma = \frac{\overline{\psi}}{\hat{\psi}}, \qquad (31)$$

$\overline{\psi} = \overline{\Phi} - \overline{F}$, and $\hat{\psi} = \sqrt{\hat{\Phi}^2 + \hat{F}^2}$.

$\Phi(\gamma)$ — the probability integral:

$$\Phi(\gamma) = \frac{1}{\sqrt{2\pi}} \int_0^\gamma \exp\left(-0.5 \cdot x^2\right) dx. \qquad (32)$$

Thus, the γ value is the number of standards falling within the range from $\psi = 0$ to $\psi = \overline{\psi}$. By converting the equation, we obtain:

$$\gamma = \frac{\overline{\Phi} - \overline{F}}{\sqrt{\hat{\Phi}^2 + \hat{F}^2}}, \qquad (33)$$

where: $\overline{\Phi}$ — the mathematic expectation of the load-bearing capacity of an element;

$\overline{F}$ — the mathematic expectation of the bending moment from the load;

$\hat{\Phi}$ — the standard of distribution of the load-bearing capacity;

$\hat{F}$ — the standard of distribution of the bending moment from the load.

To determine the mathematical expectation of the load-bearing capacity of an element, it is necessary to multiply the modulus of its section by the limit of proportionality of steel of which the element under consideration is made:

$$\overline{\Phi} = \sigma_{0.2} \cdot W_y. \qquad (34)$$

We will determine the mathematical expectation of the bending moment from the load by the design model of the buildings in SCAD. The standards

of distributions can be found by multiplying the mathematical expectations by the variation coefficients. They are determined based on the reference data. The variation coefficient of the load-bearing capacity of steel is 0.01, and that of the bending moment from the load is 0.15.

We will compare the obtained values of the safety characteristics of the structures with their regulatory values according to Table F.2 of GOST R ISO 2394-2016.

The frame of the industrial building can be attributed to the major consequences of failure since the building can contain a large amount of expensive equipment. The cost of safety measures can be classified as moderate. Because of the small number of the frame structures in the small-sized building, additional safety measures (in percentage terms) can significantly increase the total weight of the frame, therefore, the relative cost of safety measures can be classified as high. The consequences of failure, in turn, can be classified as minor since structural failure will not lead to any significant consequences. Thus, the resulting values of the safety characteristics are compared with their regulatory values from Table 1 and a conclusion can be made about the compliance or non-compliance of the frame structures with the reliability requirements when applying the probabilistic method to summarize loads.

Results and discussion

Based on the calculation results for the considered frames in SCAD, sections of structural elements were selected for the deterministic and probabilistic calculation methods. In the case of the industrial building, the section dimensions decreased only at the top and bottom chords of the truss. Below you can find a table with the calculation of the total weight of the frames with initial (deterministic method) (Table 2) and adjusted (probabilistic method) (Table 3) sections.

Thus, the gains from the reduced material consumption in the building structures from the use of the probabilistic method to summarize loads amounted to 3.2 tons, which is 3.4 % of the total weight of the frame when applying the deterministic method.

Let us compile a similar table for the frame of the small-sized building. In this case, the use of the probabilistic method made it possible to reduce the sections for columns and longitudinal beams (Table 3).

The total weight of the frame with the adjusted sections decreased by 0.156 tons, which is 27% of the initial frame weight.

Table 1. **Target values of the safety characteristics**

Relative cost of safety measures	Consequences of failure			
	Minor	**Notable**	**Moderate**	**Major**
High	0	1.5	2.3	3.1
Moderate	1.3	2.3	3.1	3.8
Low	2.3	3.1	3.8	4.3

Table 2. **Weight of the structural elements of the frame in the industrial building**

Structural element	Section	Weight, r. m	Length, quantity	Total weight, kg
Top chord	180x100x6	24.52	30.14·16	739.03
	160x100x6	22.63		682.07
Bottom chord	180x100x7	27.91	27·16	753.57
	160x100x6	22.63		611.01
Diagonal members R1, R6	50x4	5.45	8.56·16	46.65
Diagonal member R2	70x4	7.97	4.02·16	32.04
Diagonal members R3, R5, R7, R8, R9, R10	40x4	4.2	30.06·16	126.25
Diagonal member R4	60x4	6.71	4.44·16	29.79
Columns	30K1	87	9·32	25,056
Framework	25K1	80.2	9·8	5774.4
Purlins	24P	24	88·11	23,232
Struts	50x4	5.45	88·11	5275.6
Upper cross braces	140x4	16.76	234.9	3936.9
Crane girders	50x4	5.45	410	2234.5
V-shaped members	40x4	4.2	41.04	172.4
Side cross braces	120x4	14.25	67.12	956.5
		Per building	Initial	93,852.2
			Adjusted	90,659.8

Thus, comparing the obtained gains from the reduced material consumption in the structures of the two frames, we can conclude that it is most rational to use the probabilistic method to summarize loads for the frame of a small-sized building, since the gains for the frame of an industrial building will be neutralized by the possible consequences of structural failure or the cost of equipment inside the building.

Let us move on to the calculation of the reliability of the building structures by the Rzhanitsyn method in order to justify that it is safe to reduce the size of the structural elements and use the probabilistic method to summarize loads. Let us summarize the calculation results for the safety characteristics for the deterministic and probabilistic methods, obtained in the calculations according to Eq. (33), in a table.

Reliability characteristics of the initial sections of the industrial building:

Reliability characteristics of the adjusted sections of the industrial building:

It makes sense to compare the safety characteristics by their minimum values. In both cases, the purlin turned out to be a critical element of the scheme. For the deterministic method, the value of the safety characteristic of the purlin amounted to 4.29, and for the probabilistic method, it increased to 5.65 (Tables 4 and 5). This is due to the fact that for the deterministic method these values are guaranteed by the 50-year useful life of the building, and for the probabilistic method — by the 20-year period. In turn, both of these values meet the limit value, which is 3.8 for this type of building.

Let us move on to assessing the reliability of the small-sized building. For the initial sections, the safety characteristics turned out to be as follows:

For the adjusted sections:

The longitudinal beam with a safety characteristic of 0.45 for the deterministic method with a 50-year period and 0.59 for the probabilistic method with a 5-year period (Tables 6 and 7) turned out to be a critical structural element of the small-sized building. These values correspond to the regulatory values, therefore, the application of the probabilistic method to summarize loads can be considered reasonable.

Table 3. **Weight of the structural elements of the frame in the small-sized building**

Structural element	Section	Weight, r. m	Length, quantity	Total weight, kg
Columns	100x6	16.98	3·6	305.64
	100x3.5	10.36		186.48
Longitudinal beams	80x5	7.97	9·2	202.86
	80x4	6.71		165.96
Cross beams	50x2	2.93	3·3	26.37
Beams in the middle of the columns	40x2	2.31	9·2	41.58
			Initial	576.45
			Adjusted	420.39

Table 4. **Calculation results for the safety characteristics**

Structural element	$\bar{F}$	$\hat{F}$	$\bar{\Phi}$	$\hat{\Phi}$	γ
Column	111.28	16.692	309.95	3.1	11.70
Top chord	4.51	0.6765	42.19	0.42	47.26
Bottom chord	5.57	0.8355	42.19	0.42	39.13
Purlin	36.15	5.4225	59.54	0.59	4.29
Cross braces over the truss	6.95	1.0425	23.73	0.24	15.69
Diagonal member R1	0.02	0.003	3.27	0.03	98.97
Diagonal member R2	0.03	0.01	7.1	0.07	99.38
Diagonal member R3	0.02	0.003	1.41	0.01	96.42

Table 5. **Calculation results for the safety characteristics**

Structural element	$\bar{F}$	$\hat{F}$	$\bar{\Phi}$	$\hat{\Phi}$	γ
Column	97.38	14.61	309.95	3.1	14.23
Top chord	3.36	0.50	42.19	0.42	59.08
Bottom chord	3.78	0.57	42.19	0.42	54.35
Purlin	32.12	4.82	59.54	0.59	5.65
Cross braces over the truss	4.55	0.68	23.73	0.24	26.54
Diagonal member R1	0.02	0.003	3.27	0.03	98.97
Diagonal member R2	0.03	0.01	7.1	0.07	99.38
Diagonal member R3	0.02	0.003	1.41	0.01	96.42

Table 6. **Calculation results for the safety characteristics**

Structural element	$\bar{F}$	$\hat{F}$	$\bar{\Phi}$	$\hat{\Phi}$	γ
Columns	3.93	0.58	18.67	0.19	23.84
Beams in the middle of the columns	0.06	0.01	1.04	0.01	71.29
Longitudinal beams	9.22	1.14	9.85	0.10	0.45
Cross beams	0.03	0.00	1.70	0.02	94.96

Table 7. **Calculation results for the safety characteristics**

Structural element	$\bar{F}$	$\hat{F}$	$\bar{\Phi}$	$\hat{\Phi}$	γ
Columns	2.74	0.4	12.13	0.12	21.92
Beams in the middle of the columns	0.06	0.01	1.041	0.01	71.29
Longitudinal beams	7.64	1.15	8.32	0.08	0.59
Cross beams	0.03	0.01	1.698	0.02	94.96

Thus, comparing the safety characteristics obtained in the calculations by the Rzhanitsyn method of reliability assessment, we can conclude that the use of the probabilistic method to summarize loads is reasonable in terms of reliability for both frames of the buildings under consideration.

Conclusions

In a number of design situations, the use of the probabilistic method to summarize loads reduces the loads applied to the frame of the industrial building by 13 % for wind loads and by 14% for snow loads when going from the 50-year return period to the 20-year return period. The loads applied to the frame of the small-sized building, with the use of the probabilistic calculation method when going from the 50-year return period to the 5-year return period, decreased by 29 % for wind loads and by 19 % for snow loads. The reduced loads make it possible to reduce the stiffness properties of the sections. As a result, the total weight of the frame of the industrial building decreased by 3 %, and the that of the small-sized building — by 27 %. Hence, it is more rational to apply the method proposed in this work for small-sized buildings since in large buildings the economic gains will be neutralized by the consequences of structural failure and the cost of equipment inside the building. In turn, the Rzhanitsyn method showed that despite the reduction in the geometric parameters of the sections of the structural elements, their reliability does not decrease during the entire useful life of the elements.

References

Benjamin, J. R. and Cornell, C. A. (2014). *Probability, statistics, and decision for civil engineers*. Mineola, New York: Dover Publications, Inc., 685 p.

Bulanchik, D. Yu. and Lalin V. V. (2021). Determining loads with account for the useful life of a construction facility as a factor of reducing material consumption in load-bearing structures. In: *Week of Science at the Institute of Civil Engineering: Proceedings of the All-Russian Conference*. In 3 parts. Part 2. Saint Petersburg: Peter the Great St. Petersburg Polytechnic University, pp. 431–433.

CEN (2001). *EN 1990:2002. Eurocode - Basis of structural design*. Brussels: CEN, 116 p.

Dubrovin, V. M. and Semenov, K. S. (2018). Modelling of quasi-static reliability of technical system design. *Mathematical Modeling and Computational Methods*, No. 3 (19), pp. 38–48. DOI: 10.18698/2309-3684-2018-3-3848.

Gordeeva, T. E. (2012). Application of the method two moments to determine structural reliability. News of Higher Educational Institutions. *Construction*, No. 10, pp. 88–91.

Krasnoschekov, Y. V. and Zapoleva, M. Y. (2015a). The calculated values of wind load with a given probability. *The Russian Automobile and Highway Industry Journal*, No. 2 (42), pp. 64–67. DOI: 10.26518/2071-7296-2015-2(42)-81-89.

Krasnoshchekov, Y. V. and Zapoleva, M. Yu. (2015b). Probabilistic design of a structure by the given level of reliability. *The Russian Automobile and Highway Industry Journal*, No. 1 (41), pp. 68–73.

Kurguzov, K. V., Fomenko, I. K., and Shubina, D. D. (2020). Probabilistic and statistical modeling of loads and forces. *Vestnik MGSU (Monthly Journal on Construction and Architecture)*, Vol. 15, Issue 9, pp. 1249–1261. DOI: 10.22227/1997-0935.2020.9.1249-1261.

Makhinko, A. V. and Makhinko, N. A. (2015). The calibration rationale for combination factors dead load, snow and wind loads in design of steel structures with DSTU-N B EN 1990. *Metal Constructions*, Vol. 21, No. 2, pp. 81–98.

Nadolsky, V. V. and Veryovka, F. A. (2018). Specifics of determining the reliability index for different frequency periods. In: *Perspective Directions of Innovative Development of Construction Industry and Engineering Training: Proceedings of the 21st International Research and Methodological Workshop*. In 2 parts. Part 1. Brest: Brest State Technical University, pp. 205–212.

Perelmuter, A. V. and Pichugin, S. F. (2014). Issues on estimation of building structure vulnerability. *Magazine of Civil Engineering*, Issue 5 (49), pp. 5–14. DOI: 10.5862/MCE.49.1.

Pshenichkina, V. A., Glukhov, A. V., and Glukhova, S. G. (2019). Probabilistic load parameter modeling in resolving the safety and lifetime assessment problems for buildings and constructions. *The Donbas Constructor*, Issue 2 (7), pp. 58–63.

Rzhanitsyn, A. R. (1982). *Construction mechanics*. Moscow: Vysshaya Shkola, 400 p.

Spaethe, G. (1994). *Reliability of load-bearing building structures*. Moscow: Stroyizdat, 288 p.

Vrouwenvelder, T. (1997). The JCSS probabilistic model code. *Structural Safety*, Vol. 19, Issue 3, pp. 245–251. DOI: 10.1016/S0167-4730(97)00008-8.

ВЛИЯНИЕ ВЕРОЯТНОСТНОГО МЕТОДА СБОРА НАГРУЗОК НА НАДЕЖНОСТЬ И МАТЕРИАЛОЕМКОСТЬ СТРОИТЕЛЬНЫХ КОНСТРУКЦИЙ

Кулигин Дмитрий Дмитриевич*, Школяр Филипп Сергеевич

Санкт-Петербургский политехнический университет Петра Великого, Санкт-Петербург, Россия

*E-mail: dmitrykul17@gmail.com

Аннотация
Введение. Величины нагрузок являются одними из основных факторов, влияющих на оценку надежности строительных конструкций. Все нагрузки по природе имеют вероятностное происхождение, однако наиболее показательными для данного исследования являются кратковременные нагрузки, так как их характер является наиболее стохастическим по сравнению с другими видами нагрузок. Согласно нормативным документам, сбор кратковременных нагрузок на здание необходимо осуществлять, основываясь на базовый период их повторяемости — 50 лет. Из-за многообразия расчетных ситуаций невозможно оптимально унифицировать методы расчета для всех видов зданий, поэтому период повторяемости 50 лет берется для всех видов зданий вне зависимости от их необходимого срока службы, что в некоторых случаях может приводить к закладыванию излишнего запаса надежности. **Методы.** Для сбора нагрузок на конструктивные схемы зданий используются два метода: детерминистский, основанный только на данных из нормативных документов, и вероятностный, принимающий во внимание вероятностную сущность происхождения нагрузок. Оценка надежности проводится по методу предельных состояний и методу А.Р. Ржаницына. **Результаты.** Применение вероятностного метода сбора нагрузок в ряде случаев позволяет снизить жесткостные характеристики сечений, за счет приравнивания периода повторяемости вероятностных нагрузок к необходимому сроку службы здания. Таким образом, гарантия надежности дается не на 50 лет, как при детерминистском методе, а на срок эксплуатации здания, вследствие чего надежность строительных конструкций не снижается на всем закладываемом в них периоде эксплуатации. Данный метод позволил снизить общую массу каркаса производственного здания на 3 %, а малогабаритного — на 27 %, что свидетельствует о более рациональном применении предложенного метода для малых по габаритам схем зданий, так как в крупных схемах выгода в материалоемкости конструкций будет нивелироваться последствиями их отказа и стоимостью оборудования внутри здания.

Ключевые слова: надежность строительных конструкций, характеристики безопасности, период повторяемости, метод предельных состояний

SIMPLIFICATION OF THE REINFORCED CONCRETE ARCHED ROOFING CONSTRUCTION

Irakli Kvaraia*, Ioseb Giorgobiani

Faculty of Civil Engineering, Georgian Technical University, Georgia

*Corresponding author's e-mail: irakvara@yahoo.com

Abstract

In this paper, we discuss issues arising in the construction of cast-in-situ reinforced concrete arched roofs and ways to simplify their design. Despite the versatility of existing mold systems in construction, shell-type roofing structures are entirely different from other structural elements widely used in construction practice in terms of their outline and overall dimensions. Therefore, to erect them, it is necessary to build an individual mold system, which would provide the appropriate spatial shape for cast-in-situ reinforced concrete roofing. Due to the scale of shell roofs, the installation of such mold systems is often associated with significant difficulties as it requires a large, bulky structure above the ground surface with the use of load-bearing scaffolding and planking. This results in issues of building individual elements and the entire mold system and accurately placing them in the design position, which can be solved quite easily using the experience gained from similar works. As a demonstration of this, an example of the arched roof construction for the church named after the Mother of God of Iveria, the second largest church in Georgia, was given a few years ago. At the time, the main difficulty was manufacturing and installing wooden arch molds, which was quickly overcome due to considering several practical measures in advance.

Keywords: shell, mold, column, roofing, reinforced concrete.

Introduction

Due to the dome and vault structural solution of the temple, the central, most significant, cast-in-situ reinforced concrete slab and beam roof served as the unifying part for the columns and walls. The roofing was intended to cover the space with dimensions of 10x24 m. A schematic representation of the roof is given in Fig. 2, where the arrangement of the shell roof and supporting arched beams is indicated, showing the corresponding circumference radii.

`From the schematic representation, it is clear that the arrangement of the arched beam and roof molds requires excellent precision. If we consider section 1-1 (Fig. 1) as a cross-section of the mold, there is a possibility to align and fix the forms within only 0.2 meters of the 10-meter-long beam. Therefore, the most crucial task was to arrange the five arched beam molds to create a complete spatial mold system. It was impossible to manufacture them directly at the site, on the planks arranged on the load-bearing scaffolding. In view of the fact that the ready-made forms must be placed between the reinforced frames of the columns and walls, and their axis of symmetry must coincide with the axes of the columns, it was decided to manufacture the arched beam forms using wooden material. This material made it possible to slightly adjust the dimensions of the molds when installed in the design position, which is impossible in the case of molds made of other materials (metal, plastic, etc.)

(Artebyakina and Shcherbina, 2017; Ezugbaia et al., 2018; Kapanadze and Jankarashvili, 2021; Khmelidze et al., 2018; Kvaraia, 2017; Kvaraia and Firosmanishvili, 2019; Lebanidze et al., 2017; Obukhov et al., 2015; Yunusov, 2016).

During the construction of the arched beam molds, it was necessary to consider some issues in advance so that the installation of the entire mold system could be carried out as efficiently as possible. The most difficult was to comply with one of the seemingly contradictory conditions. In particular, the mold structure, in addition to high strength and stiffness, had to ensure the slightest possibility of expansion and contraction in the longitudinal direction so that, if necessary, it could be accurately fixed according to the design coordinates (Kvaraia, 2015; Kvaraia and Kanchashvili, 2015).

When lifted with a crane and delivered to the work area, the ready-made molds require the arrangement
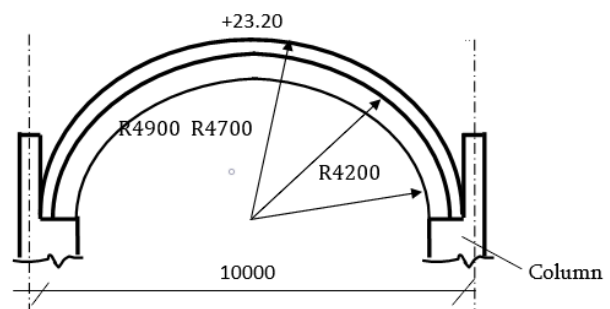

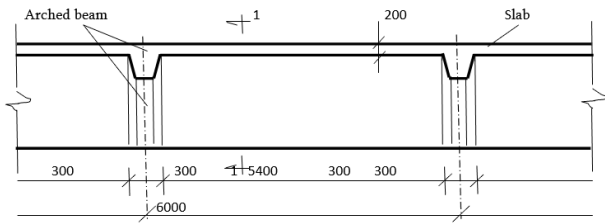Fig. 1. Schematic representation of the shell roof

Fig. 2. Section 1-1

of additional reinforcements so that their separate constituent elements are not deformed during transportation and the overall dimensions of the mold are not changed. In addition, during the construction of the beam mold, it is necessary to consider the arrangement of nodes connecting the roofing arch slab to the mold to obtain a continuous mold system (Kvaraia and Dvalishvili, 2014a, 2014b).

Molding method

The arched beam mold was manufactured directly at the site, mainly using existing wooden planks, beams and plywood, which covered the mold surfaces. All five semi-circular molds 10 meters long and 5 meters high were made of the precise wooden details, and each of them represented a sizeable independent structure (Fig. 3). When being moved to the work site, to maintain strength, each of them was additionally reinforced with wooden frames, which allowed the mold structure to be attached to the crane and delivered to the site (Fig. 4).

The issue of fixing the supporting parts of the frame in the design position was also solved quite easily. For this purpose, directly at the work site, a movable wooden belt was arranged at the bottom of the mold, which, during the mold installation, allowed its supporting parts to move forward and backward using steel screw rods (Fig. 5). It should be noted that the presence of such a belt greatly facilitated the process of forming the concrete beam.

Fig. 4. Transportation of the arched beam molds

After fixing the arched beam mold in the design position, it was also easy to arrange the mold for the roofing slab. For this purpose, shelves made of laminated plywood strips were placed on both sides of the entire perimeter for laying the wooden planks connecting the molds of the adjacent beams (Fig. 6). Paired semi-circular (arched beam outline) laminated plywood elements were also used to reinforce the roofing slab mold, which was installed every 70 cm using jacks (Fig. 7).

After the arched roof mold system was built and adequately reinforced, the reinforcement work was carried out without any problems. The only difficulty was related to concreting the inclined surfaces near the arch supports and maintaining the design thickness of the shell. For this, it was necessary to install and fix the external molds, but within the minimal area, in the case of arranging a standard mold, it would be almost impossible to build it in full after concreting. A non-standard decision was made here as well. A flexible mold was arranged along the entire length of the arched roof, consisting

Fig. 3. Assembly of the arched beam molds

Fig. 5. Movable lower assembly of the arched beam mold

of plywood and spaced planks attached to it. The elastic structure was fixed using reinforcement rods placed every 50 cm from the sides of the planks, which, while maintaining the thickness of the shell, were fastened to the reinforcement frame of the roofing slab with a tie rod (Fig. 8).

Results

The arrangement of the mold of the supporting nodes made it possible to perform continuous concreting of the roof, which went from one support to another (Fig. 9) and finally took the form shown in Fig. 10.

Discussion

To maintain mold stiffness for complex shape building it is necessary to use non-standard mold, which is specifically designed for specific sections of the building. This method also reduces number of mold materials, which itself reduces construction cost.

Conclusion

In the construction of cast-in-situ reinforced concrete arched roofs, it is of particular importance to simplify the process of building the arched beam mold, which requires an individual solution for each

Fig. 8. Assembly of the flexible external mold

Fig. 9. Concreting of the shell roof

Fig. 6. Connection between the roof slab and the beam mold

Fig. 10. Finished shell roof
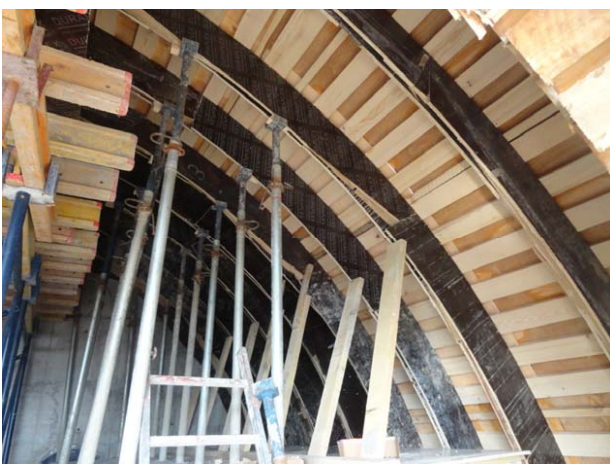

Fig. 7. Reinforcement of the roof slab mold

specific case. The need to create non-standard mold systems is due to the wide variety of the outlines and overall dimensions of envelope roofs, which radically differ from forms for other structural elements widely used in construction practice.

When constructing an arched beam mold, it is necessary to consider in advance several

problematic issues that may occur during their on-site installation. Among them, the most important is the possibility of the slight movement of the mold's supporting parts, allowing them to be accurately fixed in the design position. In this regard, the most effective is the arrangement of a movable belt, which allows the longitudinal expansion and contraction of the mold structure.

When constructing arched roofs, it is difficult to concrete the inclined surfaces near the supports and maintain the design thickness of the concrete shell in these places. When conventional molds are installed, it is almost impossible to shape them further. In this regard, it is better to arrange flexible forms by gluing flexible plywood in a specific manner, which significantly simplifies the process of maintaining the thickness of the slab and concreting the places close to the supports.

Funding

References

Artebyakina, G. I, and Shcherbina, V. A. (2017). Review of structural solutions for durable roofing of public buildings. *Young Scientist*, No. 6 (140), pp. 29–31.

Ezugbaia, Z., Kvaraia, I., Iremashvili, I. & Mskhiladze, N., 2018. *Construction production technology.* 1st ed. Tbilisi: Georgian Technical university.

Kapanadze, L. & Jankarashvili, D., 2021. Calculation of shells and slabs (literature review). *Construction,* I(57), pp. 116–120.

Khmelidze, T., Kipiani, G. & Khmelidze, K., 2018. *Monuments of Georgian architecture.* 1st ed. Tbilisi: Universal.

Kvaraia, I., 2015. *Solving arising problems during concreting of reinforced concrete shells.* 1st ed. Tbilisi: Georgian Technical University.

Kvaraia, I., 2017. *Methods of building mold systems for reinforced concrete dome-arch roofs and examle of their use.* 1st ed. Tbilisi: Georgian Technical University.

Kvaraia, I. & Dvalishvili, T., 2014. Arranging the mold of reinforced concrete arched beams. *Construction,* II(33), pp. 102–104.

Kvaraia, I. & Dvalishvili, T., 2014. Simplification of reinforced concrete constructions. *Construction,* III(34), pp. 75–77.

Kvaraia, I. & Firosmanishvili, A., 2019. Technological features of the arrangment of reinforced concrete arch beams. *Construction,* I(50), pp. 53–55.

Kvaraia, I., Kanchashvili, S. & Dvalishvili, T., 2015. Arrangement of simple moving nodes during the construction of reinforced concrete formwork systems. *Construction,* IV(39), pp. 54–56.

Lebanidze, A., Maisuradze, G. & Vardiashvili, D., 2017. Large reinforced concrete constructions. *Construction,* III(46), pp. 41–44.

Obukhov, A. Ye., Leonovich, S. N., and Bursov, N. G. (2015). Technology of constructing temple structures out of cast-in-situ reinforced concrete in modern formwork systems. In: Zverev, V. F., Koleda, S. M., and Delendik, S. N. (eds.) *Current Issues of Implementing European Standards in Construction: Collected International Research and Technical Papers (Proceedings of the Research and Methodological Conference)*. In 2 parts. Part 2. Minsk: Belarusian National Technical University, pp. 58–74.

Yunusov, A. S. (2016). Arch designs demanded by the time in building sciences and architecture. *Engineering Journal of Don*, Issue 2. [online] Available at: http://www.ivdon.ru/en/magazine/archive/n2y2016/3586 [Date accessed December 1, 2016].

УПРОЩЕНИЕ ПРОЦЕССА УСТРОЙСТВА ЖЕЛЕЗОБЕТОННОЙ СВОДЧАТОЙ КРОВЛИ

Иракли Квараия* (Irakli Kvaraia), Иосеб Гиоргобиани (Ioseb Giorgobiani)

Факультет гражданского строительства, Грузинский технический университет, Грузия

*E-mail: irakvara@yahoo.com

Аннотация

В данной статье рассматриваются проблемы, возникающие при устройстве монолитных железобетонных сводчатых крыш, и способы упрощения их проектирования. Несмотря на универсальность существующих в строительстве опалубочных систем, оболочечные кровельные конструкции по своим очертаниям и габаритным размерам совершенно не похожи на другие структурные элементы, широко применяемые в строительной практике. Поэтому для их устройства необходимо формировать индивидуальную опалубочную систему, которая обеспечит соответствующую пространственную форму для монолитной железобетонной кровли. В связи с размером оболочечных покрытий устройство таких опалубочных систем зачастую сопряжено со значительными трудностями, поскольку требует возведения над поверхностью земли громоздкой конструкции с использованием несущих лесов и настилов. В результате возникают проблемы с изготовлением отдельных элементов и опалубочной системы в целом, а также их точным размещением в проектном положении, которые можно достаточно легко решить, используя опыт, полученный в ходе аналогичных работ. В качестве наглядной демонстрации несколько лет назад был приведен пример устройства сводчатой кровли для церкви в честь Иверской Божией Матери, второй по величине церкви в Грузии. В этот период основная сложность заключалась в изготовлении и установке арочных деревянных опалубочных форм, которую удалось быстро преодолеть благодаря заблаговременному применению ряда практических мер.

Ключевые слова: оболочка, опалубочная форма, колонна, кровля, железобетон.

COMPARISON OF THE SHEAR STRENGTH IN HEAVY AND SELF-COMPACTING CONCRETE

Grigory Nesvetaev, Yuliya Koryanova, Anton Chepurnenko*

Don State Technical University, Rostov-on-Don, Russia

*Corresponding author's e-mail: anton_chepurnenk@mail.ru

Abstract

Introduction. The shear strength of concrete, while not being an independently standardized indicator of concrete quality, plays an important role in the analysis of reinforced concrete structures. The concepts related to the dependence of the shear strength of concrete on the standardized compressive and axial tensile strength are quite ambiguous. Self-compacting concrete (SCC), which has been widely used recently, is somewhat different from ordinary concrete (OC) compacted by vibration in terms of structure and properties, and data on the shear strength of SCC are sparse. **Purpose of the study**: We aimed to clarify the dependence of the shear strength of concrete on the standardized compressive and axial tensile strength, and assess the shear strength of SCC in comparison with that of OC. **Methods**: We compared the shear strength of SCC with that of OC experimentally, by applying the common methodology with the use of a Mörsch specimen and performing modeling in MATLAB with the use of six strength theories. **Results**: No significant differences were found in the dependence of the shear strength of SCC in comparison with that of OC at the design age of 28 days. In terms of quantity, the excess of the shear strength of SCC relative to OC is less than 12%. The best agreement with the experimental data among those analyzed is provided by the Geniev theory. The shear strength of concretes is most likely described by the equation $R_{sh} = k\sqrt{R \cdot R_t}$ at k = 0.5–0.6.

Keywords: shear strength, self-compacting concrete, strength theories, fracture criteria.

Introduction

The shear strength of concrete is essential, for example, in the behavior of column consoles, including those made of widely used SCC (Dhanabal and Sreevidya, 2018; Prakash et al., 2021), the ultimate resistance calculation (Filatov et al., 2020), the assessment of the monolithic character of reinforced concrete structures erected with horizontal or vertical construction joints, and in other cases. A comprehensive review of the shear strength of concrete was given by Palieraki et al. (2021). It is known that the fracture of masonry materials, including concrete, can occur as a result of splitting and (or) shear (Timoshenko, 1950). When assessing the magnitude of the transverse force in reinforced concrete elements subject to bending, researchers usually take into account the limiting value of shear stresses as the main factor. This factor is considered as the resistance of concrete to shear. In the shear and ultimate resistance calculation of structures, the compressive or tensile strength of concrete are commonly used. The shear strength of concrete, in contrast to, for example, the tensile strength, is not standardized depending on the class of concrete. One of the earliest methods to calculate the ultimate resistance was to use the assessment of shear stresses and compare them to concrete properties (Talbot, 1913). The values of the shear strength of fine-grained concrete ranged from 3.7 to 6.5 MPa. The shear strength of concrete

was considered (Borishansky, 1946; Gvozdev, 1949; Morsh, 1903; Stolyarov, 1941) as the ratio Rsh/R (shear/compression) in the following form: $Rsh = k \cdot R$ at, e.g., k = 0.2 (Stolyarov, 1941), k = 0.166…0.195 (Gvozdev, 1949), k = 0.15 (Borishansky, 1946). Some dependences of the shear strength of concrete on the compressive and tensile strength are given in Table 1.

Fig. 1. Dependence of the shear strength on the compressive strength according to Table 1.

The results presented (Fig. 1) show a significant divergence of views regarding the shear strength of concrete. The available experimental data are also quite ambiguous (Dovzhenko et al., 2016). In the construction of various reinforced concrete structures, SCCs are widely used, the macrostructure and deformation properties of which are somewhat different from those of ordinary concretes compacted by vibration (Dey et al., 2021; Liu et al., 2021; Mailyan et al., 2023; Stel'makh et al., 2022; Uğur and Ünal, 2022; Zeng et al., 2021). It seems relevant to compare the available (Table 1) suggestions for assessing the shear strength of concrete depending on the standardized values of the compressive and axial tensile strength and compare the shear strength of SCC relative to OC, especially in connection with the revealed (Nesvetaev et al., 2022b) tendency of increased brittleness in SCC in the early (up to 3 days) curing period. Some results of assessing the shear strength of SCC (De Gois Laufer and Savaris,

Table 1. **Some equations to determine the shear strength of concrete**

No.	Equation	Reference	Possible representation of the equation as suggested by the authors*
1	$R_{sh} = 2 \cdot R_t$	Stolyarov, 1941	$R_{sh} = 0.58 \cdot R^{0.6*}$
2	$R_{sh} = 0.2 \cdot R$	Stolyarov, 1941	
3	$R_{sh} = 0.7\sqrt{R \cdot R_t}$	Mikhailov, 1977	$R_{sh} = 0.377 \cdot R^{0.8*}$
4	$R_{sh} = k \cdot \sqrt{R \cdot R_t}$, $k = 0.5...1$	Golyshev et al., 1990	$R_{sh} = (0.27...0.539) \cdot R^{0.8*}$
5	$R_{sh} = 0.5\sqrt{R \cdot R_t}$	Nesvetaev and Belyaev, 2016	$R_{sh} = 0.27 \cdot R^{0.8*}$
6	$R_{sh} = (0.15...0.3) \cdot R$	Krasnoschekov and Galuzina, 2016	
7	$R_{sh} = \left(0.093 \cdot (10R)^{\frac{2}{3}}\right)$	Ctcmetar.ru, 2023	$R_{sh} = 0.43 \cdot R^{2/3}$
8	$R_{sh} = 0.5 \cdot R_t$	Maximum-shear theory (Tresca–Saint-Venant)	$R_{sh} = 0.145 \cdot R^{0.6*}$
9	$Q_{b1} = 0.5 \cdot R_{bt} \cdot b \cdot h_0$	Regulations SP 63.13330.2018, Eq. 8.61	$R_{sh} = 0.5 \cdot R_{bt} = 0.22 \cdot R^{0.6*}$
10	$R_{sh} = k \cdot \sqrt{R}$, $k = f(R) = 0.41...0.58$	De Gois Laufer and Savaris, 2021	
11	$R_{sh} = 0.75 \cdot \sqrt{R \cdot R_t}$	Zhang et al., 2020	$R_{sh} = 0.4 \cdot R^{0.8}$

Note: 1 — R_{bt} — the class of concrete by axial tensile strength, R_{btn} — the axial tensile strength of concrete, $R_{btn} = 1.5 \cdot Rbt$; R, R_t — the experimental values of the compressive and axial tensile strength in the studies; * — with account for $R_t = 0.29 \cdot R^{0.6}$ (Nesvetaev et al., 2022a)

2021) show relatively low values (Fig. 1, 10, max). This study compares the shear strength of SCC with that of OC, by applying the common methodology as a function of the values of the compressive and axial tensile strength standardized for concretes. In addition to the experimental studies, the shear strength of SCC and OC was assessed with the use of six widely known strength theories.

Subject, tasks, and methods
Methodology of experimental studies
Since the methodology of determining the shear strength of concrete is not regulated by regulatory documents, various specimens are used in experimental studies. According to (Dovzhenko et al., 2016), the most common way to determine the shear strength of concrete is to use the Gvozdev specimen
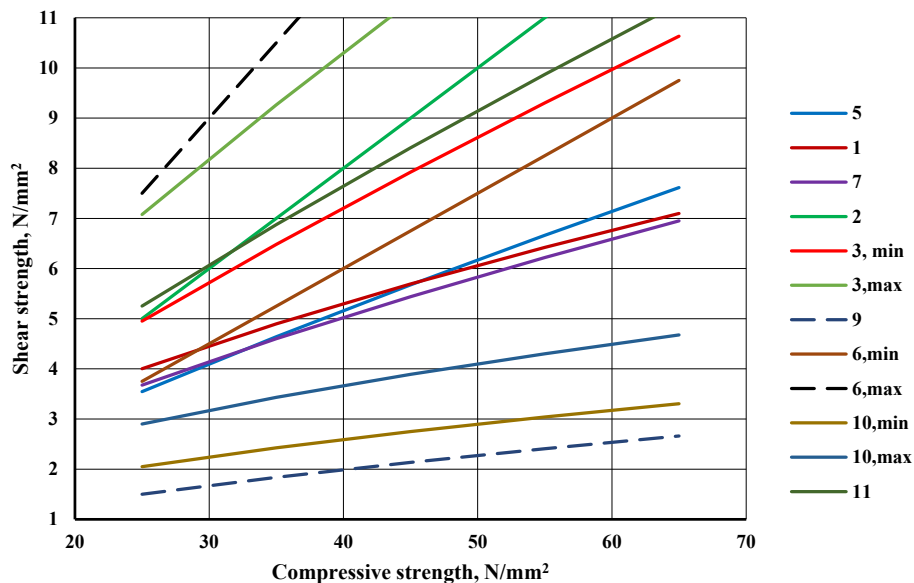

Fig. 1 graphically shows the dependences according to Table 1

or the Mörsch specimen. Both specimens provide almost identical statistical values (Dovzhenko et al., 2016). According to Dovzhenko et al. (2016), the Gvozdev specimen shows a better agreement between the theoretical and experimental values. According to Petrov (1967) and Verigin (1960), it is impossible to provide test conditions corresponding to pure shear for brittle materials, therefore, the shear strength should be excluded from the theory of brittle materials strength. However, in engineering practice, methods providing some conditional values for practical purposes are widely used in production control or comparative tests. Therefore, since the Mörsch specimen is easier to manufacture and tests involving it are quite simple and easily reproducible, we used it in our experimental studies (Fig. 2).

The experimental studies were performed with the use of four OC series made with four different W/C ratios without chemical additives and three SCC series made with three different W/C ratios using polycarboxylate-ether superplasticizers (Plank et al., 2009). In the experimental studies, ordinary concrete mixtures with consistency grade P2 according to GOST 7473-2010 for OC were used. Concrete mixtures for SCC corresponded to grade RK1 according to GOST R 59714-2021 (SF1 according to EN) with a W/C ratio from 0.4 to 0.55. The compressive strength at the design age varied for OC from 35.5 to 52.4 MPa, and for SCC — from 50.1 to 61.6 MPa. Concrete specimens 100x100x310 mm were used as Mörsch specimens (Fig. 2). To determine the compressive and tensile strength (in splitting), specimens 100x100x100 mm according to GOST 10180-2012 were used. The number of specimens in a series was taken according to GOST 10180-2012. Portland cement CEM I 42.5, crushed granite with a particle size of 5–20 mm, and quartz river sand with a particle size of 0.14–2.5 mm were used. The specimens were tested at the design age after 28 days of curing under normal conditions.

Methodology for numerical analysis

Numerical modeling was performed in two-dimensional formulation by the finite element method based on six strength criteria:

1. Maximum-shear theory (Tresca–Saint-Venant). According to this theory, the strength condition has the following form:

$$\sigma_1 - \sigma_3 \leq R_t. \tag{1}$$

2. Mohr's strength theory (Andreev et al., 2014):

$$\sigma_1 - \chi\sigma_3 \leq R_t, \quad \chi = \frac{R_t}{R}. \tag{2}$$

3. Pisarenko–Lebedev theory (Bazhenov et al., 2022):

$$(1-\chi)\cdot\sigma_0 + \frac{\sigma_i}{3}\left(3\chi + (1-\chi)\left(\sqrt{3}\cdot\cos\psi - \sin\psi\right)\right) \leq R_t;$$

$$\sigma_0 = \frac{\sigma_1 + \sigma_2 + \sigma_3}{3};$$

$$\sigma_i = \frac{1}{\sqrt{2}}\sqrt{(\sigma_1 - \sigma_2)^2 + (\sigma_2 - \sigma_3)^2 + (\sigma_1 - \sigma_3)^2};$$

$$\psi = \frac{1}{3}\mathrm{asin}\left(\frac{27 I_3}{2\sigma_i^3}\right);$$

$$I_3 = (\sigma_1 - \sigma_0)(\sigma_2 - \sigma_0)(\sigma_3 - \sigma_0). \tag{3}$$

4. Balandin's strength criterion (Andreev and Potekhin, 2019):

$$F(\sigma_1, \sigma_2, \sigma_3) = \sigma_1^2 + \sigma_2^2 + \sigma_3^2 -$$
$$- (\sigma_1\sigma_2 + \sigma_2\sigma_3 + \sigma_1\sigma_3) +$$
$$+ (R - R_t)\cdot 3\sigma_0 - R\cdot R_t \leq 0. \tag{4}$$

5. Luksha's strength criterion (Luksha, 1977):

$$F(\sigma_1, \sigma_2, \sigma_3) = \sigma_1^2 + \sigma_2^2 + \sigma_3^2 -$$
$$- 2\cdot(\sigma_1\sigma_2 + \sigma_2\sigma_3 + \sigma_1\sigma_3) +$$
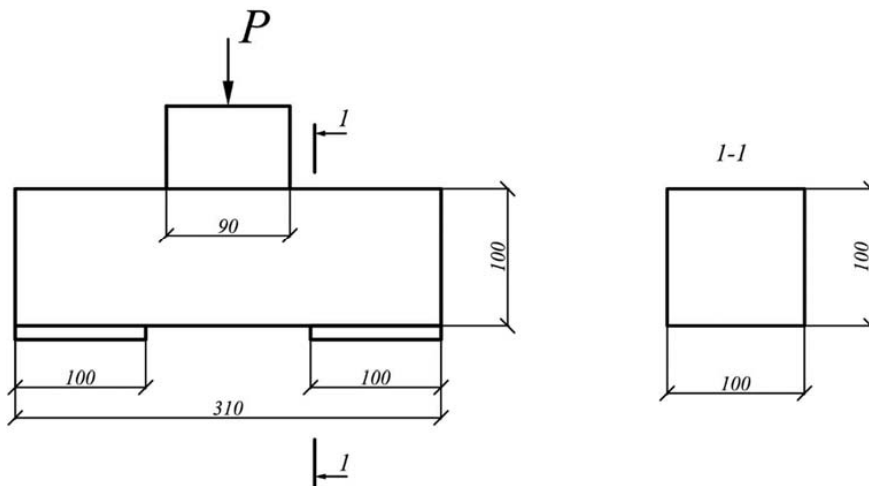$$+ (R - R_t)\cdot 3\sigma_0 - R\cdot R_t \leq 0. \tag{5}$$

Fig. 2. Test scheme

6. Geniev strength theory (Chepurnenko et al., 2021):

$$F\left(\sigma_1,\sigma_2,\sigma_3\right) = \tau_i^2 - T_c\left(T_c + \lambda\tau_i\right)\left(1+\delta\right) \leq 0;$$

$$\tau_i = \frac{1}{\sqrt{6}}\sqrt{\left(\sigma_1-\sigma_2\right)^2+\left(\sigma_2-\sigma_3\right)^2+\left(\sigma_1-\sigma_3\right)^2};$$

$$\lambda = \frac{f\sigma_0}{\tau_i}, f = \frac{3\tau_i\left(R-R_t\right)}{R\cdot R_t};$$

$$\delta = e\left(\frac{S}{\tau_i}\right)^3, S = \sqrt{3}\left[\frac{1}{2}\cdot I_3\right]^{\frac{1}{3}}, \qquad (6)$$

where T_c — ultimate shear stress intensity at pure shear.

To determine the breaking load according to the above strength criteria, a program was developed in the MATLAB environment. Because of symmetry, half of the specimen was considered. The calculation model is shown in Fig. 3.

Results and discussion

During the experimental studies with the use of the Mörsch specimen, various cases of fracture were observed (Fig. 4), which is consistent with the statement (Petrov, 1967) that the Mörsch specimen experiences shear, bending and local buckling under loading.

According to Stolyarov (1941), during tests involving the Mörsch specimen, at first, the initial crack under scheme C appears (Fig. 4). Further, fracture under scheme A ("pure" shear according
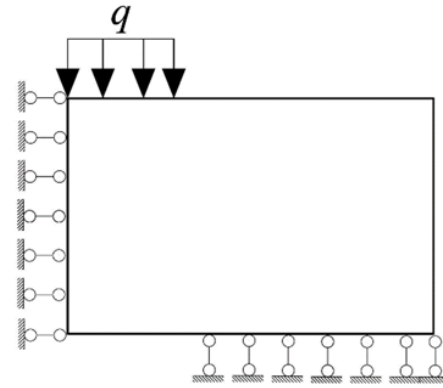

Fig. 3. Calculation model

to Stolyarov (1941)) or scheme B (i.e., bending and "pure shear") is possible. However, in our studies, all the above cases were observed as the final scheme, with only Scheme C fracture being a one-off case. This is probably due to the higher deformability of SCC.

Table 2 presents the results of modeling the Mörsch specimen fracture schemes using various strength theories in the form of mosaics of equivalent stresses.

Table 3 shows a comparison of the experimental and theoretical values of the shear strength of concrete for OC and SCC specimens. The shear strength was calculated by different strength theories (Table 2).

Fig. 4. Cases of specimen fracture when determining the shear strength of concrete: (a) by shear stresses ("pure shear" according to Stolyarov (1941)); (b) by shear and normal stresses ("shear" and "bending"); (c) by normal stresses ("bending")
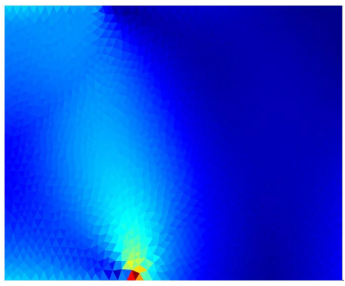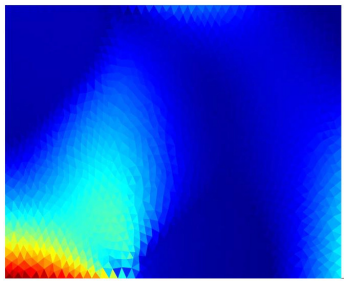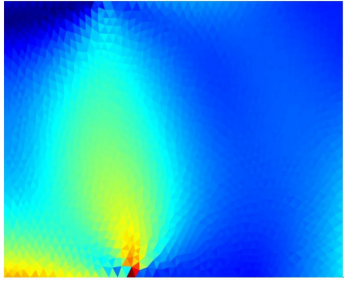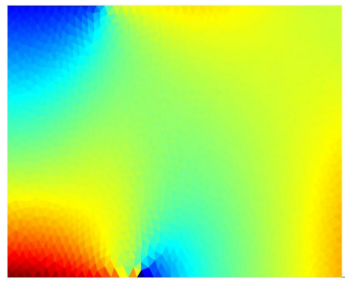
Table 2. **Numerical modeling results**

Table 2 (continued)

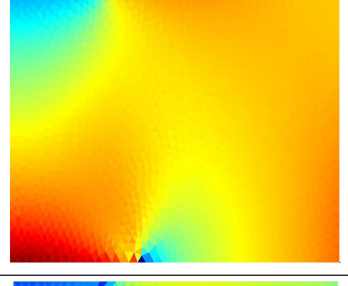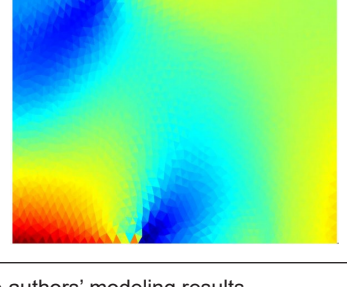| No.	Theory	Result
1	Tresca–Saint-Venant Possible fracture scheme (a), Fig. 4 Conditional shear strength[1]: $R_{sh} = 0.1 \cdot \sqrt{R \cdot R_t}$	
2	Mohr Possible fracture scheme (c), Fig. 4 Conditional shear strength[1]: $R_{sh} = 0.34 \cdot \sqrt{R \cdot R_t}$	
3	Pisarenko–Lebedev Possible fracture scheme (b), Fig. 4 Conditional shear strength[1]: $R_{sh} = 0.61 \cdot \sqrt{R \cdot R_t}$	

No.	Theory	Result
4	Balandin Possible fracture scheme (c), Fig. 4 Conditional shear strength[1]: $R_{sh} = 0.23 \cdot \sqrt{R \cdot R_t}$	
5	Luksha Possible fracture scheme (c), Fig. 4 Conditional shear strength[1]: $R_{sh} = 0.62 \cdot \sqrt{R \cdot R_t}$	
6	Geniev Possible fracture scheme (c), Fig. 4 Conditional shear strength[1]: $R_{sh} = 0.58 \cdot \sqrt{R \cdot R_t}$	

Note: 1 — based on the authors' modeling results

In the determination of the shear strength of concrete, the modeling results (Table 2) confirmed the possibility of the Mörsch specimen fracture according to the scheme presented in Fig. 4 by all options (a)–(c). Therefore, during the results processing, the shear strength of concrete in our studies in all cases was determined as the value of the breaking force based on the cross-section area, regardless of the fracture scheme.

According to Table 3, the shear strength of concrete can be represented by the following relationship:

$$R_{sh} = k \cdot \sqrt{R \cdot R_t}. \qquad (7)$$

Table 4 shows dependences for the shear strength of OC and SCC according to the authors' experimental data.

Fig. 5 shows a comparison of the experimental results for the shear strength of concrete with values from Table 2 and some dependences from Table 1.

The results of the studies show the following:

- since the difference in the values of the coefficients in the equations of Table 4 (0.59/0.53 = 1.113) for the shear strength of SCC at the design age of 28 days in comparison with OC does not exceed 12%, we can argue that, at the design age, the shear strength of SCC is insignificantly higher than that of OC; the issue of whether or not it is reasonable to consider this fact for practical purposes can be further discussed;

- the best agreement with our experimental data is provided by the Geniev strength theory, the ratio of the calculated values and average experimental values is as follows: $R_{sh,calc}/R_{sh,test}$ = 0.98 for SCC and $R_{sh,calc}/R_{sh,test}$ = 1.09 for OC;

- the Balandin criterion also provides close values: $R_{sh,calc}/R_{sh,test}$ = 1.03 for SCC and $R_{sh,calc}/R_{sh,test}$ = 1.15 for OC;

- the Luksha theory provides a good result: $R_{sh,calc}/R_{sh,test}$ = 1.05 for SCC and $R_{sh,calc}/Rsh,test$ = 1.17 for OC;

- the best agreement with our experimental data is provided by Eq. (4) in Table 1 at k = 0.5–0.6.

Conclusions

As a result of the studies, no significant difference between the shear strength of SCC and that of OC, depending on the $\sqrt{R \cdot R_t}$ value, was revealed; the difference does not exceed 12 %. The best agreement with the experimental data among those

Table 3. **Experimental and theoretical values of the shear strength of concrete with the use of the Mörsch specimen**

No.	Strength values, MPa			R_{sh}, MPa Experiment	R_{sh}, MPa Theory according to Table 2					
	R	R_t	$\sqrt{R \cdot R_t}$		1	2	3	4	5	6
SCC										
1	50.1	2.76	11.8	7.12	1.15	3.95	2.75	7.35	7.5	6.85
2	57.9	2.84	12.8	7.87	1.2	4.2	2.85	7.8	7.85	7.4
3	61.6	3.11	13.8	7.86	1.3	4.5	3.1	8.35	8.4	7.85
OC										
4	35.5	1.65	7.65	4.67	0.725	2.48	1.67	4.58	4.63	4.35
5	41.8	2.63	10.5	6.06	1.09	3.71	2.59	6.53	6.68	6.19
6	47.9	2.81	11.6	5.6	1.16	4.01	2.78	7.2	7.31	6.68
7	52.4	3.12	12.8	6.6	1.3	4.45	3.1	8	8.2	7.5
8**	21.3*	1.79*	6.2*	3.6*	0.75	2.38	1.73	4.1	4.15	3.78

Notes: 1–7 — according to the authors' data; 8 — Petrov (1967); * — according to the authors' assessment; ** — fine-grained concrete

Table 4. **Suggested equations for determining the shear strength of OC and SCC**

No.	Concrete	Equation	R^2
1	OC	$R_{sh} = 0.53\sqrt{R \cdot R_t}$	0.993
2	SCC	$R_{sh} = 0.59\sqrt{R \cdot R_t}$	0.999

analyzed is provided by the Geniev strength theory. The Tresca–Saint-Venant, Pisarenko–Lebedev and Mohr strength theories are not applicable in describing the shear behavior of concrete. The shear strength of concrete is most likely described by the equation $R_{sh} = k\sqrt{R \cdot R_t}$ at k = 0.5–0.6.
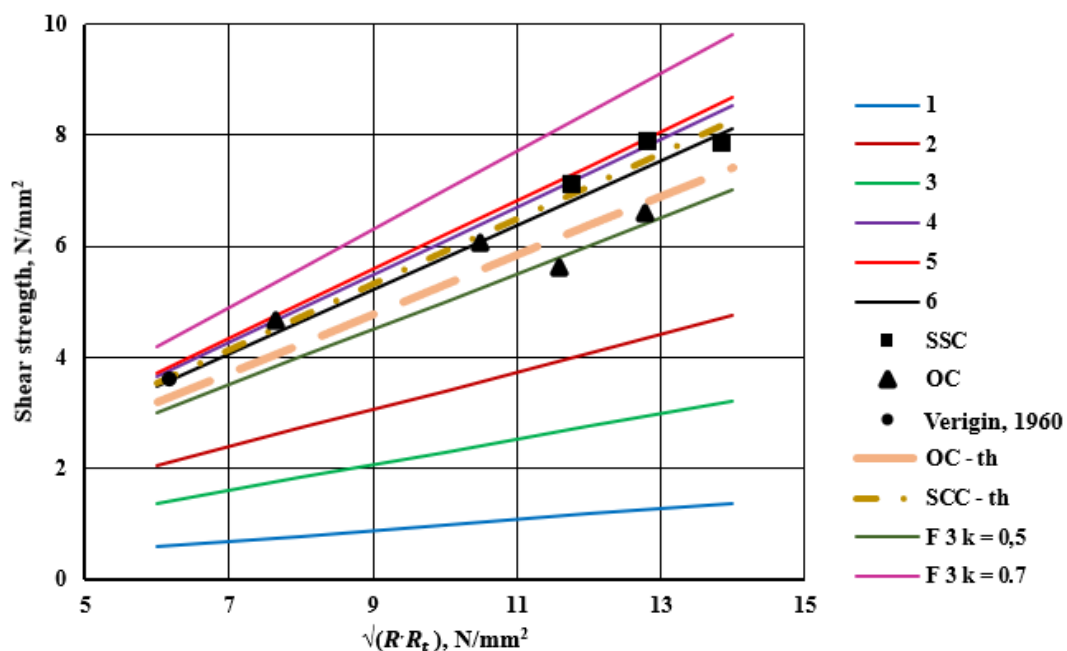

Fig. 5. Dependence of the shear strength of concrete on the compressive and tensile strength:
1–6 — the strength theories according to Table 2, respectively;
OC — experimental data for OC (Table 3);
SCC — experimental data for SCC (Table 3);
OC-th, SCC-th — by Eqs. 1, 2, Table 4;
F3 k=0.5 and 0.7 — by equations similar in structure to Eq. (4) in Table 1 at k = 0.5 and 0.7

References

Andreev, V. I., Chepurnenko, A. S., and Jazyev, B. M. (2014). Model of equal-stressed cylinder based on the Mohr failure criterion. *Advanced Materials Research,* Vol. 887–888, pp. 869-872. DOI: 10.4028/www.scientific.net/AMR.887-888.869.

Andreev, V. and Potekhin, I. (2019). Calculation of equal strength thick-walled concrete cylinder with free ends. *IOP Conference Series: Materials Science and Engineering*, Vol. 661, 012023. DOI: 10.1088/1757-899X/661/1/012023.

Bazhenov, V. G., Osetrov, S. L., Osetrov, D. L., and Ryabov, A. A. (2022). Coupled fracture model of elastoplastic materials based on a kinetic equation of damage accumulation and the Pisarenko–Lebedev strength criterion. *Journal of Applied Mechanics and Technical Physics*, Vol. 63, Issue 1, pp. 104–110. DOI: 10.1134/S0021894422010163.

Borishansky, M. S. (1946). *Calculation of bent rods and clamps in reinforced concrete elements subject to bending at the stage of failure*. Leningrad, Moscow: Gosstroyizdat, 79 p.

Chepurnenko, A., Yazyev, B., Meskhi, B., Beskopylny, A., Khashkhozhev, K., and Chepurnenko, V. (2021). Simplified 2D finite element model for calculation of the bearing capacity of eccentrically compressed concrete-filled steel tubular columns. *Applied Sciences*, Vol. 11, Issue 24, 11645. DOI: 10.3390/app112411645.

Ctcmetar.ru (2023). *Strength of concrete*. [online] Available at: https://ctcmetar.ru/stroitelnoe-materialovedenie/2137-prochnost-betona.html [Date accessed January 12, 2023].

De Gois Laufer, I. and Savaris, G. (2021). Shear strength of steel fiber self-compacting concrete beams. *Semina: Ciências Exatas e Tecnológicas*, Vol. 42, No. 1, pp. 45–62. DOI: 10.5433/1679-0375.2021v42n1p45.

Dey, S., Praveen Kumar, V. V., Goud, K. R., and Basha, S. K. J. (2021). State of art review on self compacting concrete using mineral admixtures. *Journal of Building Pathology and Rehabilitation*, Vol. 6, Issue 1, 18. DOI: 10.1007/s41024-021-00110-9.

Dhanabal, G. and Sreevidya, V. (2018). Shear strength characteristics of self compacting geopolymer concrete cast at different ages. *International Journal of Latest Engineering and Management Research*, Vol. 3, Issue 4, pp. 38–43.

Dovzhenko, O. O., Pohribnyi, V. V., Usenko, I. S., Mal'ovana, O. O., and Akopyan, M. K. (2016). Concrete elements strength under the shear action according to the variation method in the theory of plasticity and tests. *ISJ Theoretical & Applied Science*, Vol. 44, Issue 12, pp. 12–18. DOI: 10.15863/TAS.2016.12.44.3.

Filatov, V. B., Galyautdinov, Z. Sh., and Kovalenko, M. V. (2020). Experimental study of the work of a reinforced concrete floor slab under punching by column. *Engineering Journal of Don*, *Issue 6*. [online] Available at: http://ivdon.ru/en/magazine/archive/N6y2020/6518 [Date accessed January 12, 2023].

Golyshev, A. B., Bachinsky, V. Ya., Polishchuk, V. P., Kharchenko, A. V., and Rudenko, I. V. (1990). *Design of reinforced concrete structures: a reference manual*. 2nd edition. Kiev: Budivelnik, 544 p.

Gvozdev, A. A. (1949). *Calculation of bearing capacity by the method of limit equilibrium*. Moscow: Stroyizdat, 280 p.

Krasnoschekov, Yu. V. and Galuzina, R. A. (2016). Strength of concrete as fracture resistance. *Vestnik SibADI (Siberian State Automobile and Highway University)*, No. 1 (47), pp. 61–65.

Liu, Z., Chen, X., Wu, P., and Cheng, X. (2021). Investigation on micro-structure of self-compacting concrete modified by recycled grinded tire rubber based on X-ray computed tomography technology. *Journal of Cleaner Production*, Vol. 290, 125838. DOI: 10.1016/j.jclepro.2021.125838.

Luksha, L. K. (1977). Strength of thick-walled vessels of brittle materials under external pressure. *Strength of Materials*, Vol. 9, Issue 2, pp. 178–182.

Mailyan, L. R., Stel'makh, S. A., Shcherban', E. M., Kholodnyak, M. G., Smolyanichenko, A. S., Parinov, I. A., and Cherpakov, A. V. (2023). Features of electrophysical impact on mortar and concrete mixtures. In: *Management of Structure Formation and Properties of Cement Concretes. Innovation and Discovery in Russian Science and Engineering*. Cham: Springer, pp. 177–215. DOI: 10.1007/978-3-031-08919-0_9.

Mikhailov, K. V. (ed.) (1977). *New on the strength of reinforced concrete*. Moscow: Stroyizdat, 272 p.

Morsh, E. (1903). Versuche Uber schubspannugen in betoncisentregern. *Beton und Eisen*, Vol. 2, No. 4, pp. 269–274.

Nesvetaev, G. V. and Belyaev, A. V. (2016). About adhesion between structural LWA concrete and ordinary concrete in the in-situ layered slabs. *Naukovedenie*, Vol. 8, No. 4. [online] Available at: http://naukovedenie.ru/PDF/24TVN416.pdf [Date accessed January 12, 2023].

Nesvetaev, G. V., Koryanova, Y. I., Chepurnenko, A. S., and Sukhin, D. P. (2022a). On the issue of modeling thermal stresses during concreting of massive reinforced concrete slabs. *Engineering Journal of Don*, Issue 6. [online] Available at: http://ivdon.ru/en/magazine/archive/n6y2022/7691 [Date accessed January 12, 2023].

Nesvetaev, G. V., Koryanova, Y. I., and Sukhin, D. P. (2022b). On the influence of hardening conditions on the properties of self-compacting concrete. *Engineering Journal of Don*, Issue 10. [online] Available at: http://ivdon.ru/en/magazine/archive/n10y2022/7927 [Date accessed January 12, 2023].

Palieraki, V., Vintzileou, E., and Silva, J. F. (2021). Behavior of RC interfaces subjected to shear: State-of-the art review. *Construction and Building Materials*, Vol. 306, 124855. DOI: 10.1016/j.conbuildmat.2021.124855.

Petrov, A. N. (1967). On the interpretation of shear in concrete. In: *Building Structures*, Issue 6. Kiev: Budivelnik, pp. 181–188.

Plank, J., Schroefl, C., Gruber, M., Lesti, M., and Sieber, R. (2009). Effectiveness of polycarboxylate superplasticizers in ultra-high strength concrete: the importance of PCE compatibility with silica fume. *Journal of Advanced Concrete Technology*, Vol. 7, No. 1, pp. 5–12. DOI: 10.3151/JACT.7.5.

Prakash, R., Raman, S. N., Divyah, N., Subramanian, C., Vijayaprabha, C., and Praveenkumar, S. (2021). Fresh and mechanical characteristics of roselle fibre reinforced self-compacting concrete incorporating fly ash and metakaolin. *Construction and Building Materials*, Vol. 290, 123209. DOI: 10.1016/j.conbuildmat.2021.123209.

Stel'makh, S. A., Shcherban, E. M., Beskopylny, A., Mailyan, L. R., Meskhi, B., Beskopylny, N., and Zherebtsov, Y. (2022). Development of high-tech self-compacting concrete mixtures based on nano-modifiers of various types. *Materials*, Vol. 15, Issue 8, 2739. DOI: 10.3390/ma15082739.

Stolyarov, Ya. V. (1941). *Introduction to the theory of reinforced concrete*. Leningrad, Moscow: Gosstroyizdat, 447 p.

Talbot, A. N. (1913). *Reinforced concrete wall footings and column footings. Bulletin No. 67*. Urbana, Illinois: University of Illinois, 114 p.

Timoshenko, S. P. (1950). *Strength of materials: Part 1. Elementary theory and problems*. New York: Van Nostrand, 359 p.

Uğur, A. E. and Ünal, A. (2022). Assessing the structural behavior of reinforced concrete beams produced with macro synthetic fiber reinforced self-compacting concrete. *Structures*, Vol. 38, pp. 1226–1243. DOI: 10.1016/j.istruc.2022.02.051.

Verigin, K. P. (1960). Resistance of concrete to fracture under simultaneous action of axial tension and compression. *Concrete and Reinforced Concrete*, No. 10, pp. 479-480.

Zeng, Z.-P., Huang, X.-D., Yan, B., Wang, W.-D., Shuaibu, A. A., and He, X.-F. (2021). Research on the fatigue performance of self-compacting concrete structure in CRTSIII slab ballastless track under the action of heavy haul train. *Construction and Building Materials*, Vol. 303, 124465. DOI: 10.1016/j.conbuildmat.2021.124465.

Zhang, X., Zhang, W., Luo, Y., Wang, L., Peng, J., and Zhang, J. (2020). Interface shear strength between self-compacting concrete and carbonated concrete. *Journal of Materials in Civil Engineering*, Vol. 32, Issue 6, 04020113. DOI: 10.1061/(ASCE)MT.1943-5533.0003229.

СРАВНЕНИЕ ПРОЧНОСТИ НА СРЕЗ ТЯЖЕЛОГО И САМОУПЛОТНЯЮЩЕГОСЯ БЕТОНОВ

Несветаев Григорий Васильевич, Корянова Юлия Игоревна, Чепурненко Антон Сергеевич*

Донской государственный технический университет, г. Ростов-на-Дону, Россия

*E-mail: anton_chepurnenk@mail.ru

Аннотация
Введение. Предел прочности бетона на срез, не являясь самостоятельно нормируемым показателем качества бетона, играет важную роль при расчетах железобетонных конструкций. Представления о зависимости предела прочности бетона на срез от нормируемых показателей прочности на сжатие и осевое растяжение достаточно неоднозначны. Широко применяющийся в последнее время самоуплотняющийся бетон (СУБ) имеет некоторые отличия от традиционного бетона вибрационного уплотнения (ТБ) по структуре и свойствам, а данные о прочности на срез СУБ немногочисленны. **Цель исследования**: уточнение зависимости прочности бетона на срез от нормируемых показателей прочности на сжатие и осевое растяжение, оценка прочности на срез СУБ в сравнении с ТБ. **Методы**: Сравнение прочности на срез СУБ и ТБ выполнено экспериментально по единой методике с использованием образца Мерша и моделированием в среде MATLAB с использованием 6 теорий прочности. **Результаты**: Не выявлено существенного отличия зависимости предела прочности на срез в проектном возрасте 28 сут СУБ в сравнении с ТБ. Количественно превышение предела прочности на срез для СУБ относительно ТБ менее 12%. Лучшее соответствие с экспериментальными данными из проанализированных обеспечивает теория Гениева. Предел прочности бетонов на срез, наиболее вероятно, описывается уравнением $R_{sh} = k\sqrt{R \cdot R_t}$ при k = 0.5-0.6.

Ключевые слова: прочность на срез, самоуплотняющийся бетон, теории прочности, критерии разрушения.

Guide for Authors
for submitting a manuscript for publication in the «Architecture and Engineering»

The journal is an electronic media and accepts the manuscripts via the online submission. Please register on the website of the journal http://aej.spbgasu.ru/, log in and press "Submit article" button or send it via email aejeditorialoffice@gmail.com.

Please ensure that the submitted work has neither been previously published nor has been currently submitted for publication in another journal.

Main topics of the journal:

1. Architecture
2. Civil Engineering
3. Geotechnical Engineering and Engineering Geology
4. Urban Planning
5. Technique and Technology of Land Transport in Construction

Title page

The title page should include:

The title of the article in bold (max. 90 characters with spaces, only conventional abbreviations should be used); The name(s) of the author(s); Author's(s') affiliation(s); The name of the corresponding author.

Abstract and keywords

Please provide an abstract of 100 to 250 words. The abstract should not contain any undefined abbreviations or unspecified references. Use the IMRAD structure in the abstract (introduction, methods, results, discussion).

Please provide 4 to 6 keywords which can be used for indexing purposes. The keywords should be mentioned in order of relevance.

Main text

It should have the following structure:
1) Introduction,
2) Scope, Objectives and Methodology (with subparagraphs),
3) Results and Discussion (may also include subparagraphs, but should not repeat the previous section or numerical data already presented),
4) Conclusions,
5) Acknowledgements (the section is not obligatory, but should be included in case of participation of people, grants, funds, etc. in preparation of the article. The names of funding organizations should be written in full).

General comments on formatting:

- Subtitles should be printed in Bold,
- Use MathType for equations,
- Tables should be inserted in separate paragraphs. The consecutive number and title of the table should be placed before it in separate paragraphs. The references to the tables should be placed in parentheses (Table 1),
- Use "Top and Bottom" wrapping for figures. Figure captions should be placed in the main text after the image. Figures should be referred to as (Fig. 1) in the text.

References

The journal uses Harvard (author, date) style for references:
- The recent research (Kent and Park, 1990)...
- V. Zhukov (1999) stated that…

Reference list

The list of references should only include works that are cited in the text and that have been published or accepted for publication. Personal communications and unpublished works should only be mentioned in the text. Do not use footnotes or endnotes as a substitute for a proper reference list. All references must be listed in full at the end of the paper in alphabetical order, irrespective of where they are cited in the text. Reference made to sources published in languages other than English or Russian should contain English translation of the original title together with a note of the used language.

Peer Review Process

Articles submitted to the journal undergo a double blind peer-review procedure, which means that the reviewer is not informed about the identity of the author of the article, and the author is not given information about the reviewer.
On average, the review process takes from one to five months.